THE HONG KONG
POLYTECHNIC UNIVERSITY
香港理工大學
Pao Yue-kong Library
包玉剛圖書館

Copyright Undertaking

This thesis is protected by copyright, with all rights reserved.

By reading and using the thesis, the reader understands and agrees to the following terms:

1. The reader will abide by the rules and legal ordinances governing copyright regarding the use of the thesis.
2. The reader will use the thesis for the purpose of research or private study only and not for distribution or further reproduction or any other purpose.
3. The reader agrees to indemnify and hold the University harmless from and against any loss, damage, cost, liability or expenses arising from copyright infringement or unauthorized usage.

If you have reasons to believe that any materials in this thesis are deemed not suitable to be distributed in this form, or a copyright owner having difficulty with the material being included in our database, please contact lbsys@polyu.edu.hk providing details. The Library will look into your claim and consider taking remedial action upon receipt of the written requests.

Pao Yue-kong Library, The Hong Kong Polytechnic University, Hung Hom, Kowloon, Hong Kong

http://www.lib.polyu.edu.hk

Characteristics of Lead Zirconate Titanate (PZT) Films Deposited by the Sol-gel Method using Platinum and Reactive Sputtered RuO_x Electrodes

by

LAW Chi-wai

A Thesis Submitted for
the Degree of Master of Philosophy

Department of Electronic and Information Engineering

The Hong Kong Polytechnic University

1999

Pao Yue-Kong Library
PolyU • Hong Kong

Acknowledgements

Mr. K. Y. Tong, my supervisor, is the first gentleman to whom I want to express my gratitude. Without his help, inspiration, guidance and support to this investigation, to complete this project and thesis would be very difficult, if not impossible.

Mr. C. W. Lip and Dr. E. V. Jelenkovic are not only helpful in the technical support of this project but also have shown me a way to acquire a great deal of engineering sense. The author is in deep appreciation to the above nice gentlemen.

Last but not least, I would also like to acknowledge the supply of sol-gel solution by Prof. J. H. Li of Jiangsu Institute of Petrochemical Technology, China and thank Dr. Vincent Poon of HKUST for the AES measurement. The author also thanks the financial support of the research grant from the Hong Kong Polytechnic University.

Abstract

Characteristics of Lead Zirconate Titanate (PZT) Films Deposited by the Sol-gel Method using Platinum and Reactive Sputtered RuO_x Electrodes

$Pb(Zr_{0.52}, Ti_{0.48})O_3$ (PZT) thin-film capacitors with sputtered platinum (Pt) and reactive sputtered ruthenium oxide (RuO_x) electrodes were fabricated. We have studied the effect of pyrolysis temperatures between 300°C and 600°C on the materials and the ferroelectric characteristics of PZT films deposited by the sol-gel method. When using Pt electrodes, the X-ray Diffraction (XRD) patterns showed that the texture of the PZT films was mainly [111] orientation for pyrolysis temperatures below 400°C, but changed to [100] orientation for pyrolysis temperatures at or above 400°C. With RuO_x electrodes, the films were [110] preferred orientated. The [110] peak intensity dropped significantly for the pyrolysis temperatures at or above 450°C. At a final annealing temperature of 700°C for 10 minutes, the remanent polarization Pr of the films with Pt electrodes has a maximum value of $34\mu Ccm^{-2}$ at 400°C of pyrolysis temperature. However, there is no considerable effect of pyrolysis temperature on the texture of the PZT films. The PZT capacitors with RuO_x electrodes have the values of Pr about $24\mu Ccm^{-2}$ for pyrolysis temperatures between 300°C and 400°C. In both cases, pyrochlore phase also existed in the films pyrolyzed at temperatures above 400°C and hence the remanent polarization and dielectric constant dropped considerably for the pyrolysis temperatures at or above 450°C.

Applying the optimised pyrolysis temperature of 400°C from previous studies, the RuO_x/PZT/RuO_x capacitors were fabricated for the ferroelectric and fatigue measurement. The ferroelectric and fatigue properties of the PZT capacitors were investigated with different oxygen content in the RuO_x electrodes and different electrode thickness. Increase in oxygen content in the electrodes would improve the fatigue properties of the capacitors but the remanent polarization has maximum value at a relative oxygen partial pressure of 10%. Our fatigue result is consistent with the oxygen vacancy model. Considerable degradation in ferroelectric and fatigue properties of the capacitors was observed when the electrode thickness was below 230nm. Oxygen deficiency in the thin electrodes was detected through Auger Electron Spectroscopy (AES) measurement. It was testified that the effect of electrode thickness is attributed to the oxygen diffusion in the bottom electrode layers.

The I-V characteristics of the PZT capacitors with Pt and RuOx electrodes were also investigated. For the RuO_2/PZT/RuO_2 capacitors, increase in electrode oxygen content lowered the leakage current density when the applied electric field was below 120kVcm^{-1}. The leakage current density of Pt/PZT/Pt capacitors was confirmed to be lower than that of RuO_2/PZT/RuO_2 capacitors. It was found that, in the high E-field region, Pt/PZT/Pt capacitors obey the Frenkel Poole Emission conduction model.

Table of Content

Acknowledgements		II
Abstract		III
Table of Content		V
Chapter 1	Introduction	1
1.1	Ferroelectrics for Memory Applications	1
1.2	Project Objective	2
Chapter 2	Literature Review	5
2.1	Definition of Ferroelectrics	5
2.2	Structure of Ferroelectric Materials	8
2.3	Applications of Ferroelectrics	11
2.4	Fatigue of Ferroelectric Thin Films	16
2.5	Sol-gel Process for Ferroelectric Thin Films	18
2.6	Texture of Ferroelectric Thin Films	20
2.7	Electrodes and Substrates	22
Chapter 3	Ferroelectric Properties	24
3.1	Introduction	24
3.2	Experiment	26
3.3	Ferroelectric Properties and Pyrolysis Temperature	28
(a)	Effect of Pyrolysis Temperature on the PZT Films With Pt Electrodes	28
(i)	Crystallization Behavior of Pt Bottom Electrodes	28

(ii) Crystallization Behavior of the PZT Films Deposited on Pt Electrodes 28
(iii) Ferroelectric Properties of PZT Films Deposited on Pt Electrodes 32
(b) Effect of Pyrolysis Temperature on the PZT Films with RuO_x Electrodes 39
(i) Characteristics of RuO_x Bottom Electrodes 39
(ii) Crystallization Behavior of PZT Films Deposited on RuO_x Electrodes 39
(iii) Ferroelectric Properties of PZT Films Deposited on RuO_x Electrodes 43
3.4 Ferroelectric Properties and RuO_x Oxygen Content 47
3.5 Ferroelectric Properties and RuO_x Electrode Thickness 53
3.6 Conclusions 57

Chapter 4 Fatigue Properties 59
4.1 Introduction 59
4.2 Experiment 60
4.3 Properties of the RuO_x Bottom Electrodes 61
4.4 Fatigue Properties of PZT Thin Film Capacitors with Pt and RuO_2 Electrodes 63
4.5 Effect of Oxygen Content of RuO_x Bottom Electrodes 63
4.6 Effect of RuO_x Electrode Thickness 68
4.7 Inter-diffusion in RuO_x Bottom Electrodes 68
4.8 Conclusions 73

Chapter 5		Current-Voltage Characteristics	75
5.1		Introduction	75
5.2		Experiment	76
5.3		Results and Discussions	76
	(a)	J-E Characteristics of PZT Capacitors with Pt and RuO_2 Electrodes	76
	(b)	J-E Characteristics of RuO_x/PZT/RuO_x Capacitors With Different Oxygen Content	82
5.4		Conclusions	83
Chapter 6		Conclusions and Future Work Suggestion	85
6.1		Conclusions	85
6.2		Future Work Suggestion	88
References			89

Chapter ONE

Introduction

1.1 Ferroelectrics for Memory Applications

Growing demand for battery-operated devices such as personal digital assistants (PDA's) has led to extensive study of low-power high-speed microprocessors and high density memories. As developments in computer memories - whose integrated circuits combine transistors, resistors and capacitors - have accelerated, it arouse the need for better capacitors and materials.

In the race for ever better computer memories, ferroelectric materials offer unique advantages. They can also be combined with standard silicon processing or with gallium arsenide in microwave components. One of the ideas to produce higher density memories is to increase the dielectric constant of the memory dielectrics so that the size of the memory capacitor could be reduced by a certain large factor. Since ferroelectric materials often have relatively high dielectric constant compared to the conventional memory dielectrics (SiO_2), it is a better choice to use ferroelectric memories. The remanent polarization in ferroelectric materials can also be applied to make non-volatile memories. Although ferroelectrics are highly recommended to be investigated for memory applications because of their bistable polarizations and high dielectric constants, there are still several research problems that have to be further studied.

Ferroelectricity is defined as a non-linear relationship between polarization and electric field [1-2]. Ferroelectric materials with perovskite-type structures have been intensively investigated during the last fifty years. The physical structures and properties in relation to the spontaneous polarization, have been widely investigated through experimental and theoretical measures [3-4]. The application of ferroelectricity for electronic, optical and mechanical devices has been implemented by the greatly improved performance of ferroelectrics over the years [5-7]. In the past decades, ferroelectric memory devices, based on spontaneous polarization switching, have been integrated into standard CMOS technology taking the form of ferroelectric thin films. Large charge storage capacity, non-volatility, low driving voltage and low energy dissipation of ferroelectric memories are desirable. On the other hand, reliability issues have accompanied the applications of ferroelectricity. In particular, polarization fatigue, defined as loss of switchable polarization under repeated cycling, has long been a major hindrance to the application of ferroelectric memories [8-9]. Various attempts have been made to improve the fatigue performance of ferroelectric thin films via electrode modification or novel substitute materials such as layered perovskites [10-12]. Different mechanisms have also been proposed to explain fatigue and to guide further designs of ferroelectrics. Nevertheless, a fundamental understanding and a definitive mechanism for fatigue are still lacking [13-14].

1.2 Project Objective

The present study is intended to investigate the characteristics of sol-gel Lead Zirconate Titanate (PZT) thin films. The whole investigation is divided into three

aspects: Ferroelectric Properties, Fatigue Properties and Current-Voltage (I-V) Characteristics. Ferroelectric Properties include polarization states and dielectric constant. Though there have been many reports on sol-gel PZT films, a detailed study on the effect of pyrolysis temperatures is still lacking. In the aspect of Ferroelectric Properties (chapter 3), the effect of pyrolysis temperatures on the electrical and physical properties of sol-gel PZT thin films has been studied. Sol-gel PZT thin-film capacitors with sputtered Pt and reactive sputtered RuO_x electrodes were fabricated. We have studied the polarization states, dielectric constant and texture of the PZT films with varying the pyrolysis temperature from 300°C to 600°C. Other than the effect of pyrolysis temperature, the effect of RuO_x electrodes with different oxygen content and thickness on the ferroelectric properties of the PZT films has also been investigated. The work is expected to optimize the sputtering conditions for the RuO_x electrodes. We obtained different oxygen content for the electrodes by varying the relative oxygen partial pressure. In addition, the thickness of the RuO_x electrodes was obtained by taking different sputtering time. For the second aspect - Fatigue Properties (chapter 4), the issue of fatigue performance of the sol-gel PZT thin films has been addressed. It is decided to study sputtered ruthenium oxide films as electrodes of the PZT capacitors, because it is expected that oxide electrodes can improve the fatigue, aging and imprint properties. So the fatigue behavior of PZT thin-film capacitors has been investigated with (i) Pt electrodes, (ii) RuO_x electrodes with various oxygen content of the electrodes and (iii) RuO_x electrodes with various thickness. The result is found to be consistent with the established oxygen vacancy model. For the last aspect (chapter 5), we studied the I-V characteristics of the PZT thin-film capacitors with Pt and RuO_x electrodes. The leakage current density (J) of the capacitors with Pt and RuO_x electrodes has been

measured. We confirmed that the capacitors with RuO_x electrodes possess higher leakage current density than those capacitors using Pt electrodes. We also found that the leakage current density of the RuO_x/PZT/RuO_x capacitors decreased when their electrode oxygen content increased. We shall compare our results with other published results.

The results of this project would contribute to the technology involving the application of sol-gel PZT films in ULSI memories.

Chapter TWO

Literature Review

2.1 Definition of Ferroelectrics

Ferroelectricity is defined as the non-linear relationship between polarization and electric field. A ferroelectric crystal is defined as a crystal which belongs to the pyroelectric family and of which the direction of spontaneous polarization can be reversed by an electric field. The usual method to examine whether a crystal is ferroelectric or not is by applying Sawyer-Tower circuit (Fig. 2.1). When applying the Sawyer-Tower circuit, usually the AC voltage of 50-100Hz is supplied to the bridge. The voltage V applied to C_x is equal to the voltage between the electrodes 1 and 2 of the oscilloscope. Since the capacity of the electrodes of the oscilloscope is small, the electric charges stored in C_x and C_o are practically the same. If this charge is denoted as Q, the voltage between the electrodes 3 and 4 must be Q/C_o. Therefore, on the fluorescent plate of the oscilloscope the curve of Q/C_o vs. V is observed. When a hysteresis loop shown in Fig. 2.2 is observed during measurements, the crystal in C_x is called ferroelectric. The crystal which is ferroelectric in some temperature range is called a ferroelectric crystal. The charge Q above mentioned is proportional to the electric displacement D in a crystal. The relation between D and the electric field E and the polarization P is, in CGS units, $D=E+4\pi P$. In most cases where the hysteresis loop is observed, P is much larger than E and therefore the quantity Q/C_o may be considered

to be proportional to P. In such a case the Q/C_o vs. V curve on the oscilloscope can be considered as P vs. E curve (Fig. 2.2) and is conventionally called a polarization curve or P-E loop.

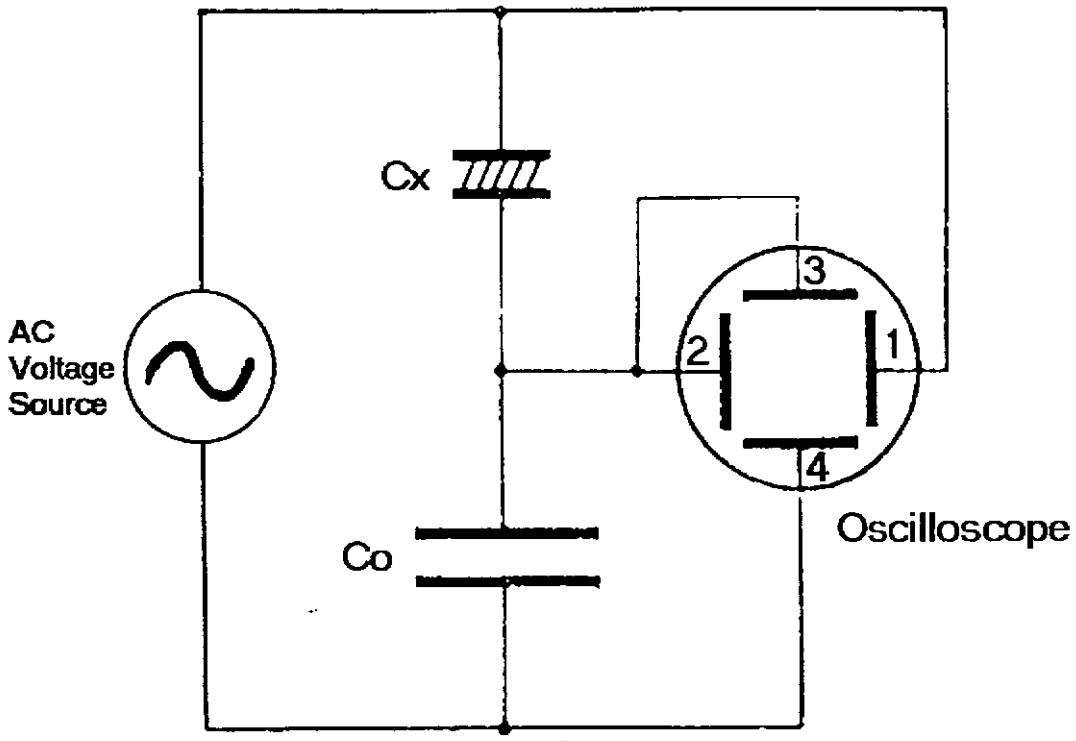

Fig. 2.1 Sawyer-Tower Circuit - A Hysteresis Bridge [14]

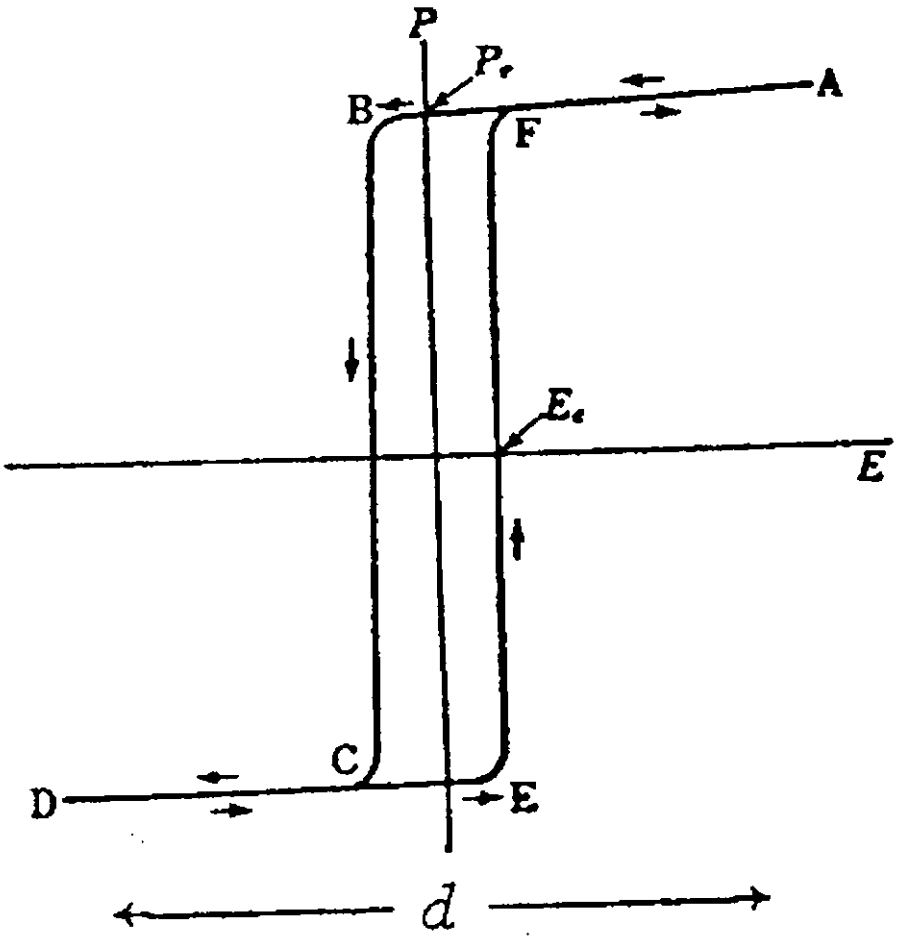

Fig. 2.2 Ferroelectric Hysteresis Loop (P-E Loop) [14]

2.2 Structure of Ferroelectric Materials

Most of the ferroelectric materials have the so-called ABO_3 type perovskite structure [1] (Fig. 2.3). This is a cubic structure with A-site cations at the corners, B-site cations at the body center and oxygen ions at the face centers. Titanates such as $BaTiO_3$, $PbTiO_3$ and $SrTiO_3$, as well as zirconates and niobates such as $PbZrO_3$ and $NaNbO_3$, all belong to the family of perovskites. The B-site is occupied by a smaller cation such as Ti^{4+}, Zr^{4+}, or Nb^{5+}. Since the structure of perovskites provides a relatively loose environment for B-site cations, they can be displaced and give rise to large polarization. Below the Curie temperature, perovskites distort into lower symmetry forms such as tetragonal, orthorhombic or rhombohedral phase from the cubic phase and permanent polarization forms on a macroscopic scale.

Lead ziconate titanate ($Pb(Zr_{1-x}Ti_x)O_3$ is the most widely investigated perovskite for ferroelectric memory and other applications. It is a solid solution system between $PbZrO_3$ and $PbTiO_3$ with several metastable phases [2]. A typical PZT phase diagram is shown in Fig. 2.4. High Zr compositions are orthorhombic and antiferroelectric but with a small lattice strain [3], while high Ti compositions are tetragonal and ferroelectric with a large lattice strain [4]. At compositions of Zr/Ti close to 52/48, there is a morphotrophical phase boundary (a phase boundary independent of temperature), where many dielectric and ferroelectric properties are found to be optimal [5].

There are other types of ferroelectric oxides which have no perovskite structure. However, they show similarity to perovskites in some way - the presence of BO_6 octahedra. Layered perovskites, also known as Aurivillius compounds, have perovskite units separated by bismuth oxide layers [6]. Typical examples of layered perovskites

include $Bi_4Ti_3O_{12}$ and $SrBi_4Ti_4O_{15}$. Pyrochlores such as $Bi_2Ti_2O_7$ assume a defected fluorite structure, while tungsten bronze structures such as (Pb, Ba)Nb_2O_6 have three types of A-site interstitials among BO_6 octahedra [7-8]. These non-perovskite structure materials have not been shown to have higher remanent polarization states than perovskites. Therefore they have been less investigated in view of the rich variety of perovskites.

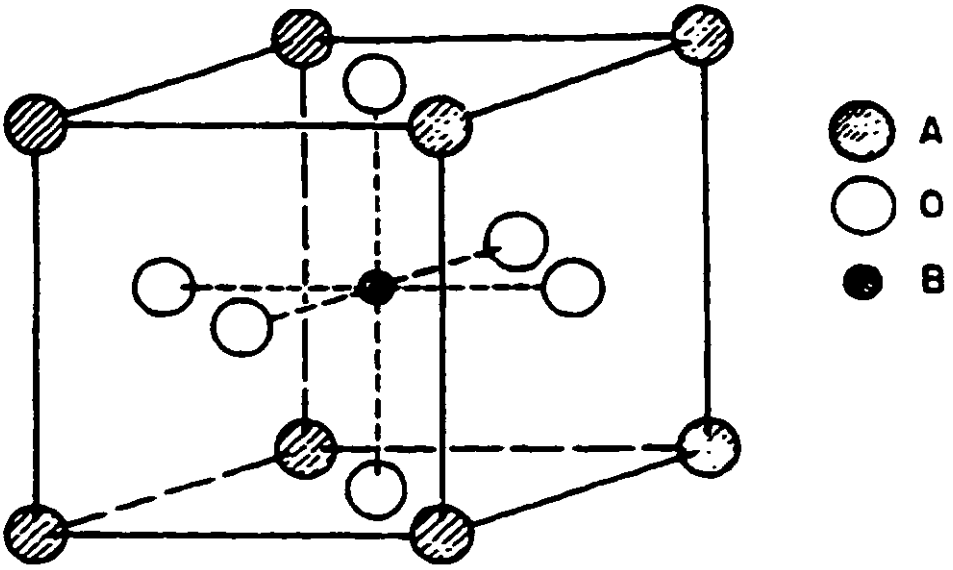

Fig. 2.3 Crystal Structure of ABO_3 Perovskite [14]

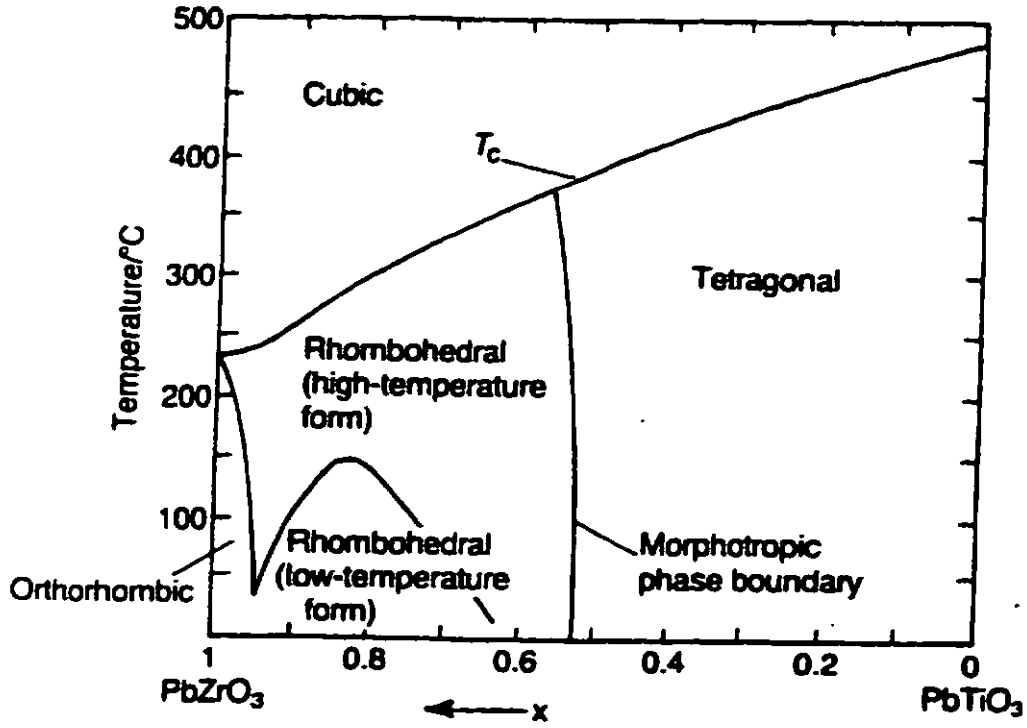

Fig. 2.4 A Typical $Pb(Ti_{1-x}Zr_x)O_3$ Phase Diagram [14]

2.3 Applications of Ferroelectrics

The ferroelectric materials with perovskite structure have received a lot of attentions in past years because of their useful ferroelectric, electro-optic, piezoelectric and pyroelectric properties [9-10]. Fig. 2.5 shows a chronology of efforts at various applications for ferroelectric films. There are several reasons for the current upsurge in ferroelectric film synthesis research:

(i) In spite of the lack of commercialization of ferroelectric film devices in the past, the promise of several economically important applications, including non-volatile and radiation-hard memory, high dielectric constant capacitors, actuators, SAW devices, and electro-optic devices, pyroelectric detectors, and IR imagers is a prime driving force of current work.

(ii) The maturity of film deposition processes such as sputtering provides more confidence in process control than existed in earlier years. A body of knowledge relating growth conditions to film properties and structure has developed, especially in the case of PZT type deposition by sputtering. Added to this is the development of new film synthesis techniques such as sol-gel, laser deposition, and MOCVD, which provide alternative, high rate synthesis routes.

Table 2.1 [10] compares various features of common deposition techniques. Film deposition techniques can be divided into "dry" and "wet" processes. The dry processes include sputtering, evaporation, and CVD, whereas the common wet processes are MOD and sol-gel. The wet processes usually use unheated substrates or low temperature deposition but dry processes use a range of temperatures, typically heated substrates, to 700°C. Regarding the deposition methods of ferroelectric thin

films, the wet methods tend to be inexpensive and fast, whereas the dry methods are expensive and slower. Also the low substrate temperature during sol-gel film deposition is a favorable point in film deposition process. This method can make the film produced with good stoichiometric ratio and low cost of production. Also it has the advantages of fine epitaxy level and low substrate temperature which are suitable for making memory devices (Table 2.1).

Ferroelectric materials that undergo first order transitions have a bi-stable polarization at zero electrical field. The two states are externally switchable under an applied field. Ferroelectric thin films seek to take advantage of these properties for microelectronic applications such as integrated circuit (IC) memory devices and optical devices [11-13]. In addition, the high dielectric constant and high electrostriction coefficients associated with some ferroelectric materials offer possible applications such as high density capacitors and microactuators. The high density, fast speed and low power dissipation of ferroelectric thin films are important attributes of these devices in electronic circuits. In particular, ferroelectric memories have been a fast growing field of development for the past decade.

There are basically two major categories of ferroelectric Random Access Memories (RAMs). One is the non-volatile RAM (NVRAM) which operates on the switching of the remanent polarization. The other is the dynamic RAM (DRAM) which operates on the charge storage capability. The later usually takes advantage of the high dielectric constant of ferroelectric materials such as (Ba, Sr)TiO_3 and PZT. Fig. 2.6 shows the cross-section of a typical ferroelectric RAM integrated circuit. From the studies of various ferroelectric materials, it was found that PZT can provide a relatively higher and stable dielectric constant (~2000) and an appropriate Curie temperature

(>200°C) [14]. For NVRAM applications, fast switching time, high remanent polarization, low coercive field, low leakage current and long term endurance are desirable. PZT seems to be promising for these requirements and have been widely investigated [15-17]. The integration of PZT thin films into standard CMOS process on Si wafers has been successful for device realization. Some research groups have made 4k-bit and 16k-bit RAMs [10]. Ramtron used sputtered PZT and a more conservative SRAM layout [18]. However, the commercial products of ferroelectric memories are still not common. In reality, there are a number of physics, engineering, and materials science issues to be solved or optimized for ferroelectric RAMs. One major hindrance for the application of PZT ferroelectric thin films is their lack of endurance. It is well known that PZT thin films on Pt/Si substrates suffer from significant degradation in polarization after repeated electrical switching [19].

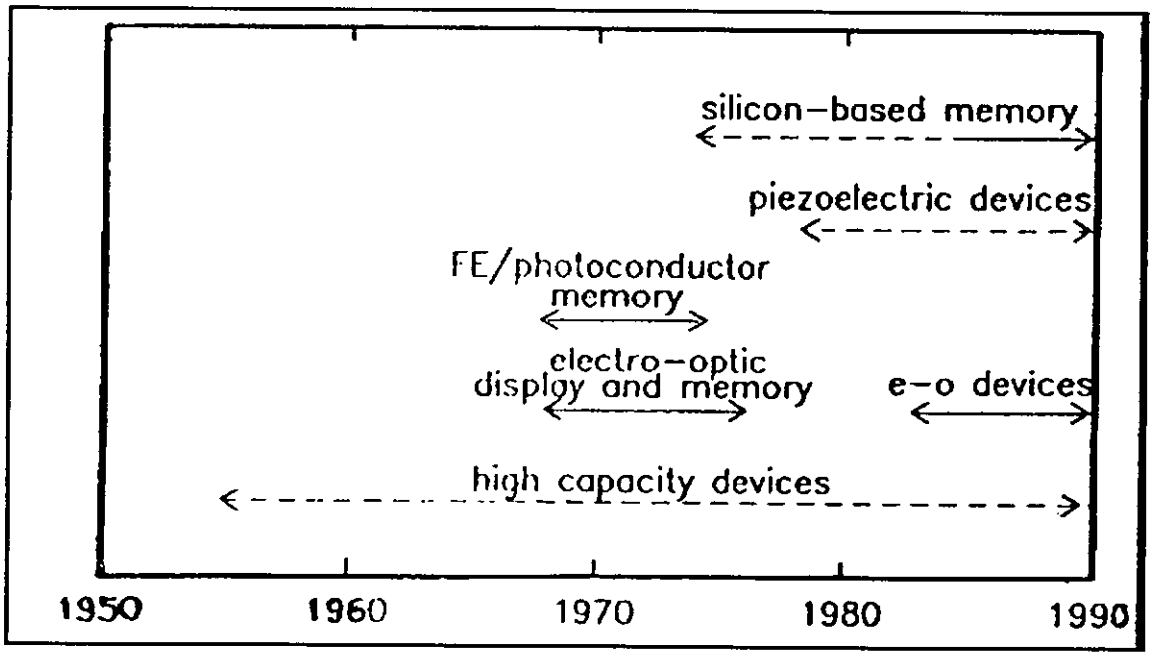

Fig. 2.5 Application History of Ferroelectric Films [10]
(Arrows indicate time span of various applications. Solid lines indicate more concerted activity)

Methods	Deposition Rate nm/min	Epitaxy 1-10	Stoichiometry 1-10	Wet / Dry	Substrate Temp. (°C)	Annealing Temp. (°C)	Devices 1-7	Cost	Problems
R. F. Sputtering	0.5-5	8	3	Dry	Room Temp. - 700	500-700	1-7	High	Negative Ions
Magnetron Sputtering	5-30	5	5	Dry	Room Temp. - 700	500-700	1-7	High	Target Surface
R. F. Magnetron Sputtering	5-10	9	5	Dry	Room Temp. - 700	500-700	1-7	High	
Ion Beam Sputtering	2-10	9	8	Dry	Room Temp. - 700	500-700	1-7	High	Uniformity
Evaporation	10-100	7	4	Dry	Room Temp. - 700	500-700	1-7	High	Rate Control
Laser Deposition	5-100	9	6	Dry	Room Temp. - 700	500-700	1,3,5	High	Debris, Uniformity
Sol-Gel	100 nm /Coating	2-8	9	Wet	Room Temp.	450-800	1,2,3,5	Low	Multiple Coating
MOD	300 nm /Coating	2	9	Wet	Room Temp.	500-800	1,3,5	Low	High Annealing Temp.
MOCVD	5-100	5	7	Dry	400-800	600	1-6	High	High Substrate Temp.

Table 2.1 Comparison of Salient Features of Various Common Methods of Ferroeletctric Thin Film Preparation [10]
(Number scale for epitaxy and stoichiometry : 1-worst, 10-best; Number classification for devices : 1-Capacitor, 2-Memory cell, 3-Actuator, 4-Electro optic, 5-Pyrodetector, 6-IR Imager, 7-SAW)

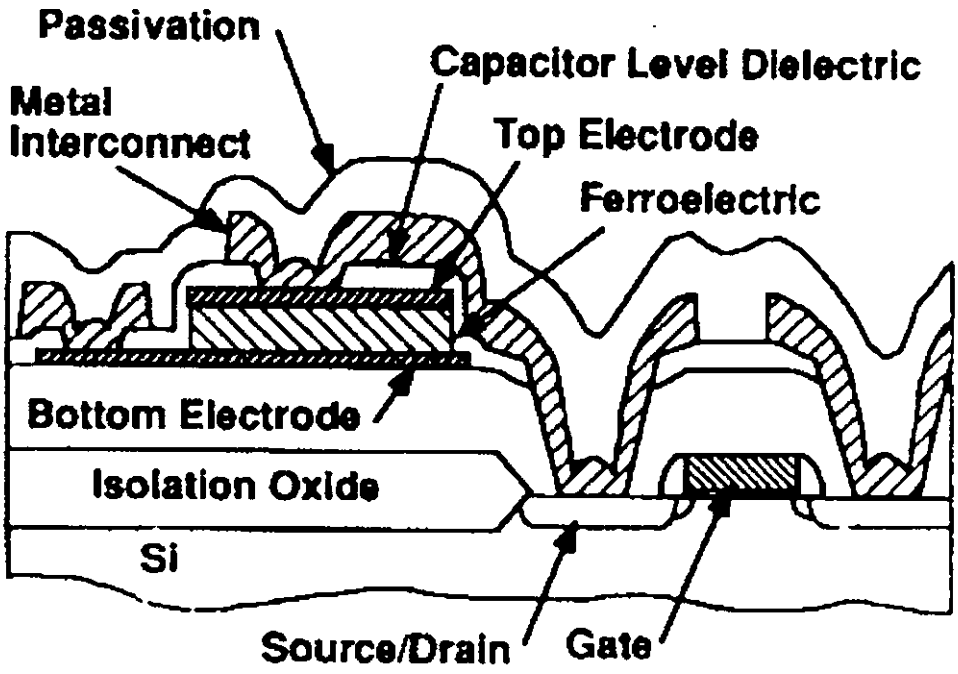

Fig. 2.6 Cross-section of a Typical Ferroelectric Random Access Memory (FERAM) Integrated Circuit [62]

2.4 Fatigue of Ferroelectric Thin Films

Reliability issues for ferroelectric thin films for memory applications include aging, retention, fatigue, imprint and DC breakdown [20-24]. Fatigue is defined as the loss of switchable polarization during bipolar cycling. This problem is known for ferroelectrics since the early stage of ferroelectric research, but it is particularly important for thin film memory applications. Several mechanisms, such as microcracking near the ferroelectric-electrode interface, domain restoration, accumulation of charged particles at the interface, and growth of conductive dendrites were suggested to be the cause of fatigue but no conclusive interpretation has been presented [25-28]. It is generally believed that fatigue is defect related, and that fatigue is also an accumulative phenomenon which requires a time dependent response and interaction of the defects. Along this line, questions of which defects, how they cause fatigue, and the type of defect-domain interaction, have emerged as essential issues to be addressed by the ferroelectric thin film community.

PZT thin films on Pt electrodes are well known for the poor fatigue resistance. Remanent polarization starts to degrade remarkably after 10^6 cycles. A number of intrinsic defects may exist in PZT thin films due to processing, some can be relatively mobile. Oxygen vacancies are known to exist in PZT as revealed by high temperature conduction study by Waser et al. [29]. It is generally believed that oxygen vacancies come from the lead loss during annealing [30]. On the other hand, PZT materials are p-type semiconductor as the work function (5.25eV) was found to be close to the valence band (Eg=3.5eV, χ=2.6eV [31]). Holes are therefore present as electronic defects. EPR study of the band structure of PZT thin films also revealed some shallow hole traps and

electron traps which are close to the valence band and the conduction band, respectively. Shallow hole traps were throught to be Pb^{+}, and Ti^{3+} was regarded as electron trap because of the mixed valency of Ti [32]. Therefore, oxygen vacancies, electrons and holes are all possible charge carriers in PZT thin films which are mobile and they may migrate during AC cycling. Fatigue mechanisms based on the oxygen vacancy model and electronic (electrons and holes) carrier model have thus been proposed.

Oxygen vacancy model envisions trapping of oxygen vacancies at the electrode interface. Since the top and bottom electrodes went through different processing, the field distribution across the film may be asymmetric [33]. Therefore, even symmetric AC field may cause asymmetric migration of oxygen vacancies. The interface may have the trapping ability due to lattice mismatch and interface states. Under AC cycling, there could be a continuous trapping of oxygen vacancies at one interface (top or bottom) which creates an internal field suppressing further domain switching. This oxygen vacancy model was supported by the Auger Electron Spectroscopy (AES) study from the report on depletion of oxygen at the electrode after fatiguing PZT thin films [34]. Another support came from the alleviation of leakage and fatigue by donor (Nb) doping of PZT films by Chang et al. (Donor doping was supposed to suppress the number of oxygen vacancies) [35].

Electronic carrier model envisions that electrons and holes injected into the film are trapped at domain boundaries. These trapped defects stablize the domain and prevent it from further switching [36]. Support for this theory came from the suppression of polarization of $BaTiO_3$ single crystals and PZT thin films by shinning UV light [37-38]. By tuning the energy of the radiation to be near the bandgap, UV light was thought to be responsible for the creation of electron and hole pairs, which

accelerated trapping and caused the suppression. Furthermore, since these trapped carriers can be removed from domain boundaries by thermal, electrical and optical means during annealing, a prolong field application, or light exposure, it should be possible to restore the polarization. This was indeed observed. Another report by Jiang et al. showed that the polarization of PZT thin films can be suppressed by e-beam exposure [39].

Practical remedies have been used to improve the fatigue endurance of PZT thin films, irrespective of these proposed mechanisms. Most of them fell into the category of choosing an appropriate oxide electrodes. Conductive oxide such as RuO_2 and IrO_2 are known to improve the fatigue but they also increase the leakage current [40-41]. P-type semiconducting perovskites such as $(La,Sr)CoO_3$, $LaAlO_3$ were also found to improve the fatigue by Tuttle et al. [42-43]. Heterostructures of the $YBi_2Cu_3O_7$/PZT have been reported to be effective as well [44]. To rationalize these results, the oxygen vacancy model interpreted the role of oxide electrodes as oxygen sinks which can compensate the oxygen vacancies at the interface. On the other hand, electronic model interpreted these oxide electrodes as p-type semiconductors which would limit the electron injection into the film during cycling.

2.5 Sol-gel Process for Ferroelectric Thin Films

Wet-chemical, also known as sol-gel, processing of ceramics can refer to a multitude of reaction processes which employ a wide variety of chemical precursors to prepare many different products. The basic idea is to use the techniques of solution chemistry to build ceramic structures from the molecular level. Wet metal-organic

precursors are applied to deposit wet layers on the substrate. Budd et al. developed a sol-gel procedure to prepare PZT thin films from metal ethoxides [45]. Solutions in sol-gel methods are allowed to undergo polymerization before deposition. The product has good film uniformity and it is relatively easy to control film composition. Sol-gel coatings can be prepared using simple, non-vacuum processes, which require only a small investment in capital, hence coatings which might be made by alternate techniques are made more cheaply using sol-gel processes [11].

Sol-gel method requires a pyrolysis step to obtain crystallized metal oxides. The pyrolysis stage in which the organic wet layers are burnt out usually leaves many pores in the film. The other problem is related to cracking of the film during pyrolysis. This is usually avoided by multiple coating with interim drying or pyrolysis between coatings. Many perovskite ferroelectric thin films including PZT, $SrBi_2Nb_2O_9$ and $SrBi_2Ta_2O_9$ have been prepared by the sol-gel method with good film quality [46].

Since ferroelectric materials are mostly complex oxides, many thin film deposition techniques, especially sol-gel technique requires post or in-situ deposition heat treatment to crystallize the film. Furthermore, crystallization process is also required to ensure good electrical contact and bonding between the ferroelectric and the electrode. For example, it has been shown that annealing of the top electrodes after the deposition improves the film properties [47]. In integration of ferroelectric memory with other electronic devices, it is desirable to lower the crystallization temperature to minimize damage to other circuit elements, since high crystallization temperature can cause undesirable reaction, diffusion and cracking of the device.

Effort has been made to lower the crystallization temperature of PZT thin films. Sol-gel method usually requires a crystallization temperature about 600-700°C.

Between 400°C and 600°C, pyrochlore formation becomes competitive which is detrimental to film properties. The phase transformations of PZT thin films from amorphous to pyrochlore to perovskite have been widely investigated [48-49]. The critical issues are temperature, composition and atmosphere. For example, Lefevre et al. showed that in pure O_2, PZT films formed perovskite at 700°C while in reducing atmosphere there was a pyrochlore formation at the same temperature [50]. If excess Pb is added, the crystallization is better because Pb is a low melting component which enhances the densification process during film crystallization. However, very few researchers have seriously investigated the pyrolysis step. The general pyrolysis temperature applied is 300°C.

2.6 Texture of Ferroelectric Thin Films

The orientation of ferroelectric thin films has some effect on the property because ferroelectricity varies between different crystallographic directions. For example, the polarization of tetragonal $BaTiO_3$ is along the (001) axis of the cubic cell. Such anistropy is an inevitable feature of ferroelectrics because spontaneous polarization is only allowed in certain directions.

To control the orientation of ferroelectric thin films, lattice matched substrates have been used. For example, MgO(100), Si(100) with Pt(100) were found suitable for the growth of (100) orientation of $BaTiO_3$, PZT and $SrBi_2Ta_2O_9$ thin films [51-53]. The epitaxial relationship between the substrate and the ferroelectric film minimizes the stress during crystallization and retains epitaxial growth. Another example is the growth of (001) oriented PZT or PLZT thin films on (001) LSCO or YBCO layers.

TEM studies revealed a perfect epitaxial relation between the substrates and the film [54]. However, the variety of candidate materials for lattice matched substrates are limited and many of them still have significant lattice mismatch. For example, the widely used Pt(111)/Si substrates have 30% lattice mismatch with PZT materials. Therefore, many substrates yielded a polycrystalline thin film rather than a single crystal thin film even if the substrate was a single crystal.

Another method is through nucleation control. A buffer layer served as nucleation sites for a specific orientation is introduced before the deposition or the crystallization of the film. This buffer layer retains some similarity to the upper ferroelectric layer on a specific crystallographic plane and it sometimes comes from the ferroelectric material itself. For instance, during crystallization, some intermediate phase might form which can serve as nucleation sites. This intermediate phase may eventually decompose when the crystallization is complete and is thus transient in nature. An example of this is the PZT thin films made by the sol-gel method on Pt(111)/Si substrates [55-56]. Both (100) and (111) orientation on the same Pt(111)/Si substrate can be facilitated by different nucleation treatments. For the nucleation of (111) orientation, a transient $Pt_{5-7}Pb$ phase was detected with (111) feature, and PZT films could directly grow into (111) orientation through this intermediate phase. On the other hand, (100) texture of PZT can also be obtained on the same substrate if the film had a PbO buffer layer. Growth control is applicable if all the films will grow into the same orientation when the final heat treatment is the same and sufficiently dominant. The nucleation theory stresses the importance of intermediate step controlling the final orientation. In general, temperature, chemistry and substrate materials play an important role in the formation of these intermediate phases.

2.7 Electrodes and Substrates

A good substrate material for ferroelectric deposition should satisfy the following requirements: (i) good surface quality, (ii) good thermal and chemical stability, (iii) specific crystallographic orientation, (iv) lattice matching quality, (v) good electrical contact, and (vi) low cost. Single crystal Si was the first kind of substrates used for ferroelectric thin film depositions and it is still the most popular kind of substrates today [57]. There was a few attempts to use GaAs and InP as substrate [58]. Pt is usually coated onto these semiconductors as bottom electrode prior to the deposition of ferroelectric films. Oxide substrates such as MgO and sapphire, especially perovskite substrates such as $SrTiO_3$, provide lattice matching and chemical stability features [59]. Si is well known for its reaction with Pb-containing perovskites. Si diffusion is also a serious problem at high temperature and has been known to degrade the ferroelectric properties. The prevention of such effects is by introducing some diffusion barrier such SiO_2 and Ti layers. Thus a typical substrates architecture for ferroelectric thin films is single crystal Si/oxide layer/diffusion barrier/bottom electrode on which the ferroelectric film layer is deposited. $Pt/Ti/SiO_2/Si$, a most popular substrate, has this configuration [60]. Substrate materials have great influence on the orientation of the ferroelectric thin films. For example, Si(100)/Pt(100) favors (100) oriented PZT thin films while Si(111)/Pt(111) favors the PZT (111) orientation.

Electrodes for ferroelectric thin films directly influence their electrical properties. Platinum is a metal with good conductivity and chemical stability for the crystallization of the ferroelectric thin films. The electrode/ferroelectric interface may

differ from system to system. Recently, $Pt/Ti/SiO_2/Si$ has been the most popular electrode/substrate system used for ferroelectric memories because of its stability and integration potential. This configuration has been demonstrated in previous report [60] to endure high temperature processing of the ferroelectric thin films and to maintain a distinct interface with little diffusion problem.

Due to the work function difference between the Pt electrode and PZT materials, a Schottky barrier or a space charge layer could form when they are in contact [61]. This feature was believed by several investigators to be responsible for the poor fatigue endurance of PZT thin films on Pt electrode. Recently, conductive oxide electrodes such as RuO_2 and IrO_2 have been used to alleviate the fatigue problem of PZT thin films [40-41]. While RuO_2 electrode is known to reduce the fatigue of PZT thin films, it also increases the leakage current. The deposition of RuO_2 and IrO_2 is usually through sputtering. There are not much detail studies of the relation between the RuO_2 sputtering process and the PZT properties.

Chapter THREE

Ferroelectric Properties

3.1 Introduction

PZT films have been an interesting research topic because of their ferroelectric, pyroelectric and piezoelectric properties. Many reports show that the sol-gel deposition technique has the advantage of better stoichiometry, simplicity and low cost [1-3]. The ferroelectric properties of PZT thin films have been widely investigated not only for memory applications but also for other device applications (e.g. sensors).

In this chapter, we would investigate the ferroelectric properties of the PZT thin films in three aspects: (a) Effect of Pyrolysis Temperature, (b) Effect of Oxygen Content of RuO_x Electrodes and (c) Effect of RuO_x Electrode Thickness.

In the preparation of PZT films using the sol-gel technique, a precursor solution is first spin coated on the substrate and pyrolyzed at a low temperature before final annealing at a higher temperature. Concerning the choice of thermal conditions in the preparation of PZT films, in the past most attention was paid to the effect of the annealing process on the characteristics of the crystallized films, such as the annealing temperature and the use of rapid thermal annealing [4-7]. Many reported results were based on a pyrolysis temperature of about 300°C. There were only a few studies [8-9] on the effect of varying the pyrolysis temperature on the microstructure of the PZT film after crystallization, but the electrical properties were not described. In the first part of

this chapter (Section 3.3), we shall report on both the textures and ferroelectric properties of PZT films prepared at different pyrolysis temperatures of the precursor solution, all with the same final annealing conditions. Our work shows that a proper choice of the pyrolysis temperature is important in optimizing the ferroelectric properties with a low thermal budget.

In ferroelectric thin film technology, platinum (Pt) film electrodes have widely been used for the thin film capacitors. In the past years, platinum has been proposed as an electrode material for PZT capacitor [10]. However, along with poor adhesion and etching characteristics, interface-related degradation problem such as fatigue accelerated the research for alternate electrode materials to replace conventional Pt films [11-13]. Recently, highly conductive electro-ceramics such as ruthenium dioxide (RuO_2) have been considered as alternatives [14]. This interest arised from the excellent fatigue properties of the ferroelectric films on these electrodes [15]. RuO_2 is one of the most stable conductive oxides and has a bulk resistivity of 46 $\mu\Omega$-cm [13,16-17]. Excellent etching of RuO_2 films using conventional dry etching techniques has been demonstrated, and the application of RuO_2 films as the electrodes of PZT ferroelectric thin-film capacitors has been actively investigated [18-19]. Although there are some studies on the properties of reactive sputtered RuO_2 thin films, in-depth investigation of RuO_x/PZT/RuO_x capacitors is still needed [20-22]. In particular, the optimization of RuO_x sputtering process to obtain the most desirable ferroelectric and fatigue properties is of great practical interest. In the second and third part of this chapter (Section 3.4 & 3.5), we shall report the effect of oxygen content and thickness of the RuO_x electrodes respectively on the ferroelectric characteristics of the PZT thin films. We would reveal that the ferroelectric properties of the PZT capacitors would be degraded when their

electrode thickness is too small. We also would show that the PZT capacitors possess the highest remanent polarization when using RuO_x electrodes with 10% oxygen partial pressure for the fabrication condition.

3.2 Experiment

(a) Effect of Pyrolysis Temperature: $Pb(Zr_xTi_{1-x})O_3$ films were prepared from organometallic precursor solutions including a mixture of $Pb(CH_3COO)_2$, $ZrO(CH_3COO)_2$ and $Ti(OC_4H_9)_4$. The composition was chosen to be near the morphotropic phase boundary ($x \approx 0.52$). The solution contained 5 mol% excess Pb in order to account for the loss of Pb during the later thermal treatment.

The substrate was a (100) Si wafer oxidized to 600nm SiO_2. Pt/Ti layers of thickness 80 nm and 15 nm respectively were deposited on the substrate by r.f. sputtering. XRD measurement on the Pt layer confirmed that the Pt was strongly (111) orientated. Another set of substrates used was RuO_x films. Reactive sputtered RuO_x thin films of 220nm were grown on SiO_2/Si substrates. The relative oxygen partial pressure during sputtering was 10%. RBS measurement was conducted to confirm the O/Ru atomic ratio of the as deposited films to be 2.0 (i.e. RuO_2). A filtered 0.5M precursor solution as described above was then applied to the Pt or RuO_2 coated substrates by spin-on coating at 3000 rpm for 30s. The films were then pyrolyzed at several temperatures ranging from 300°C to 600°C in oxygen ambient for 5 minutes in a rapid thermal processor. The above coating and pyrolysis process was repeated a few times in order to obtain a PZT thickness of about 300 nm. Finally the samples were annealed in oxygen at a temperature of 700°C for 10 minutes to crystallize the PZT

films. Top Pt electrodes with $2x10^{-2}$ cm^2 area were deposited by r.f. sputtering through a shadow mask. Another set of samples were also made but with RuO_x coated substrates (RuO_x(200nm)/SiO_2(600nm)/Si). The fabrication conditions were the same as that of the samples with Pt electrodes.

The physical structures of the films were observed using scanning electron microscopy (SEM) and X-ray diffraction (XRD). The X-ray diffractometer used was Philips type PW3710 using Cu target. The polarization vs. electric field was measured using the Sawyer-Tower circuit. The small signal permittivity was extracted from the measured capacitance at 1 kHz on an HP4284A impedance analyzer.

(b) Effect of RuO_x Electrodes: N-type silicon wafers with (100) orientation were chosen as the substrates. Silicon dioxide (SiO_2) was grown by thermal oxidation to a thickness of 600nm on the surface. RuO_x thin films were reactively sputtered by rf-sputtering of ruthenium target in a mixture of Ar and O_2. The relative partial pressure of oxygen to the total gas pressure, $p(O_2)/p(O_2+Ar)$, was varied from 0% to 20%. The film thickness of the bottom electrode was also varied from 80nm to 380nm. Fabrication conditions of the top electrode layers are the same as that of the corresponding bottom electrode layers. Prior to sputtering, the system was pumped down to a base pressure of less than $5x10^{-7}$ Torr. During sputtering, the input power was 150W, the substrate temperature was 350°C and the total pressure was 6mTorr. Post-annealing at 550°C in N_2 for 30 minutes was performed to lower the resistivity of the RuO_x bottom electrodes.

PZT films of 400nm were prepared using the same method mentioned in 3.2(a) above. The film was pyrolyzed at 400°C in oxygen ambient for 5 minutes in a rapid thermal processor and finally annealed in oxygen at a temperature of 700°C for 10

minutes to crystallize it. A top RuO_x electrode with $2x10^{-2}$ cm^2 area was deposited by rf-sputtering through a shadow mask.

The RuO_x film composition was studied with Rutherford Backscattering Spectrometry (RBS). The physical structures of the films were observed using X-ray diffraction (XRD). The polarization vs. electric field was measured using the Sawyer-Tower circuit at 100Hz. The small signal permittivity was extracted from the measured capacitance at 1 kHz on an HP4284A impedance analyzer. All resistivity measurements were performed using the 4-point probe technique.

3.3 Ferroelectric Properties and Pyrolysis Temperature

(a) Effect of Pyrolysis Temperature on PZT Films with Pt Electrodes

(i) Crystallization Behavior of Pt Bottom Electrodes

The resistivity of the platinum film (Pt/Ti/SiO_2/Si substrate) was measured as 30.3 μΩcm (ρ = 10.8μΩcm for bulk platinum). After different thermal treatment (300°C-700°C), there was no considerable change in the resistivity observed. Fig. 3.1 shows the XRD patterns of the as deposited Pt bottom electrodes. Diffraction peak of Pt (111) was observed and showed strong intensity which indicates that the Pt films deposited were completely crystalline.

(ii) Crystallization Behavior of PZT Films Deposited on Pt Electrodes

The orientation of grains in the crystallized PZT films after annealing at 700°C was observed by XRD measurement. In Fig. 3.2 showing the θ-2θ XRD patterns for samples pyrolyzed at different temperatures, no splitting is observed for the (100),(001) peaks or (200),(002) peaks. This is because the splitting of such peaks in tetragonal

PZT films close to the morphotropic phase boundary was too close to be observed after accounting into the broadening effect of the peaks due to small grain sizes [23]. For simplicity the term (100) will be used in this chapter to label the (100,001) group. The XRD pattern in Fig. 3.2 showed that:

(1) At the pyrolysis temperature of 400°C, strong (100) (200) peaks existed without pyrochlore phases. In films pyrolyzed at temperatures of 450°C and above, weak (100) (200) peaks were observed, and in addition to pervoskite phases, diffraction peaks corresponding to pyrochlore phases appeared. This means that pyrochlore phases were formed during the pyrolysis process at higher temperatures and would still remain even after the 700°C annealing for 10 minutes.

(2) For lower pyrolysis temperatures below 400°C, only strong (111) peaks occurred in the pervoskite phase, and no pyrochlore phases were observed. The change of texture at a temperature around 400°C agrees with a previous report [9] investigating the effect of pyrolysis temperatures between 350°C and 450°C with a final annealing at 600°C for 5 minutes.

The change of preferred orientation has been explained from the grain nucleation and growth mechanisms [9]. During the annealing process, the amorphous film first transforms into a metastable nanocrystalline pyrochlore phase. The (111) grains then nucleate from the interface with the (111) Pt substrate, and rapidly grow into the film to replace the pyrochlore phase. This is possible because the interfacial energy of (111) grains with the Pt substrate is lower than that of other orientations. For (100) grains the nucleation rate is substantially lower, but [100] is the energetically favoured growth direction. Therefore columnar (100) grains could only be observed (with the existence of pyrochlore phase) when the growth of (111) grains is suppressed. In Ref. [9] it was

argued that the suppression of (111) grains were due to the incorporation of more oxygen at higher temperatures, which results in the formation of the more stable pyrochlore $Pb_2(Ti,Zr)_2O_{7-x}$ and slows down the transformation from the metastable pyrochlore to pervoskite structures.

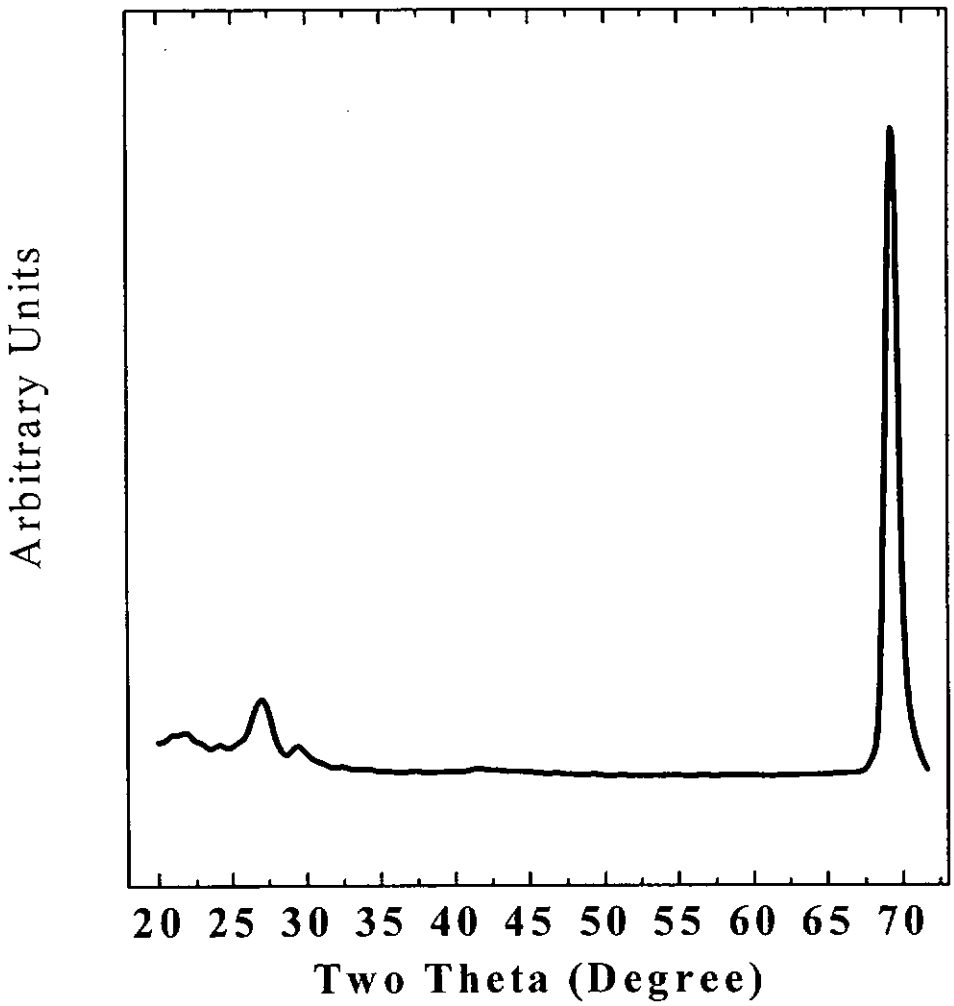

Fig. 3.1 XRD Pattern of Platinum Film Deposited on Ti Coated Substrate

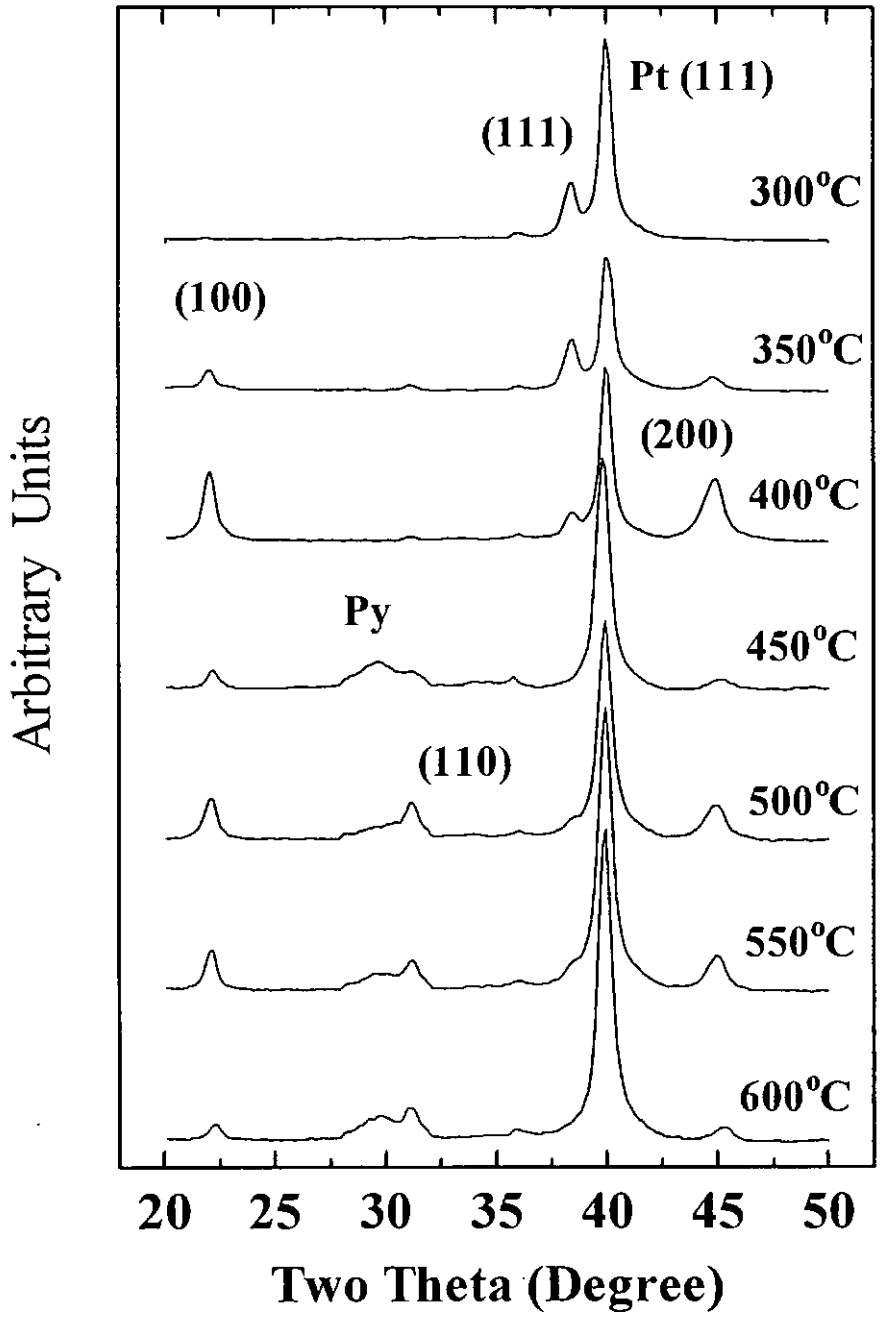

Fig. 3.2 **XRD Pattern of PZT Films Pyrolyzed at Different Temperatures (Pt Electrodes)**
(Py - Pyrochlore Phase)

(iii) Ferroelectric Properties of PZT Films Deposited on Pt Electrodes

The remanent polarization Pr of the PZT films varied considerably between 9 and 34μCcm^{-2} with the pyrolysis temperature (Fig. 3.3). Pr had a maximum value of 34μCcm^{-2} at the pyrolysis temperature of 400°C, and decreased at either lower or higher temperatures. The small signal relative permittivity Kr (Fig. 3.4) had the values between 1000 and 1100 at pyrolysis temperatures between 300°C and 400°C, but dropped significantly to values between 500 to 700 at temperatures at or above 450°C. It was found that our results are not too far away from the previous report [24-25].

SEM micrographs revealed grain structures of size about 0.5-1.0 μm after annealing for samples pyrolyzed at different temperatures (Fig. 3.5). Our results show that both the grain size and the number of pores on film surface seem to increase slightly when the pyrolysis temperature increases. Columnar structures were observed in Fig. 3.5(c) with the cross-sectional view micrograph. It was found that the columnar structures did not change considerably with the pyrolysis temperatures.

Previous reports on the effect of pyrolysis temperature on grain size in PZT films are quite diversified. It has been reported in Ref. [8] that smaller grains of size less than 0.25nm with columnar growth would be obtained if the films were pyrolyzed at 600°C, as compared to the coarse grains with banded domain structures formed in films pyrolyzed at 300°C. However, according to Ref.[9], small columnar grains (0.1-0.2μm) were obtained at 350°C pyrolysis temperature as compared to large columnar (0.5-1.0μm) grains at 420°C. Our results seem to agree more with the trend described in Ref.[9].

L. L. Hench et al. [26] have mentioned from their studies in $BaTiO_3$ that there is a relationship between the size of the crystalline structure and the equilibrium positions

of titanium ions in the polarized state. In ultrafine powders there exists little or no orientational relationship. Likewise, the increase in dielectric constant is much less for ultrafine particles. This shows the interrelationship between the microstructure and the ferroelectric domains. However, the trend of variation in remanent polarization obtained by us did not match with that of the grain size. We cannot attribute the variation in ferroelectric properties of the PZT films to the growth of grains.

PZT thin films with preferred orientations such as (100), (001), (110) and (111) have been demonstrated to have superior properties over randomly oriented films [27]. Much higher polarization as well as dielectric constant was observed in these oriented PZT films. Among the preferred orientations, it is generally believed that near morphotropic phase boundary, the polarization mainly lies in the (111) direction so c-axis PZT films are preferable. (001) oriented PZT thin films on YBCO electrodes can have very high polarization states as reported by Wu et al. [28]. The ferroelectric properties of our films measured above can be explained based on the observed XRD patterns:

(1) The decrease of Pr or Kr for pyrolysis temperatures above 400°C can be attributed to the formation of pyrochlore phase which is non-ferroelectric. Further experiments with longer annealing times showed that the pyrochlore phase could be removed (most likely by conversion into the pervoskite phase) if films pyrolyzed at higher temperatures were finally annealed at 700°C for more than 20 minutes. Measurements also showed that removal of the pyrochlore phase by prolonged annealing resulted in a significant improvement of the remanent polarization.

(2) Fig. 3.2 shows the XRD intensity of PZT films plot against different pyrolysis temperatures. At a pyrolysis temperature of 400°C when the Pr is maximum, the film

has (100) texture without any pyrochlores. For lower pyrolysis temperatures below 400°C, P_r decreases with a corresponding changing of texture from (100) to (111). Since there is no splitting of (100) peak, the observed peak may be caused by a-domains (100 orientation) or c-domains (001 orientation). Because c-domains contribute to the larger value of measured polarization, our data showing a maximum Pr at 400°C implies that the film should consist of dominantly c-domains for the pyrolysis temperature at 400°C. This agrees with the conclusion in a previous report [29] which showed that based on stress measurements the (100) orientated domains in as-prepared PZT samples could be changed to (001) orientation after poling. We found that prolonged annealing time to more than 20 minutes did not alter the change of texture at a pyrolysis temperature of 400°C.

(3) The significant drop in relative permittivity at or above 450°C pyrolysis temperature is due to the presence of pyrochlore phase in the films, similar to the case of the remanent polarization. The permittivity has a highest value at 300°C when the grains in the film are mainly (111) orientated. At 350°C the slight decrease in permittivity corresponds to a similar decrease in the XRD (111) peak intensity. At 400°C the orientation in the film becomes dominantly (100), and the permittivity also increases slightly compared to 350°C. It appears that the permittivity due to (111) grains formed at 300°C pyrolysis temperature is slightly higher than that due to (100) grains at 400°C.

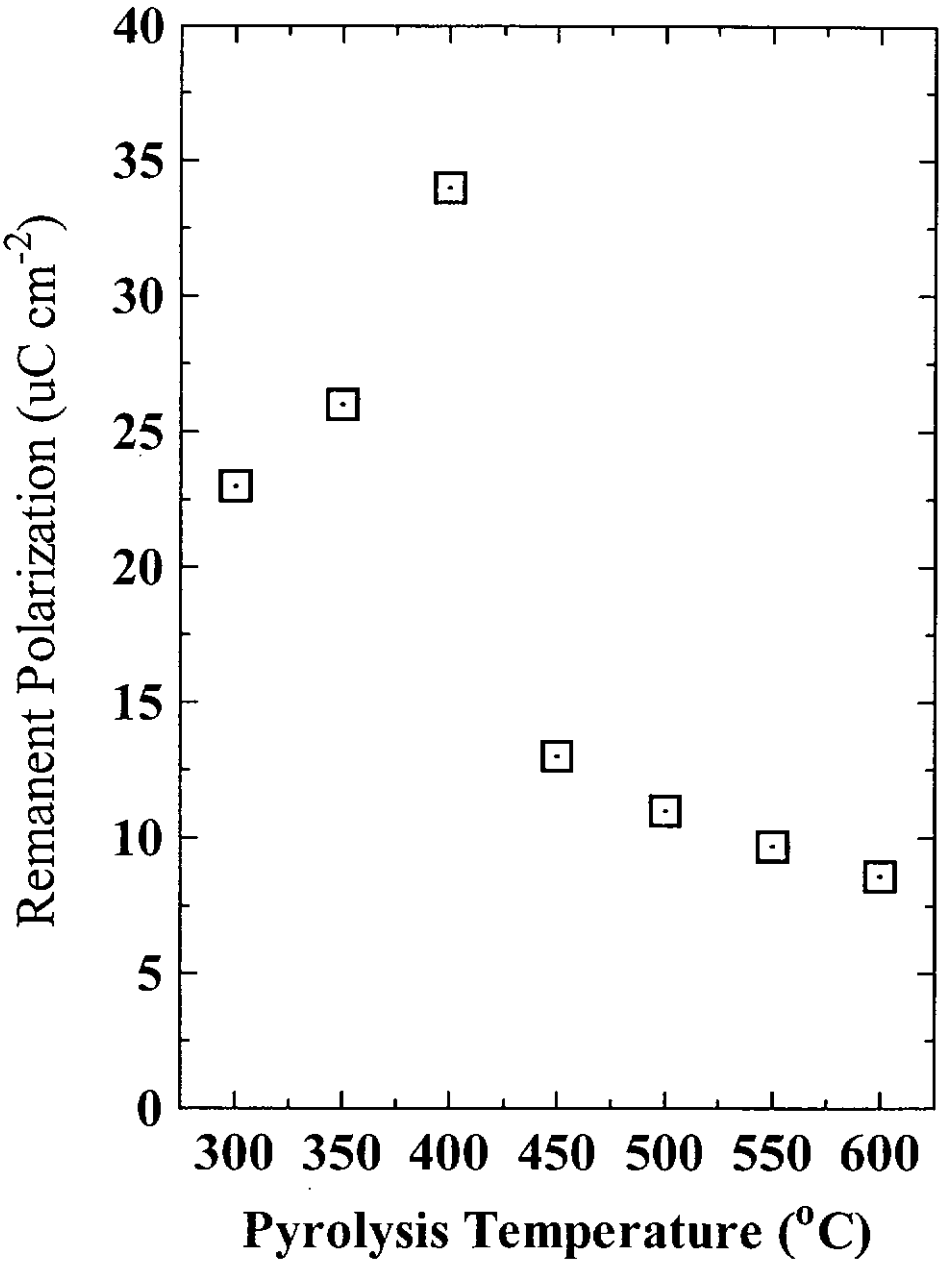

Fig. 3.3 Remanent Polarization of PZT Films Pyrolyzed at Different Temperatures (Pt Electrodes)

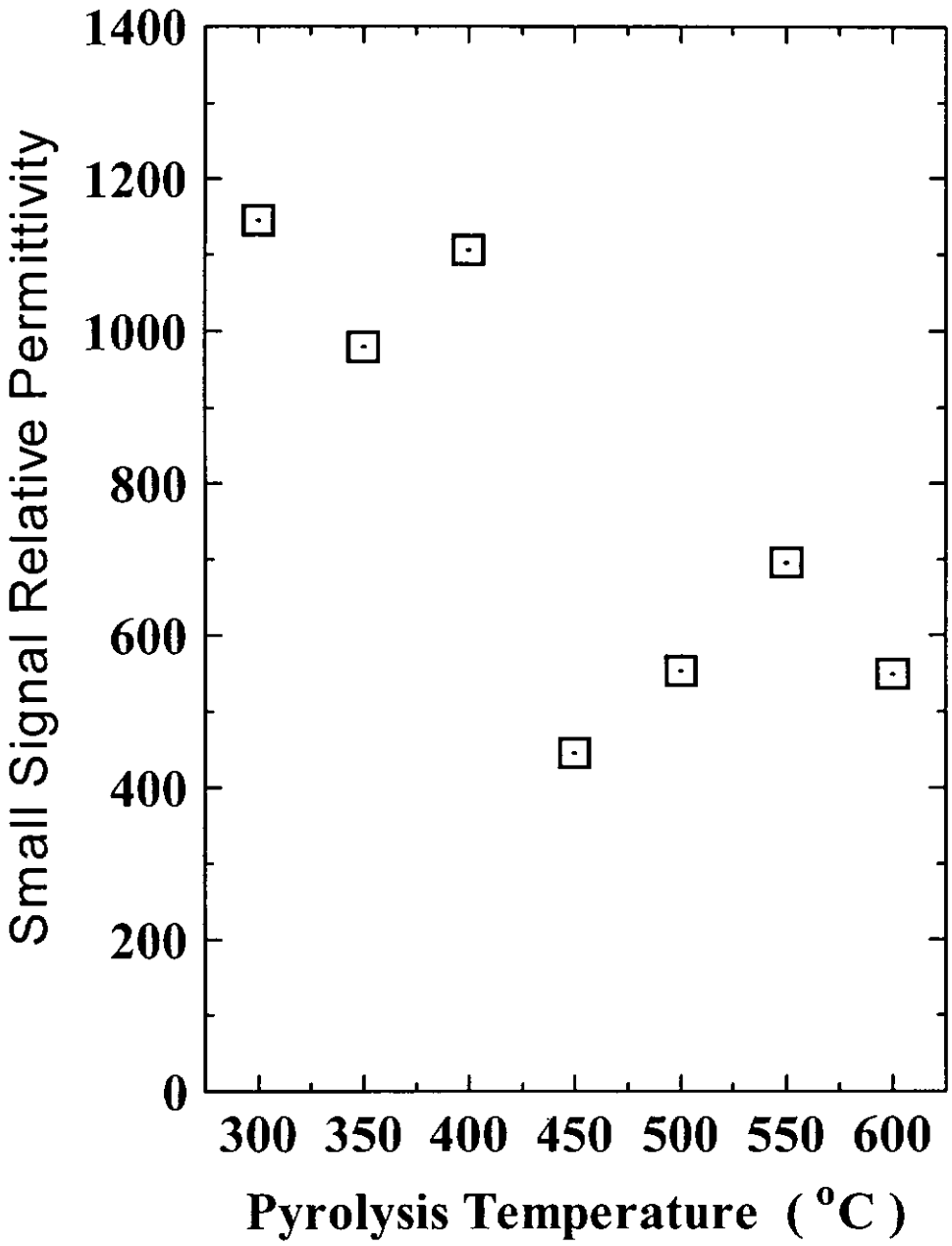

Fig. 3.4 **Small Signal Relative Permittivity of PZT Films Pyrolyzed at Different Temperatures (Pt Electrodes)**

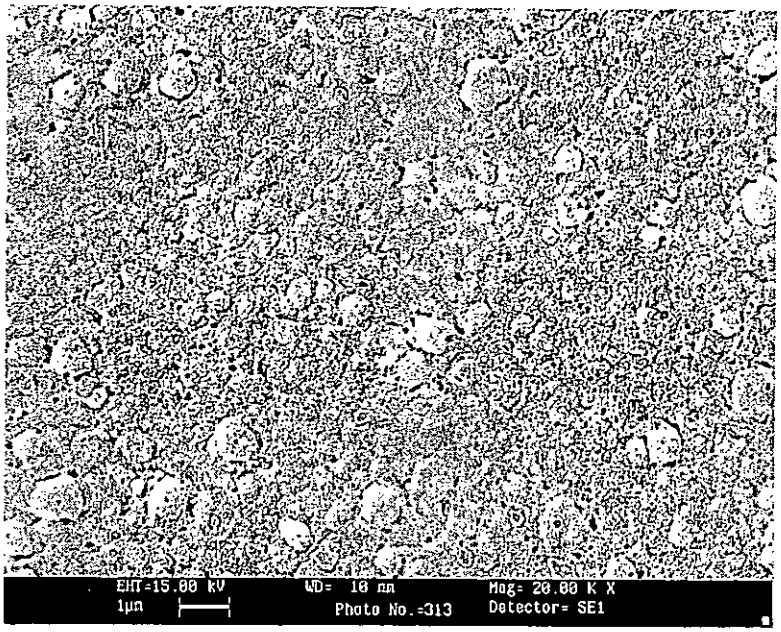

Fig. 3.5(a) SEM Micrograph of Sol-gel PZT Film Pyrolyzed at 400°C for 5 minutes and Annealed at 700°C for 10 minutes (Pt Electrodes)

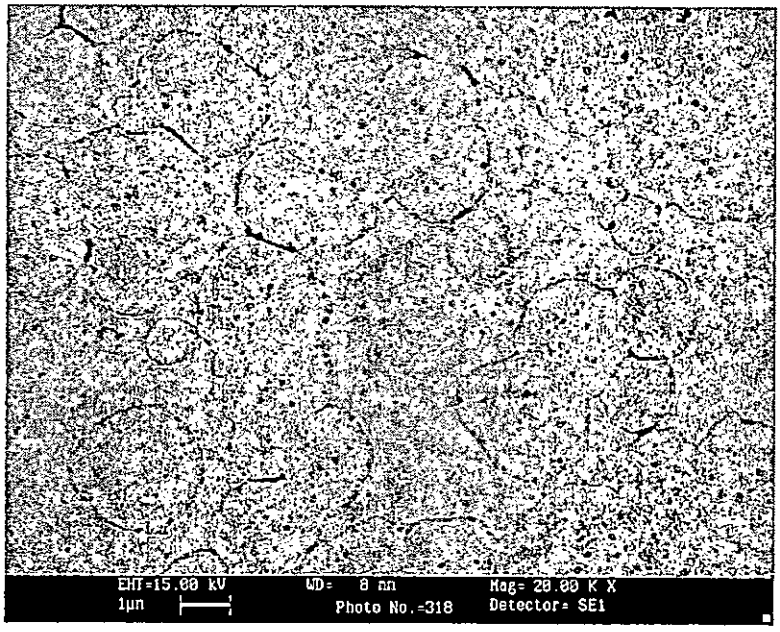

Fig. 3.5(b) SEM Micrograph of Sol-gel PZT Film Pyrolyzed at 600°C for 5 minutes and Annealed at 700°C for 10 minutes (Pt Electrodes)

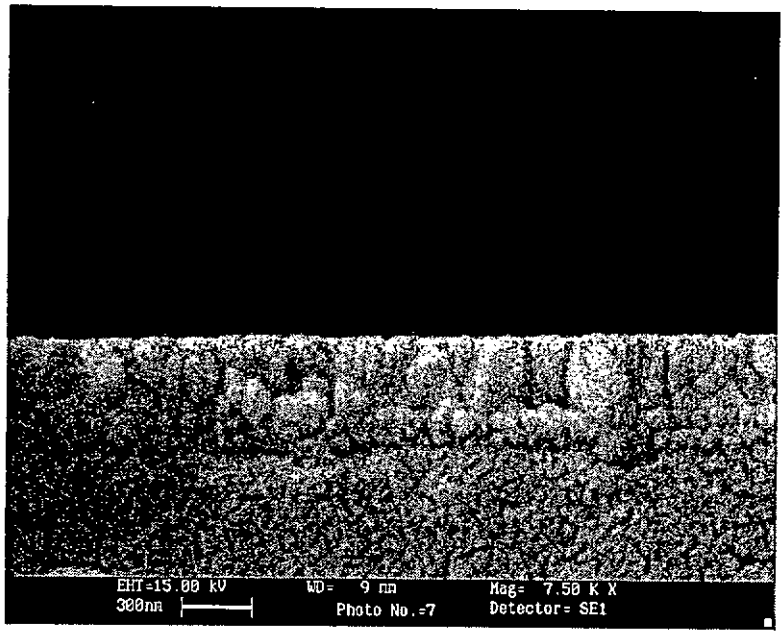

Fig. 3.5(c) SEM Micrograph (Cross-section View) of Sol-gel PZT Film Pyrolyzed at 400°C for 5 minutes and Annealed at 700°C for 10 minutes (Pt Electrodes)

(b) Effect of Pyrolysis Temperature on the PZT Films with RuO_x Electrodes

(i) Characteristics of RuO_x Bottom Electrodes

During the reactive sputtering of ruthenium oxide thin films, the oxygen partial pressure of 10% was applied. According to the corresponding RBS spectra, the structure of the as deposited film is RuO_2 thin film. Fig. 3.6 shows the resistivity of the RuO_2 films after annealing of different temperatures (350°C - 850°C) for 30 minutes in N_2 atmosphere. The resistivity was kept at about 87 μΩcm after 550°C annealing. The XRD pattern (θ-2θ scan) of the RuO_2 thin films was shown in Fig. 3.7. The intensity of the reflection peaks increased slightly after heat treatment. Typically, the RuO_2 films were (101) preferred oriented. Therefore, we can employ 550°C annealing process to lower the resistivity of the bottom electrodes before depositing the PZT layers.

(ii) Crystallization Behavior of PZT Films Deposited on RuO_x Electrodes

With fixed fabrication conditions of the bottom electrodes, the crystallization behavior of the PZT thin films deposited on the RuO_2 electrodes was displayed in Fig. 3.8. With varying pyrolysis temperature from 300°C to 400°C, the XRD patterns of the PZT films seem to have no considerable change. From 450°C to 600°C, the intensity of the reflection peaks obviously dropped, and reflections of pyrochlore phases were observed in the patterns. The PZT films pyrolyzed at any temperature were (110) preferred oriented. We found that the pyrochlore phases still exist in the PZT films after they were pyrolyzed at 450°C or above and annealed at 700°C for 10 minutes. The effect of pyrolysis temperature on these PZT films was not as sensitive as those on the PZT films deposited on Pt coated substrates.

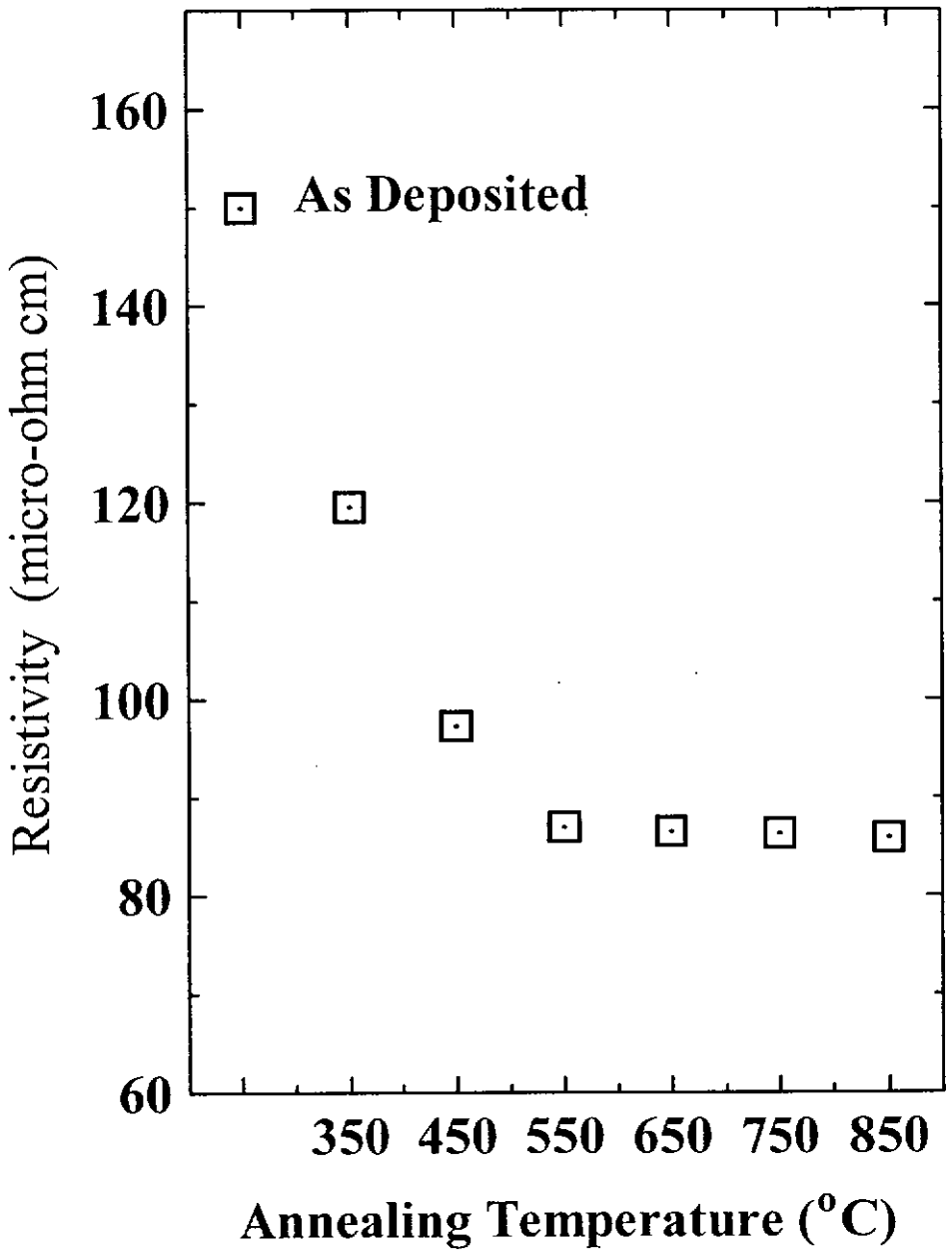

Fig. 3.6 **Resistivity of RuO_x Films with Different Annealing Temperatures**

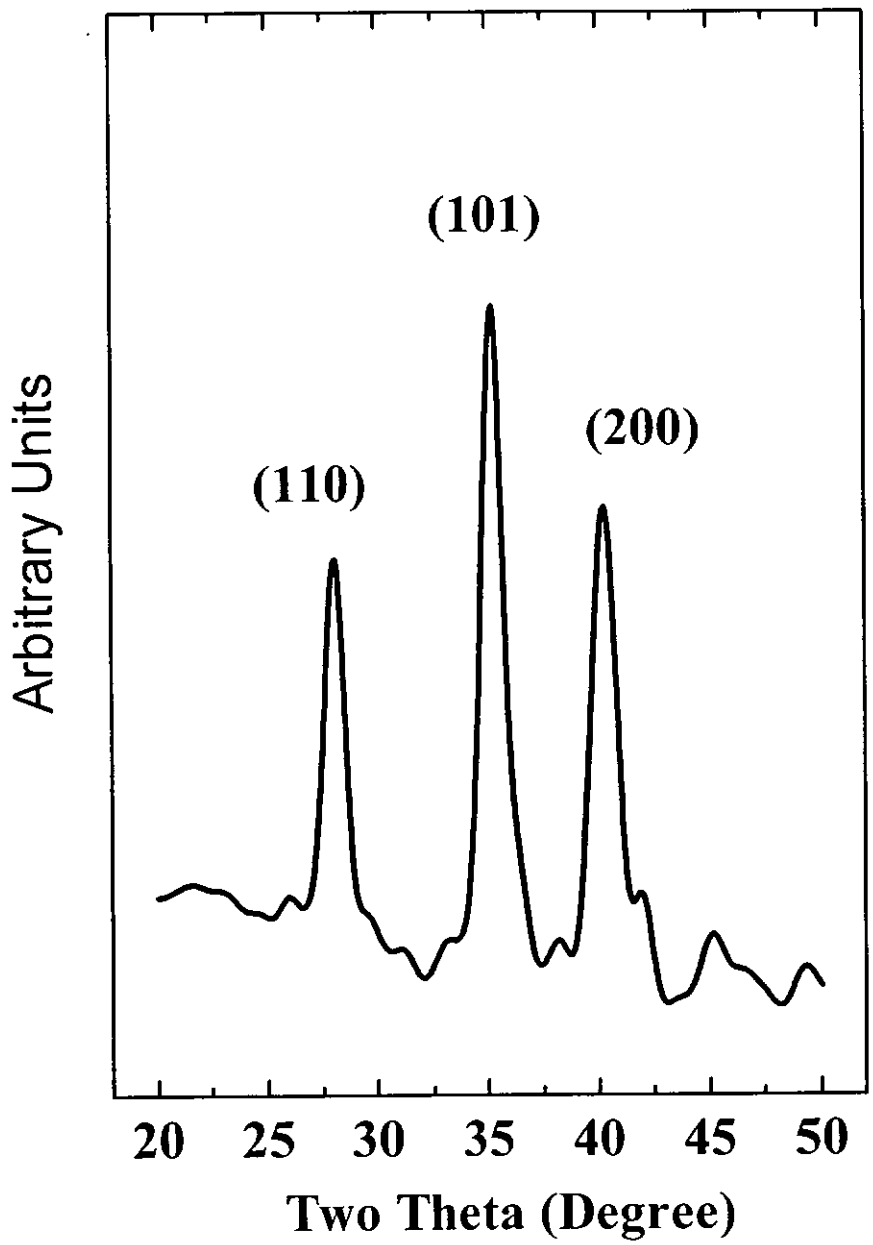

Fig. 3.7 **XRD Pattern of RuO_x Film with 10% Relative Oxygen Partial Pressure**

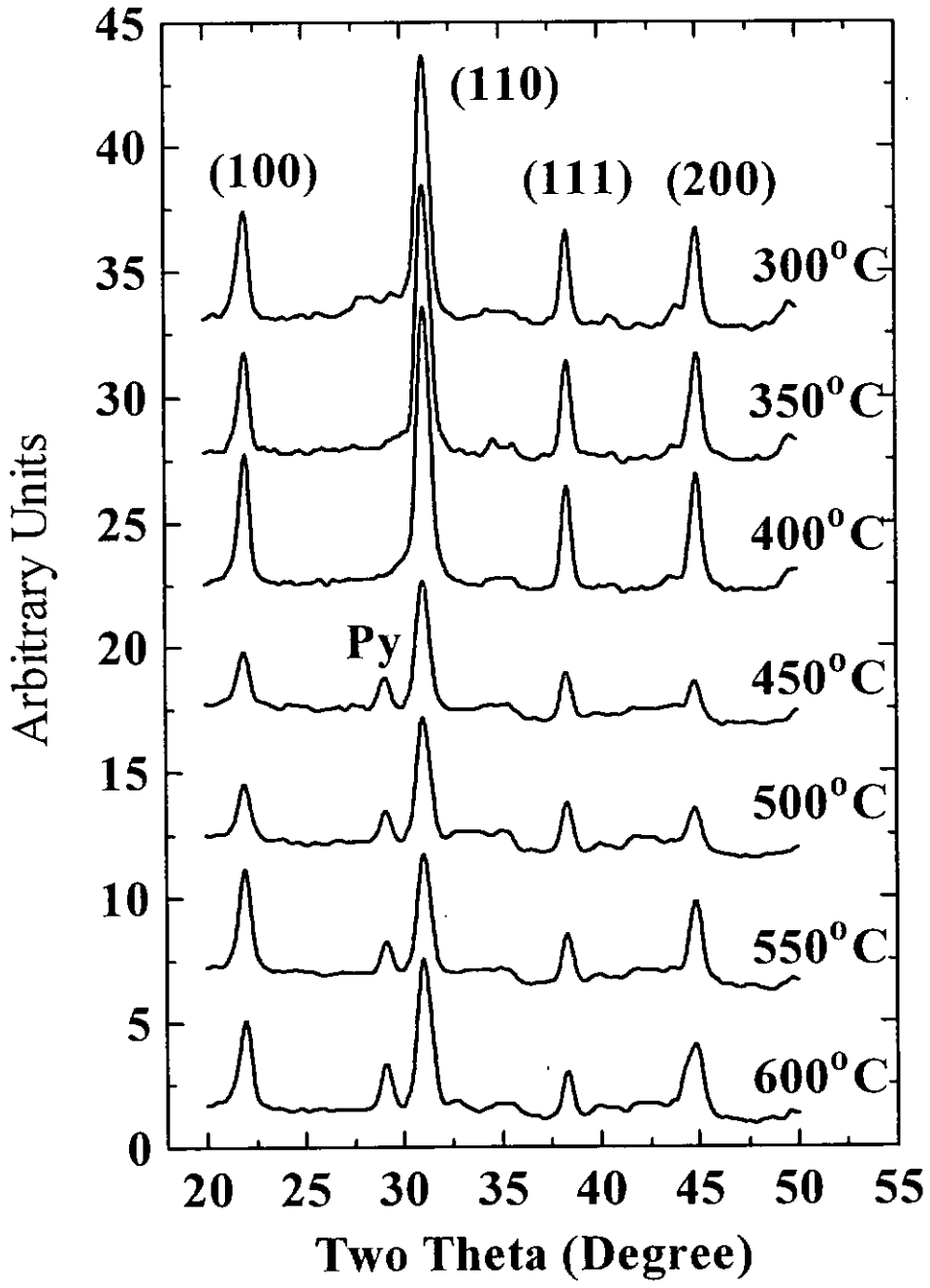

Fig. 3.8 **XRD Pattern of PZT Films Pyrolyzed at Different Temperatures (RuO_x Electrodes) (Py - Pyrochlore Phase)**

(iii) Ferroelectric Properties of PZT Films Deposited on RuO_x Electrodes

The ferroelectric properties (remanent polarization Pr & small signal relative permittivity Kr) of the PZT films deposited on the RuO_2 electrodes were reported in Fig. 3.9 and Fig. 3.10. The RuO_2/PZT/RuO_2 capacitors possessed characteristics different from the Pt/PZT/Pt capacitors. For the pyrolysis temperatures between 300°C and 400°C, the remanent polarization Pr of the PZT films with RuO_2 electrodes was about 23 μCcm^{-2} and the relative permittivity Kr was about 770. Both the Pr and Kr were lower than that of those films with Pt electrodes. The Pr decreased down to 16μCcm^{-2} at the pyrolysis temperature of 450°C and continued to decrease with further increasing the pyrolysis temperature. The relative permittivity of the films dropped to the values between 310 and 480 with further increasing the pyrolysis temperature to above 450°C. Both the remanent polarization Pr and relative permittivity Kr have very slight variations for the pyrolysis temperature between 300°C and 400°C. When the pyrolysis temperature increased to 450°C or above, both Pr and Kr dropped significantly.

If we refer to the XRD patterns in Fig. 3.8, it is believed that the sudden drop in Pr and Kr at the pyrolysis temperature of 450°C or above is due to the existence of pyrochlore phase in the PZT films. In the films pyrolyzed at temperature between 300°C and 400°C, strong (110) peaks existed without any pychlore phases. At the pyrolysis temperature of 450°C or above, weak reflections of pervoskite phases were observed and reflections of pyrochlore phases were also detected. The preferred orientation has not changed for all pyrolysis temperatures. The grain nucleation and growth mechanisms previously discussed were not suitable for describing the PZT grain growth on the RuO_2 coated substrates. We believed that the RuO_2 films would favour the (110) grain nucleation of the PZT films.

Regarding the ferroelectric properties of the PZT films and their texture characteristics, we believed that the decrease of Pr and Kr for pyrolysis temperatures above 400°C was attributed to the formation of non-ferroelectric pyrochlore phases. Again, the pyrochlore phase could be converted into pervoskite phase if the films pyrolyzed at higher temperatures were finally annealed at 700°C for a prolonged period. A factor affecting the Pr and Kr was believed to be the reflection intensity of the pervoskite phase. Comparatively, strong reflections of the pervoskite phase and (110) preferred orientation in the PZT films were obtained when the films were pyrolyzed at the temperartures between 300°C and 400°C.

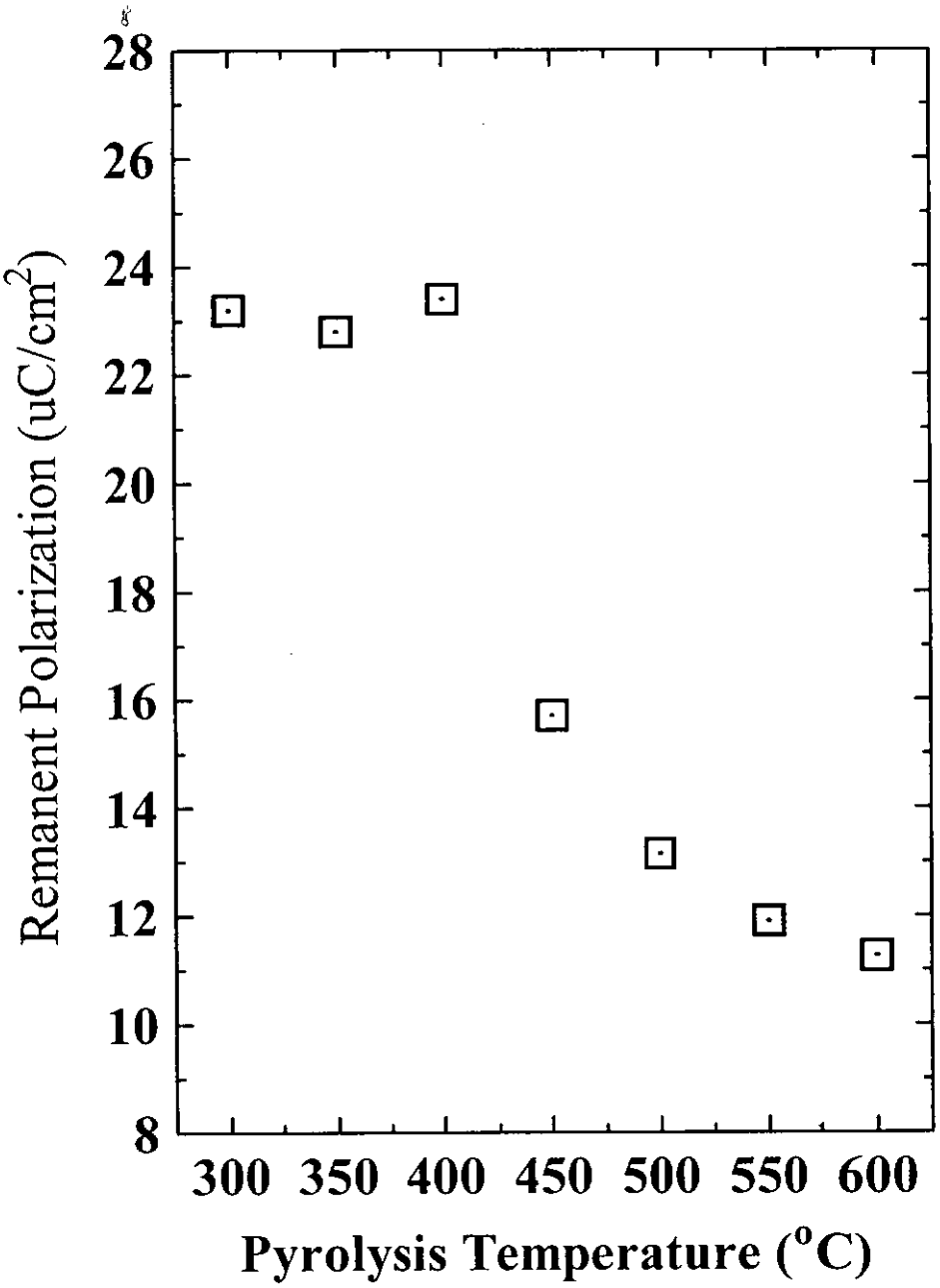

Fig. 3.9 **Remanent Polarization of PZT Films Pyrolyzed at Different Temperatures (RuO_x Electrodes)**

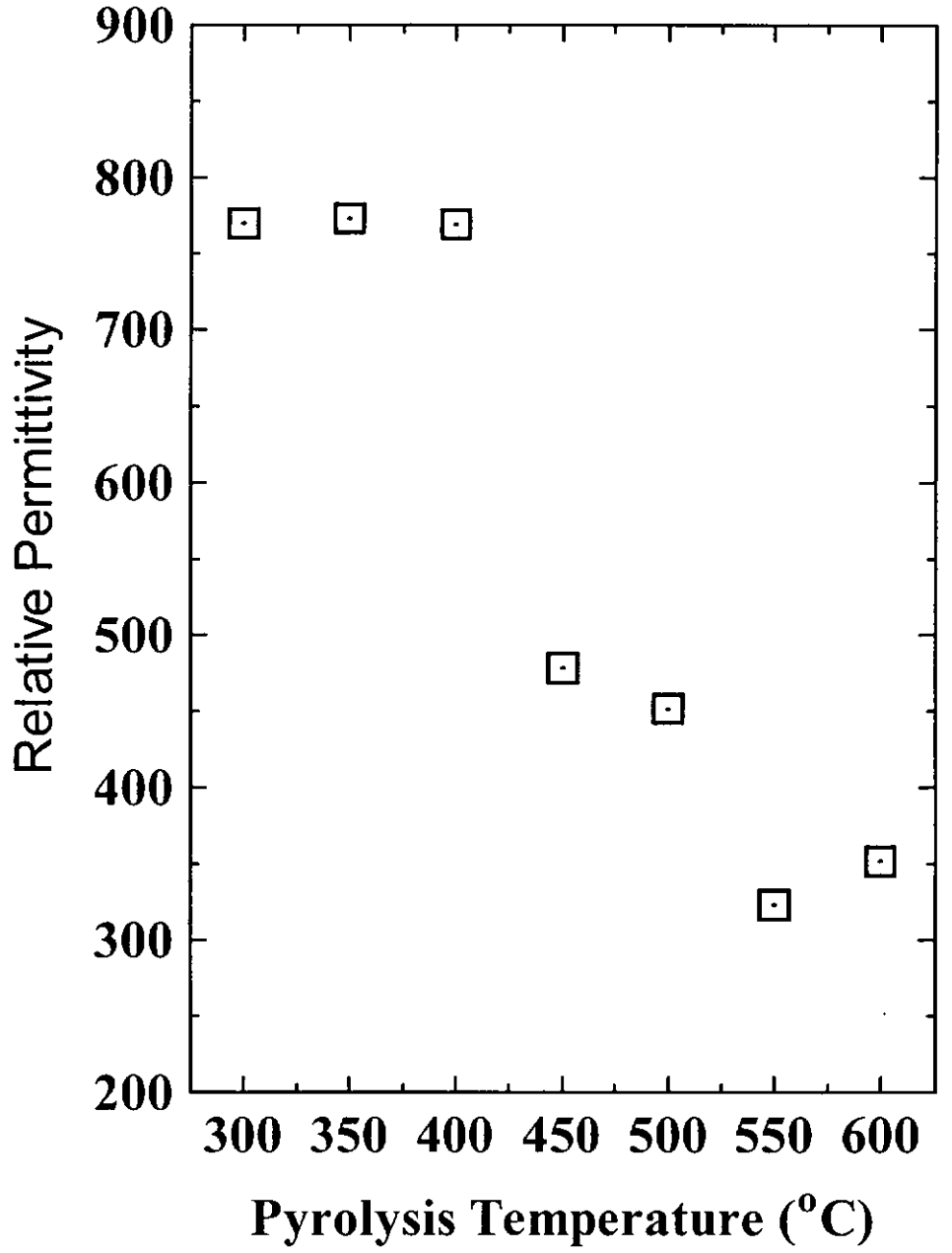

Fig. 3.10 Small Signal Relative Permittivity of PZT Films Pyrolyzed at Different Temperatures (RuO_x Electrodes)

3.4 Ferroelectric Properties and RuO_x Oxygen Content

The oxygen content of the RuO_x electrodes was controlled by the oxygen partial pressure during sputtering. Fig. 3.11 and Fig. 3.12 show the remanent polarization, Pr, and the small signal permittivity, Kr, of the RuO_x/PZT/RuO_x capacitors respectively against different oxygen partial pressure. The maximum Pr, 26μCcm^{-2}, was observed at 10% partial pressure in Fig. 3.11. Pr decreased with increasing or decreasing the partial oxygen pressure from 10%. The dielectric constant decreased from 1520 to 660 when the pressure increased from 0% to 20% (Fig. 3.12).

The remanent polarization of ferroelectric thin film is always affected by their preferred orientation because ferroelectricity varies between different crystallographic directions. PZT thin films with preferred orientations such as (001), (111) and (110) have been demonstrated to have superior properties over randomly oriented films [27]. To understand why Pr in our PZT films is dependent on the oxygen content, it is valuable to look into their XRD patterns.

The XRD θ-2θ scans of PZT thin films (Fig. 3.13) deposited on RuO_x coated substrates show preferred (100) and (110) reflections of perovskite phase. It indicates that the maximum Pr of the PZT thin film at 10% relative oxygen pressure corresponds to the strongest (100) and (110) reflections. The reason for this correlation should be traced back to the texture of the RuO_x films. From the XRD patterns of the RuO_x films in Fig. 3.14, it can be seen that: (1) RuO_x thin films of 10% pressure possessed strong (110) texture; (2) When the pressure was at 0% & 5%, almost no reflections of RuO_2 films was observed and reflections of Ru dominated the patterns. We believe that Ru was dominant in the films when the pressure was below 10%. When the pressure was

increased from 10% to 20%, both the (110) and (101) intensity decreased. This is consistent with the report from J. Lee et al. [21] which stated that (110) RuO_2 grains were preferentially grown in the film deposited at a lower oxygen partial pressure. When the pressure was below 10%, weak reflection of PZT perovskite phase was observed due to the existence of Ru phase. At 10% pressure, the (110) texture of the RuO_x film was the strongest and it favoured the formation of (110) perovskite phase of the PZT films.

The trend of dielectric constant is very different from that of remanent polarization. The dielectric constant decreased continuously with increasing the partial oxygen pressure during sputtering. We guess that the dielectric constant is affected by the presence of an interfacial layer between the PZT and RuO_x electrode. Our data shows that the effective capacitance of the interfacial layer decreases with increasing oxygen content in the electrode.

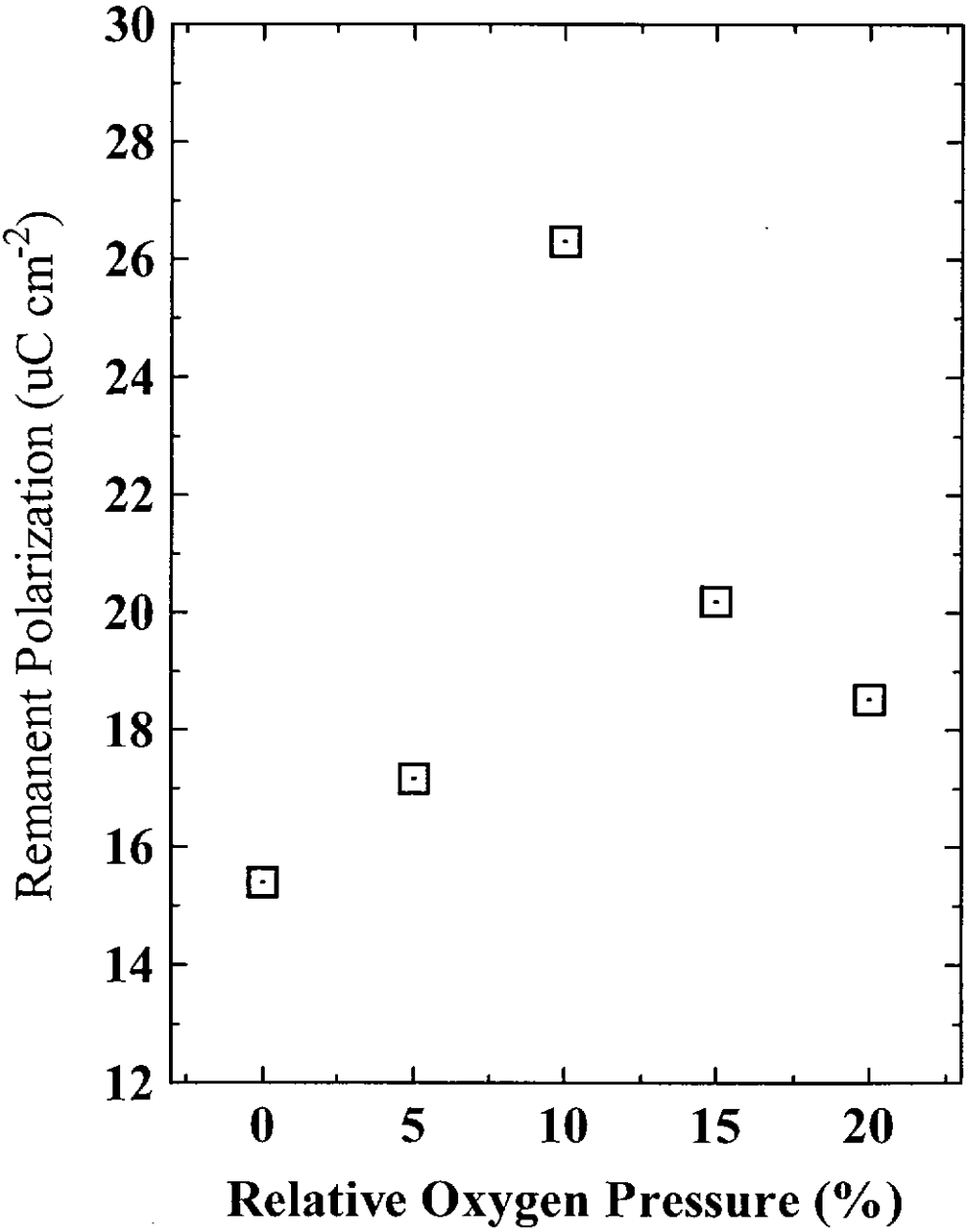

Fig. 3.11 **Variation of Remanent Polarization of PZT Capacitors with Relative Oxygen Partial Pressure for RuO_x Electrodes**

Pao Yue-Kong Library
PolyU • Hong Kong

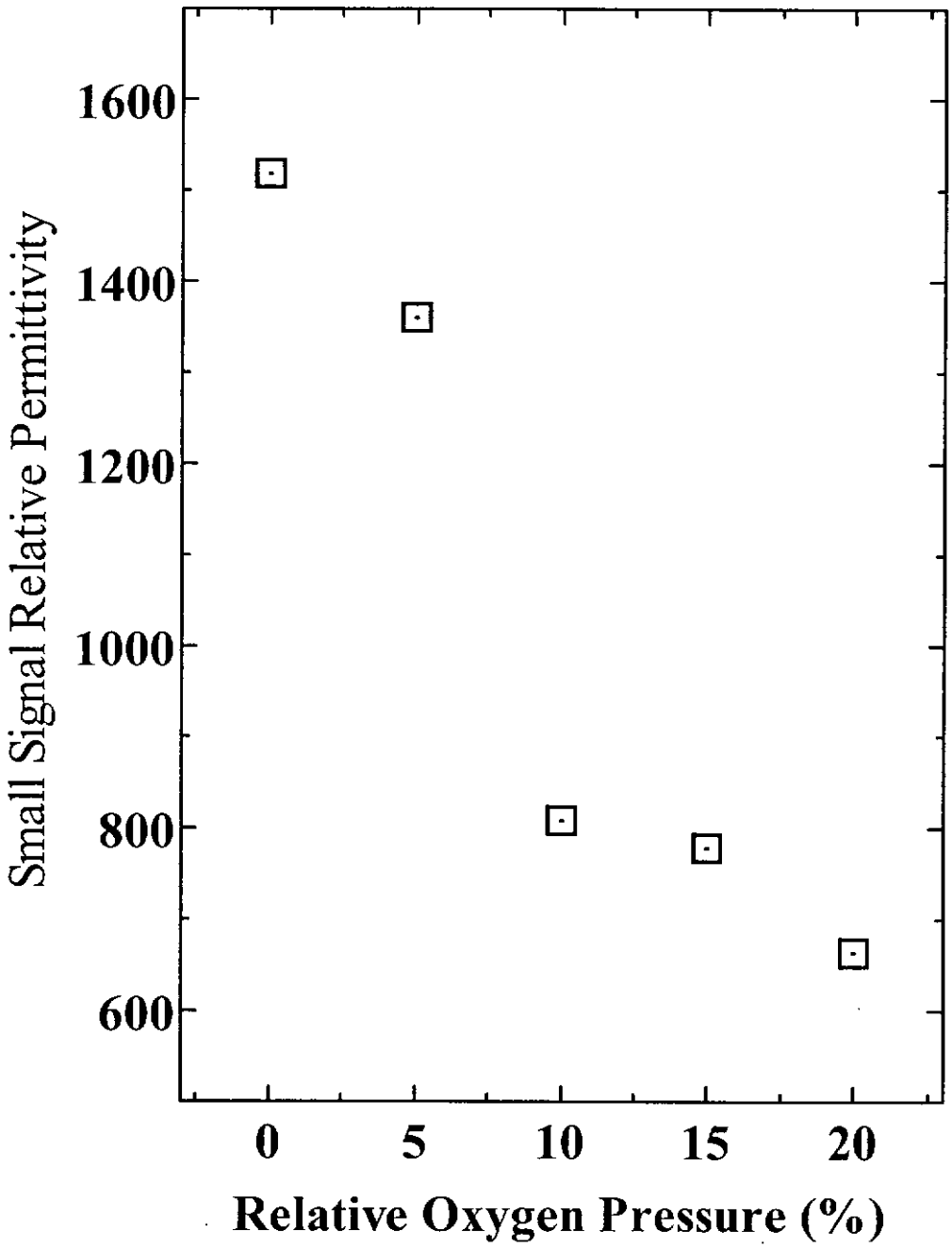

Fig. 12 **Variation of Small Signal Relative Permittivity of PZT Capacitors with Relative Oxygen Partial Pressure for RuO_x Electrodes**

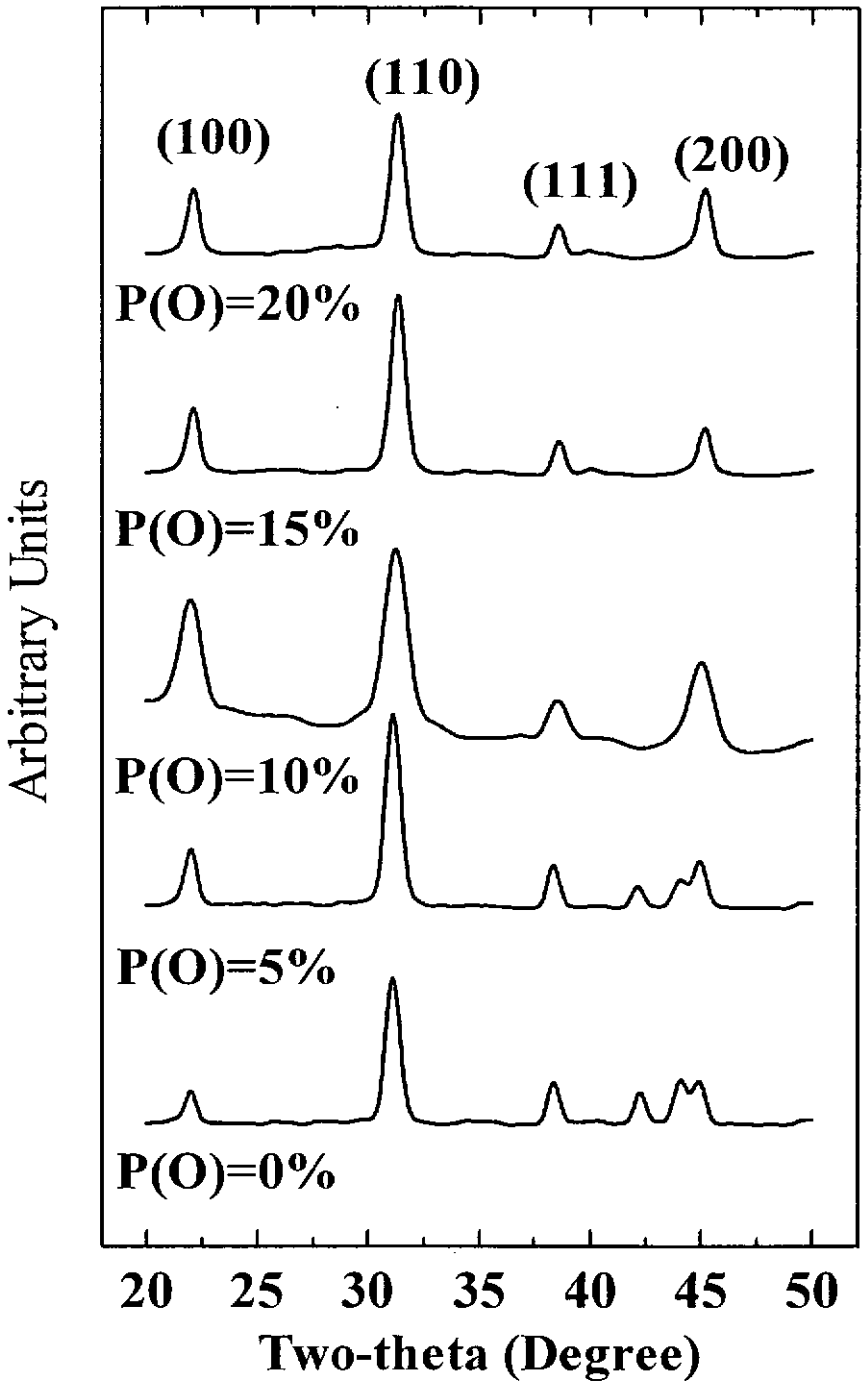

Fig. 3.13 XRD Pattern of PZT Film Deposited on RuO_x Electrodes with Different Relative Oxygen Partial Pressure

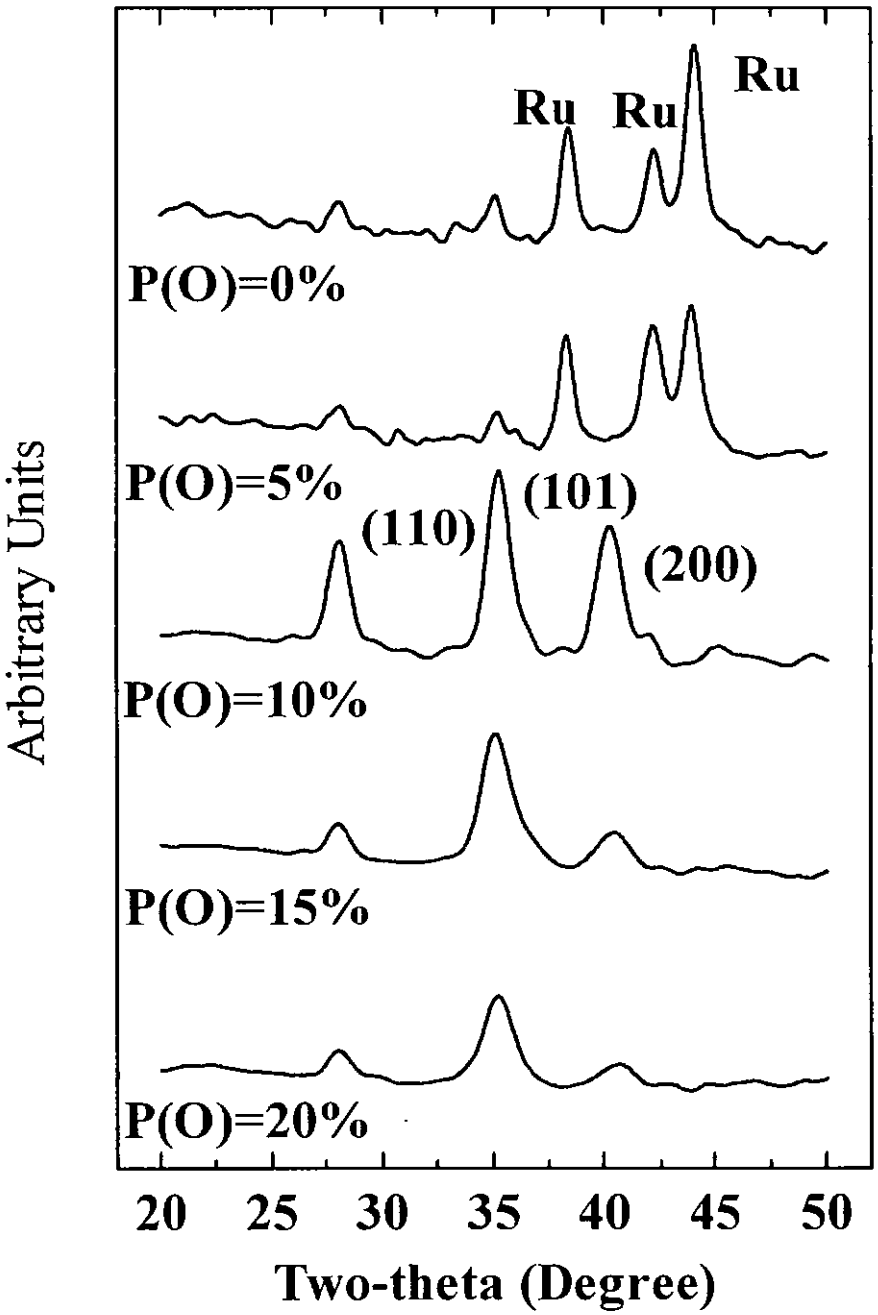

Fig. 3.14 XRD Pattern of Reactive Sputtered RuO_x Film with Different Relative Oxygen Partial Pressure

3.5 Ferroelectric Properties and RuO_x Electrode Thickness

Fig. 3.15 and Fig. 3.16 show the remanent polarization and dielectric constant of the PZT capacitors against different bottom electrode thickness. The relative oxygen sputtering pressure for the RuO_x film was 10%. The thickness was varied from 80nm to 380nm. The two figures show that Pr increased from 9 to 26μCcm^{-2}, whereas Kr increased from 530 to 840 when the electrode thickness was increased from 80nm to 380nm. When the thickness was above 230nm, both Pr and Kr were almost independent of the thickness. Both Pr and Kr dropped considerably when the thickness was decreased from 230nm.

The XRD patterns for PZT thin films deposited on 80nm and 230nm bottom-electrodes are shown in Fig. 3.17. Relative weak reflection peaks of perovskite phase were observed for PZT thin films with 80nm electrode. Therefore, the drop in Pr and Kr in thin electrodes was due to the incomplete perovskite phase in the PZT thin films.

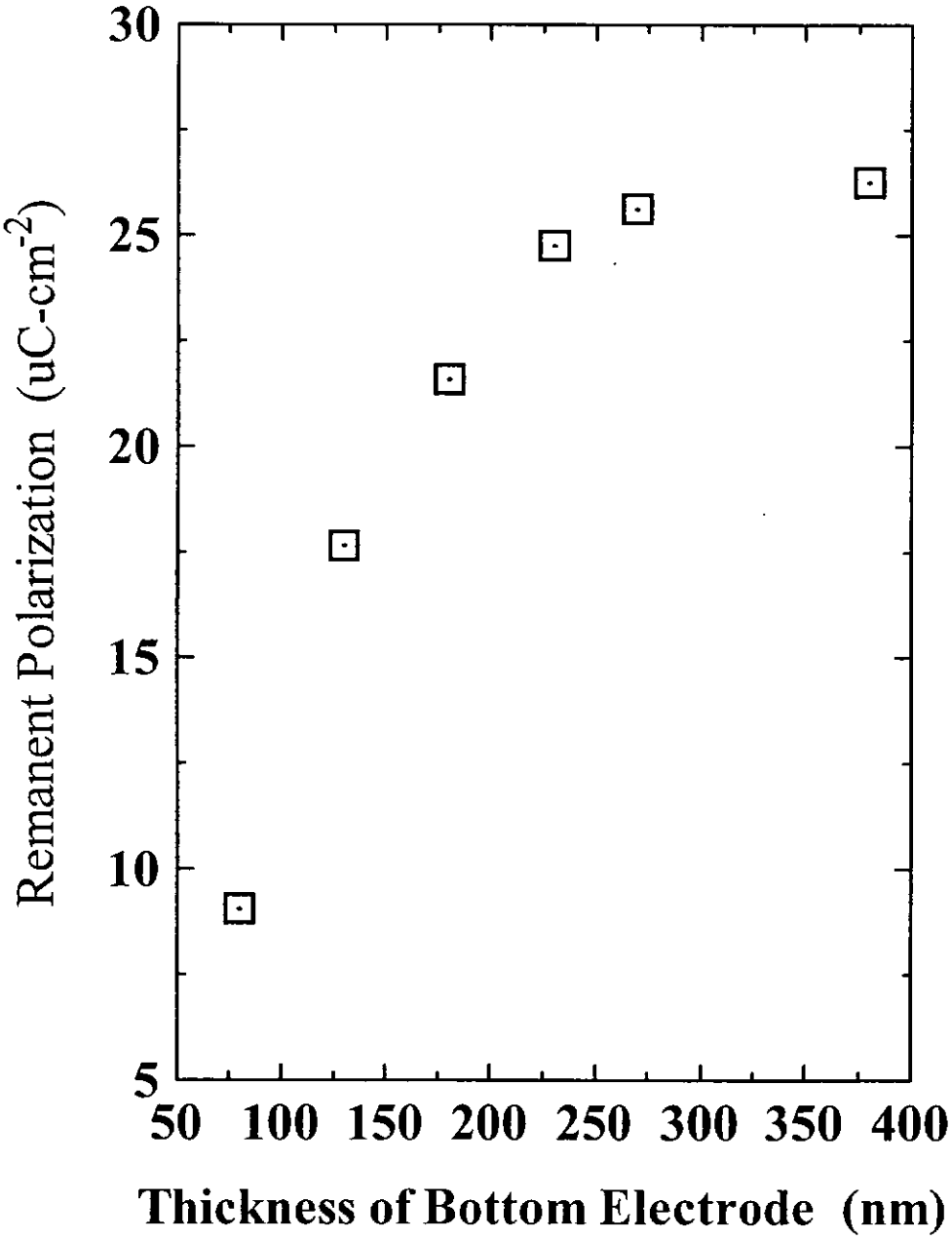

Fig. 3.15 Variation of Remanent Polarization of PZT Capacitors with RuO_x Bottom Electrode Thickness

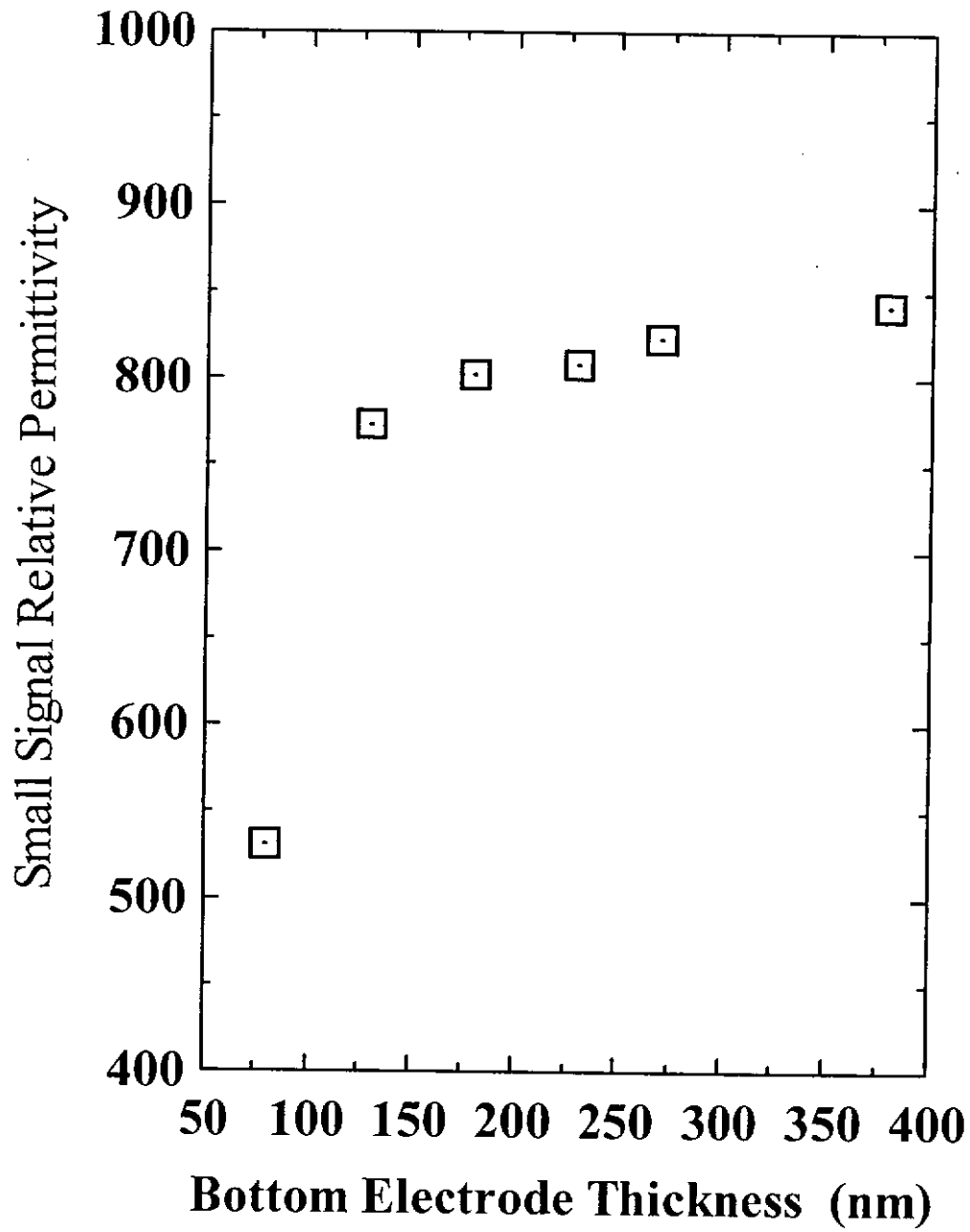

Fig. 3.16 **Variation of Small Signal Relative Permittivity of PZT Capacitors with RuO_x Bottom Electrode Thickness**

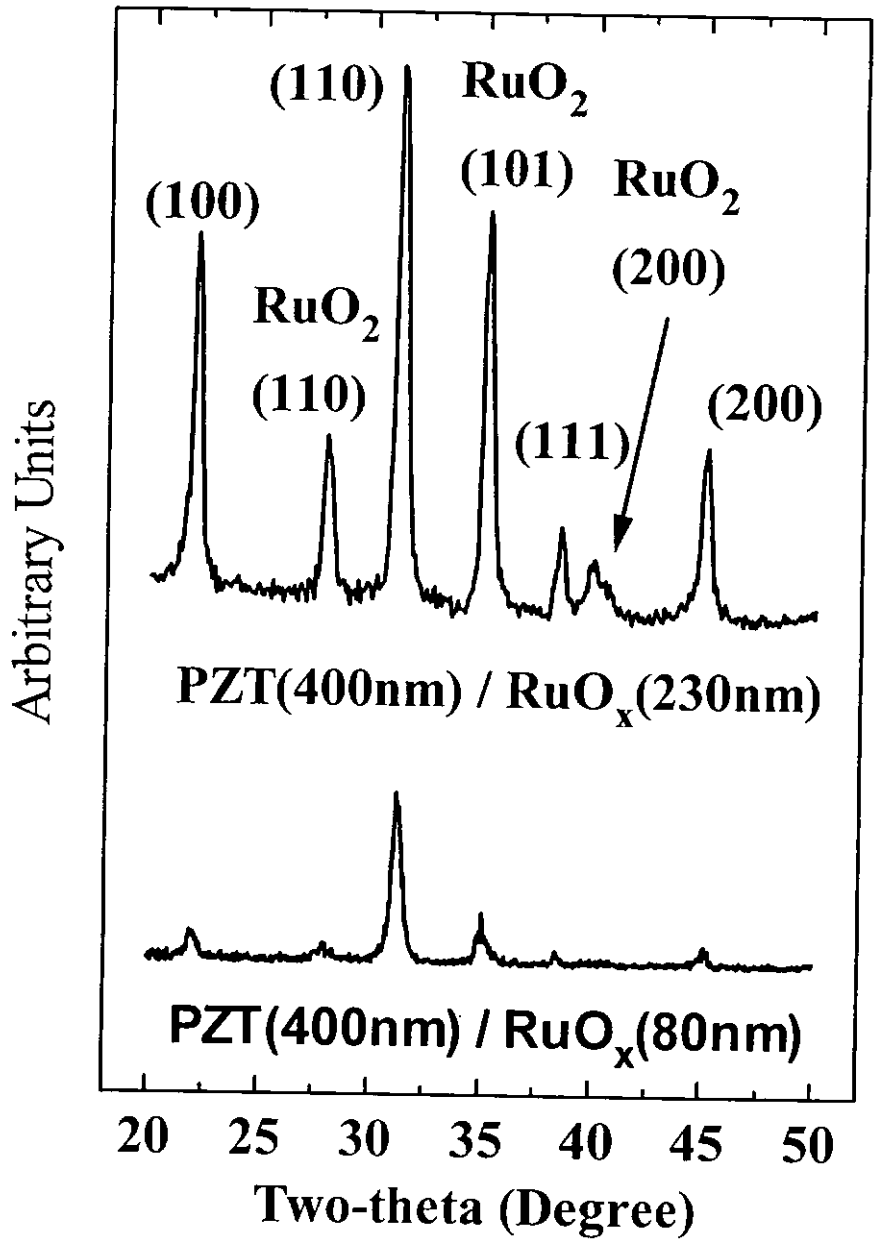

Fig. 3.17 **XRD Pattern of PZT Film Deposited on RuO_x Electrodes with Different Bottom Electrode Thickness**

3.6 Conclusions

In summary, the effect of pyrolysis temperatures between 300-600°C on sol-gel PZT films grown on Pt and RuO_2 coated substrates was investigated under the same final annealing condition (700°C for 10 minutes). SEM showed that the grain size increased slightly with the pyrolysis temperature.

With Pt coated substrates for the PZT films, it was observed that the value of the pyrolysis temperature can affect the nucleation of grains and the preferred orientation. XRD patterns showed that the texture was mainly [111] orientation for pyrolysis temperatures below 400°C, but changed to [100] orientation for pyrolysis temperatures at or above 400°C. As a result, the remanent polarization obtained in the films varies with the pyrolysis temperature, and has a maximum value at a pyrolysis temperature of 400°C under the final annealing temperature of 700°C. With RuO_x electrodes for the PZT films, the pyrolysis temperature can not affect the grain nucleation and preferred orientation. The PZT films grown on the RuO_2 coated substrates were all (110) preferred oriented. The Pr was about 23 μCcm^{-2} at the pyrolysis temperatures between 300°C and 400°C and dropped to about 16 μCcm^{-2} at or above 450°C. Both Pr and Kr degraded when the pyrolysis temperature is above 450°C due to the existence of pyrochlore phases in the PZT films.

For both cases, the samples pyrolyzed in the higher temperature (450°C or above) range always possess pyrochlore phase in the PZT films. If the annealing time was elongated, the value of Pr for films pyrolyzed at higher temperatures could be increased. It was believed that increasing the final annealing time can convert the pyrochlore phase into pervoskite phase and improved the remanent polarization.

However, since a low thermal budget is important for applications of PZT films in VLSI circuits, the use of shorter annealing time is more desirable. With shorter final annealing time, the choice of pyrolysis temperature is important in order to optimize the remanent polarization eventually obtained in the PZT films. In the following studies, we have unified the fabrication conditions of the PZT thin films. The pyrolysis temperature of 400°C for 5 minutes was employed, with 700°C final annealing temperature for 10 minutes in oxygen atmosphere.

Besides, sol-gel PZT thin-film capacitors with reactive sputtered RuO_x electrodes were fabricated. We have investigated the dependence of the ferroelectric properties of sol-gel PZT thin films on the reactive sputtered RuO_x electrodes, including the effects of the electrode oxygen content and the thickness of the bottom electrodes.

Regarding the effect of electrode oxygen content, our results show that the remanent polarization has maximum value at a partial oxygen pressure of 10%. Maximum remanent polarization of 26 μCcm^{-2} was obtained when the relative oxygen pressure was at 10% during sputtering. However, the maximum dielectric constant was found in capacitors with Ru only electrodes.

We would further discuss the issue of oxygen deficiency in the thin electrodes in Chapter 4, where we showed that the effect of electrode thickness is attributed to the oxygen diffusion in the bottom electrode layers based on AES measurement. The above results provide useful information for the RuO_x sputtering process in order to optimize the ferroelectric properties of the PZT films.

Chapter FOUR

Fatigue Properties

4.1 Introduction

In the ferroelectric thin film technology, recently highly conductive electro-ceramics such as ruthenium dioxide (RuO_2) have aroused great interest due to the excellent fatigue properties of the ferroelectric films on these electrodes [5-6]. RuO_2 is one of the most stable conductive oxides and has a bulk resistivity of 46 μΩ-cm [4,7-8]. Excellent etching of RuO_2 films using conventional dry etching techniques has been demonstrated, and the application of RuO_2 films as the electrodes of PZT ferroelectric thin-film capacitors has been actively investigated [9-10].

Although there are some studies on the properties of reactive sputtered RuO_2 thin films, in-depth investigation of RuO_x/PZT/RuO_x capacitors is still needed [11-13]. In particular, the optimization of RuO_x sputtering process to obtain the most desirable ferroelectric and fatigue properties is of great practical interest. In Chapter 3, we have reported the ferroelectric properties of the RuO_x/PZT/RuO_x capacitors with different oxygen content and bottom electrode thickness. In this chapter we shall report the study on the effect of oxygen content and thickness of the RuO_x electrodes on the fatigue properties of the PZT thin film capacitors. We shall show that the fatigue property of our capacitors is consistent with the oxygen vacancy fatigue model. We would also

reveal that the fatigue properties of the PZT capacitors would be degraded when their bottom electrode thickness is too small.

4.2 Experiment

RuO_x thin film substrates were prepared using the method described in Chapter 3. The relative partial pressure of oxygen to the total gas pressure, $p(O_2)/p(O_2+Ar)$, was varied from 0% to 40%. The film thickness of the bottom electrode was also varied from 80nm to 380nm. Fabrication conditions of the top electrode layers are the same as that of the corresponding bottom electrode layers. Prior to sputtering, the system was pumped down to a base pressure of less than $5x10^{-7}$Torr. During sputtering, the input power was 150W, the substrate temperature was 350°C and the total pressure was 6mTorr. Post-annealing at 550°C in N_2 for 30 minutes was performed to lower the resistivity of the RuO_x bottom electrodes.

PZT films of 400 nm were prepared using the same method mentioned in Chapter 3. The film was pyrolyzed at 400°C in oxygen ambient for 5 minutes in a rapid thermal processor. The above coating and pyrolysis process was repeated a few times in order to obtain a PZT thickness of about 400 nm. Finally the PZT film was annealed in oxygen at a temperature of 700°C for 10 minutes to crystallize it. A top RuO_x electrode with $2x10^{-2}$ cm^2 area was deposited by rf-sputtering through a shadow mask.

The RuO_x film composition was studied with Rutherford Backscattering Spectrometry (RBS). The physical structures of the films were observed using scanning electron microscopy (SEM) and X-ray diffraction (XRD). The interdiffusion phenomena at the PZT-RuO_x and RuO_x-SiO_2 interface were investigated by Auger

Electron Spectroscopy (AES). The polarization vs. electric field was measured using the modified Sawyer-Tower circuit at 100Hz. The fatigue tests were performed using a triangular wave voltage with amplitude of 5V and a frequency of 1MHz. The small signal permittivity was extracted from the measured capacitance at 1 kHz on an HP4284A impedance analyzer.

4.3 Properties of the RuO_x Bottom Electrodes

The oxygen composition of the as-deposited RuO_x films determined from their RBS spectra and the corresponding resistivity measured using the 4-point probe technique were shown in Fig. 4.1. The O/Ru atomic ratio, x, increased from 0 to 2.2 with increasing the relative oxygen pressure from 0% to 20%. The value of x was kept at 2.2 with further increasing the relative oxygen pressure above 20%. This indicates that sufficient oxidation of ruthenium takes place at the partial pressure of 20%. The trend of the film resistivity agrees with that of the atomic ratio, and suggests that the resistivity is strongly affected by the amount of excess oxygen incorporated in the films.

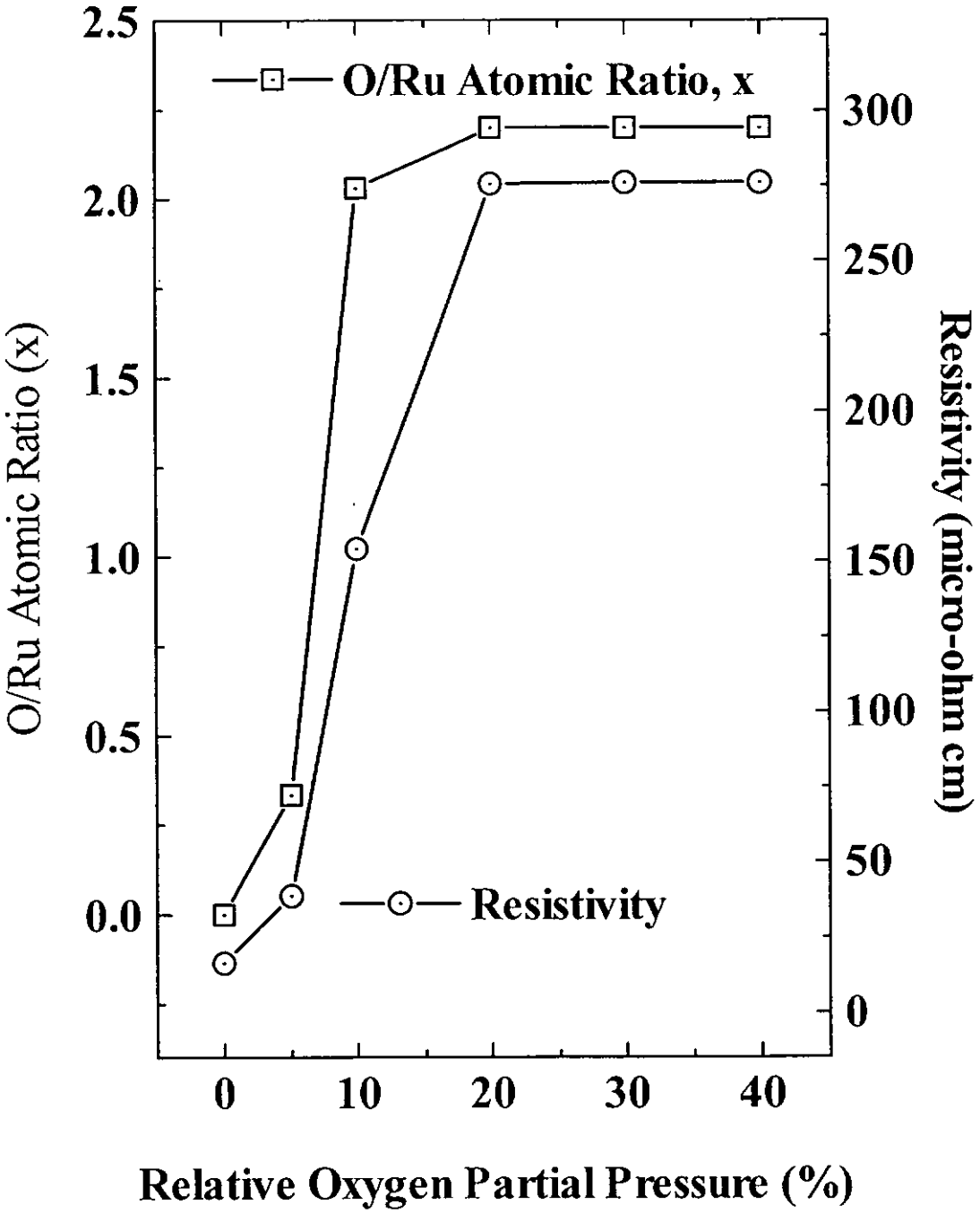

Fig. 4.1 **Variations of Oxygen Composition and Resistivity in the As-deposited RuO_x Films with Relative Oxygen Partial Pressure**

4.4 Fatigue Properties of PZT Thin Film Capacitors with Pt and RuO_2 Electrodes

The fatigue curves of typical Pt/PZT/Pt and RuO_2/PZT/RuO_2 capacitors were shown in Fig. 4.2. Almost fatigue-free capacitors were obtained when the RuO_2 electrodes were employed. These capacitors show no fatigue up to nearly 10^9 cycles whereas the Pt/PZT/Pt capacitors have 20% reduction in remanent polarization after 10^9 cycles. These results imply that the fatigue behavior depends on the electrode type and using RuO_2 electrodes alleviates the fatigue problem of PZT capacitors. Our results are consistent with reports in Ref. [5] and [6].

4.5 Effect of Oxygen Content of RuO_x Bottom Electrodes

It was observed from Fig. 4.3 that the number of fatigue free cycles increased when the relative oxygen pressure of the RuO_x electrodes increased. Quantitatively, the PZT capacitors were almost fatigue free up to 10^{11} switching cycles when the pressure was at 20%. Besides, the reduction in Pr decreased with increasing the pressure. The largest Pr reduction, 20%, after 10^{11} switching cycles, was obtained at 0% pressure whereas only 3% reduction was obtained at 20% pressure. The fatigue property, in other words, was improved by increasing the oxygen content of the electrodes.

There are several types of fatigue mechanism described by different research groups [19-23]. Our result is consistent with the oxygen-vacancy fatigue mechanism [14-15]. It suggested that fatigue behavior in ferroelectric thin films is due to the existence of trapped oxygen vacancies at or near the electrode interfaces, which results in the suppression of further domain switching. This postulate has been testified in many

reports by replacing Pt electrodes of the ferroelectric capacitors with RuO_2 or other conductive oxide electrodes [3,5,9,16]. Fig. 4.4 shows a model for the behavior of oxygen vacancies during the fatigue [18]. Oxygen vacancies are uniformly distributed in the film in the initial state. During the fatigue process, positively charged oxygen vacancies move only in any one direction. Therefore the oxygen vacancies were trapped at the electrode/film interface. Because of the oxygen vacancy layer, the total applied voltage is divided into two parts, V_i and V_B. Since V_B is smaller than the external applied voltage for increasing numbers of switching cycles, the measured polarization must decrease. Also, the newly created C_i is connected to C_B in series; thus, the total capacitance is smaller than that of the bulk. The final conclusion is that conductive oxide electrodes can provide oxygen to fill up the oxygen vacancies of the ferroelectric thin films. As the amount of oxygen vacancy decreases, the domains will continue to switch without suppression and hence the fatigue properties can be improved. Our result shows that electrodes with lower oxygen content resulted in poor fatigue properties of the capacitors. We believe that lower oxygen content in the electrodes provides less amount of oxygen to fill up the vacancies.

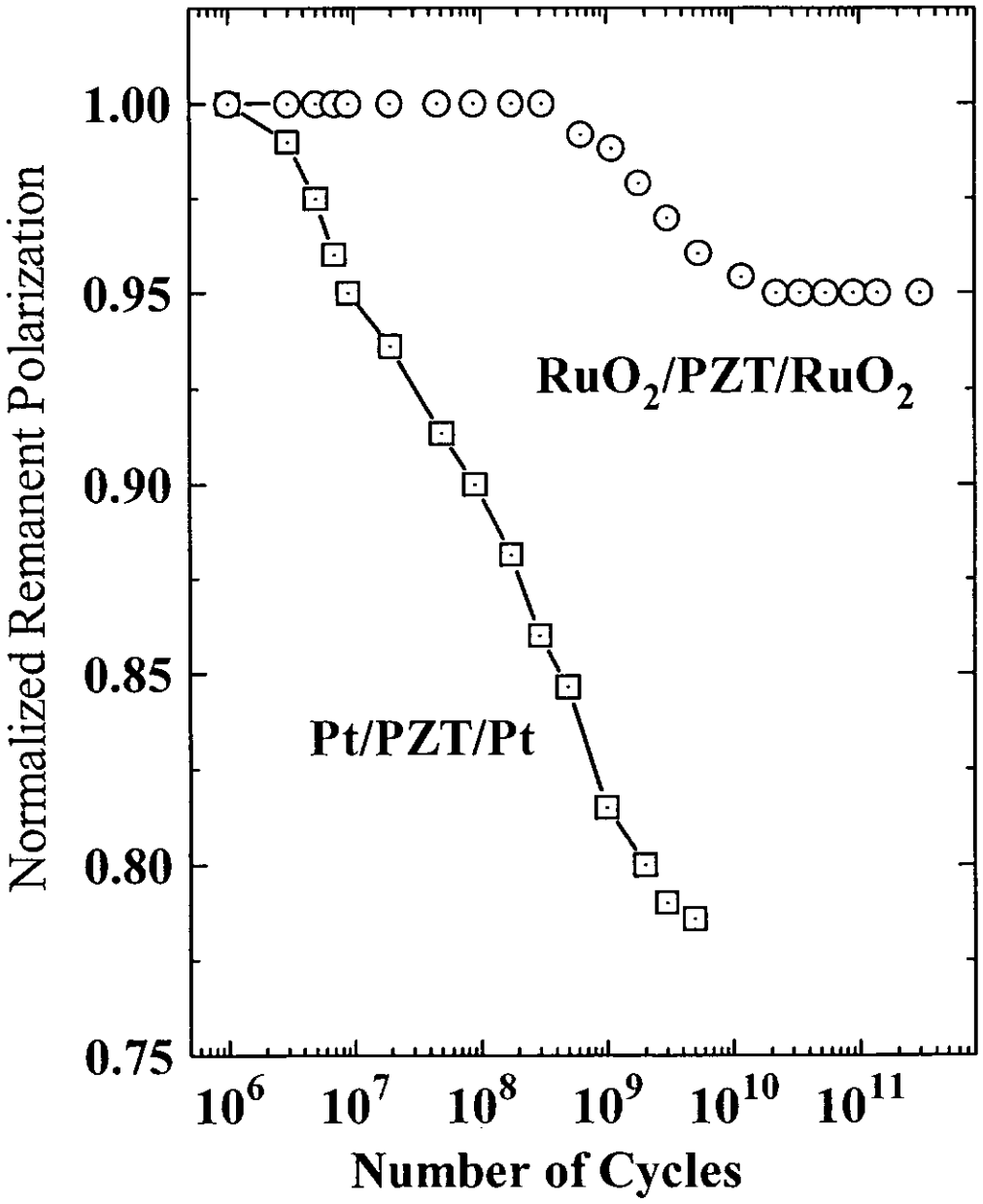

Fig. 4.2 **Fatigue Curves of Pt/PZT/Pt and RuO_2/PZT/RuO_2 Capacitors**

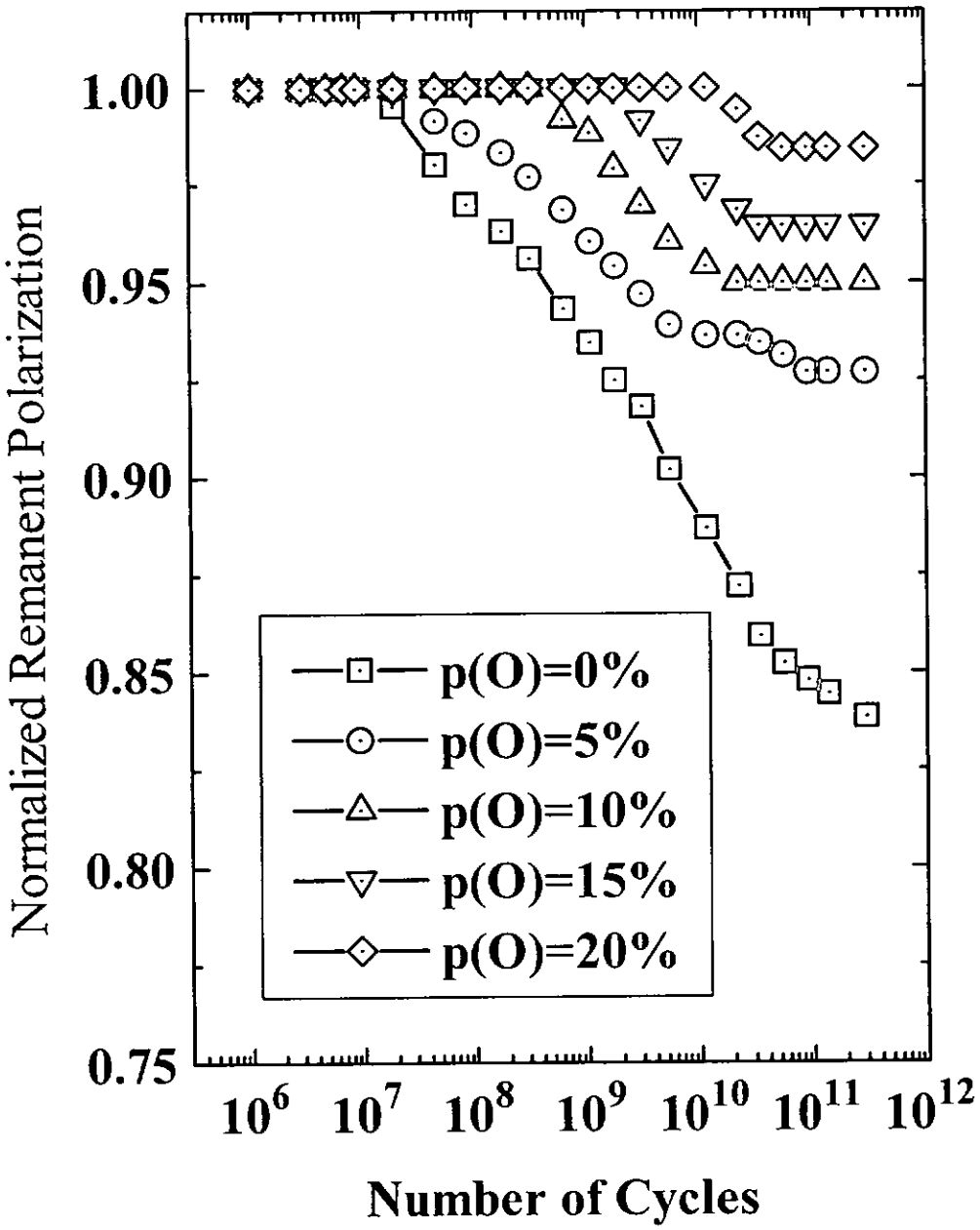

Fig. 4.3 **Fatigue Curves of RuO_x/PZT/RuO_x Capacitors with Different Relative Oxygen Partial Pressure for the RuO_x Electrodes**

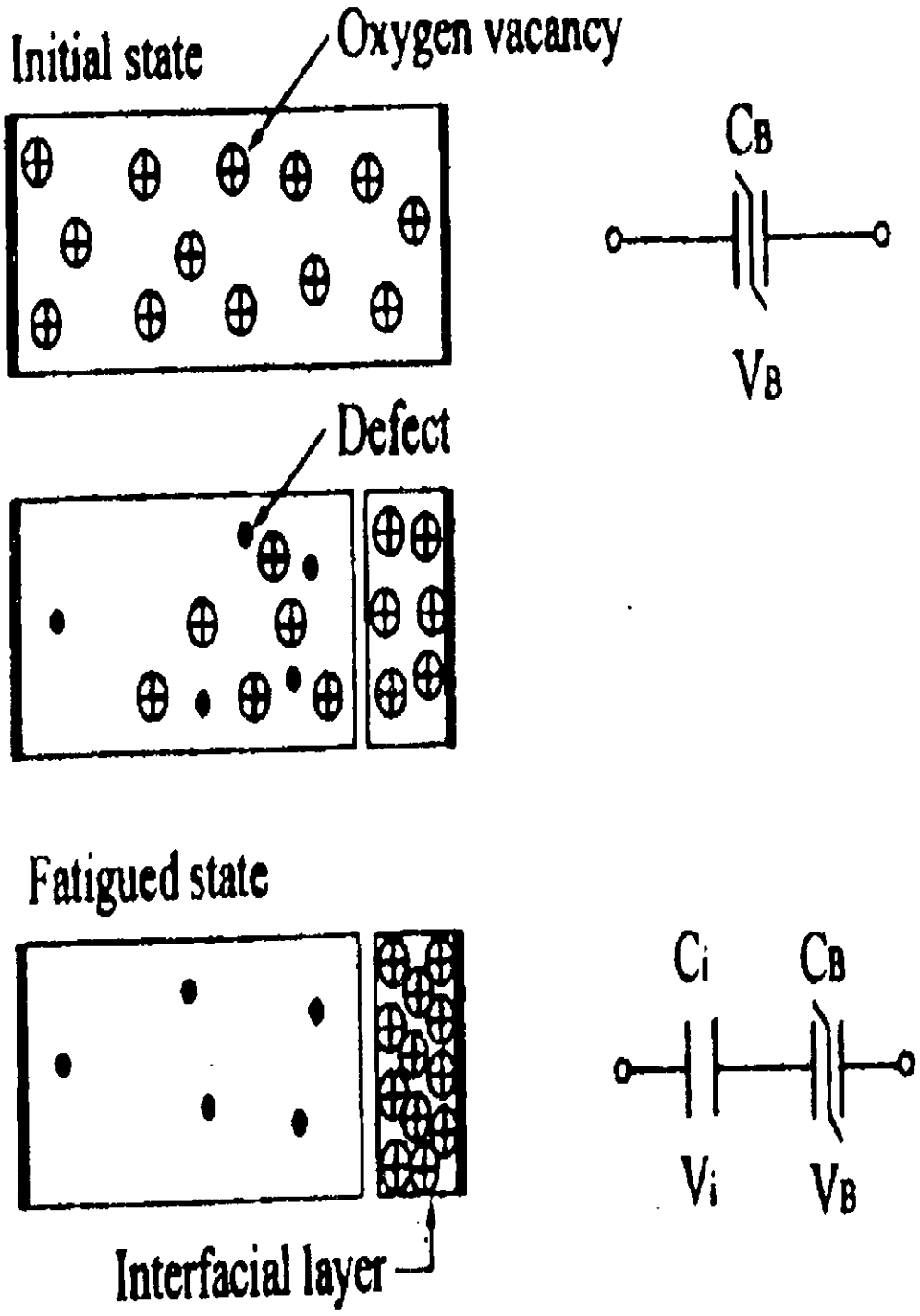

Fig. 4.4 **Modeling of the Oxygen Vacancies Behavior in the Fatigue Process [18]**

4.6 Effect of RuO_x Electrode Thickness

PZT capacitors with electrode thickness above 230nm exhibited better fatigue property (Fig. 4.5). After 10^{11} switching cycles, there were 3% and 47% Pr reduction for the capacitors with electrode thickness of 380nm and 80nm respectively. Both the number of fatigue free cycles and the Pr reduction greatly degraded when the bottom electrode thickness was below 230nm.

If we refer to the oxygen vacancy mechanism, there is one point that we can draw from our results. That is the amount of oxygen content in the bottom electrodes might be decreased when the thickness is too thin. So the capacitors with thin electrodes provided poor fatigue property due to lack of oxygen amount for filling up the oxygen vacancies at interfaces. To provide an explanation of the above thickness dependence, we need to look into the inter-diffusion behavior at the interface.

4.7 Inter-diffusion in RuO_x Bottom Electrodes

From the above discussion, we have introduced a postulate for the effect of thinner bottom electrode on the PZT capacitor properties. The cross sectional SEM micro-graphs of PZT film on $RuO_x/SiO_2/Si$ was displayed in Fig. 4.6. From Fig. 4.6(a), we found that both the PZT film and the 240nm RuO_x film were very clearly distinguishable. However, the clear boundaries were not observed in Fig. 4.6(b) when the RuO_x bottom electrode thickness was 80nm. The induction from these micro-graphs is the property that very thin RuO_x bottom electrode would be dominated by significant inter-diffusion in the $PZT/RuO_x/SiO_2/Si$ system. AES measurement was taken to provide more details on the inter-diffusion.

The AES spectra of PZT thin film on RuO_x layer with different thickness (100nm & 240nm) was shown in Fig. 4.7(a) and Fig. 4.7(b). For the sample with RuO_x film of 240nm thickness, there was a clearly defined region with the composition of RuO_x where x is about 1.3. However for the samples with thin RuO_x of 100nm between the PZT and SiO_2 substrate, there was only an interfacial layer in which oxygen concentration decreases rapidly from the PZT side and Ru concentration varies with a triangular shape. In such sample, no RuO_x layer of proper stoichiometric ratio was formed. As shown in section 3.1 the crystallization in the PZT film was strongly dependent on the grain orientation of the bottom RuO_x layer. Therefore the PZT crystallization in very thin RuO_x samples is incomplete and resulted in low Pr and Kr values.

The fatigue property of PZT capacitors with such thin bottom electrode was degraded due to the low oxygen content in the bottom electrode. Kohta Yoshikawa et al. [17] have demonstrated the oxygen diffusion from the RuO_2 layer to the Ru/Si substrate when the RuO_2 layer thickness is 50nm after 600°C annealing for 1 hour. This in fact confirms that very thin RuO_x bottom electrode possess relative thinner layer with improper stoichiometric ratio such that the film was dominated by significant inter-diffusion layer. The degraded performance of the PZT capacitors with thin RuO_x bottom electrodes was believed to be due to the low oxygen content in their electrodes.

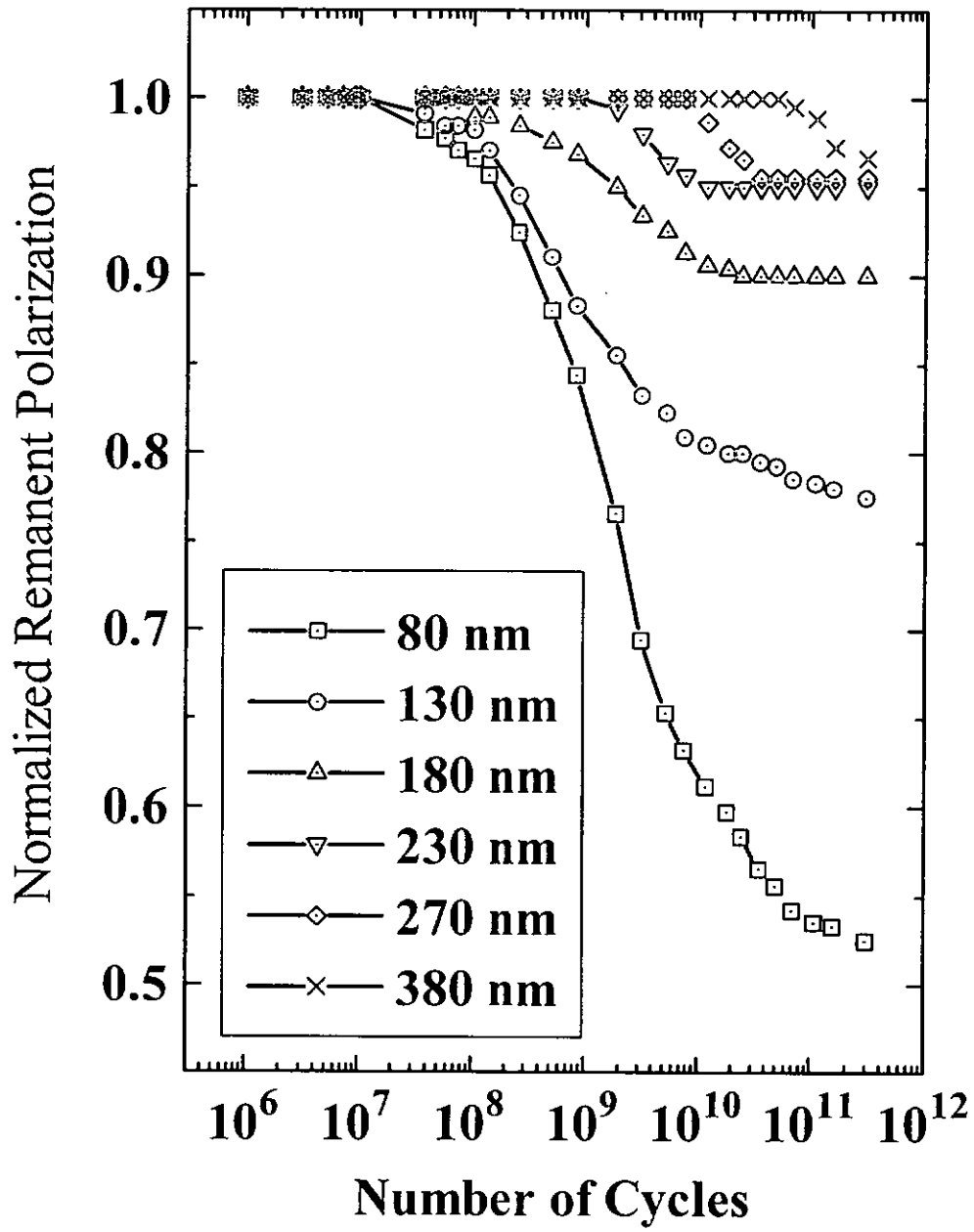

Fig. 4.5 **Fatigue Curves of RuO_x/PZT/RuO_x Capacitors with Different Bottom Electrode Thickness**

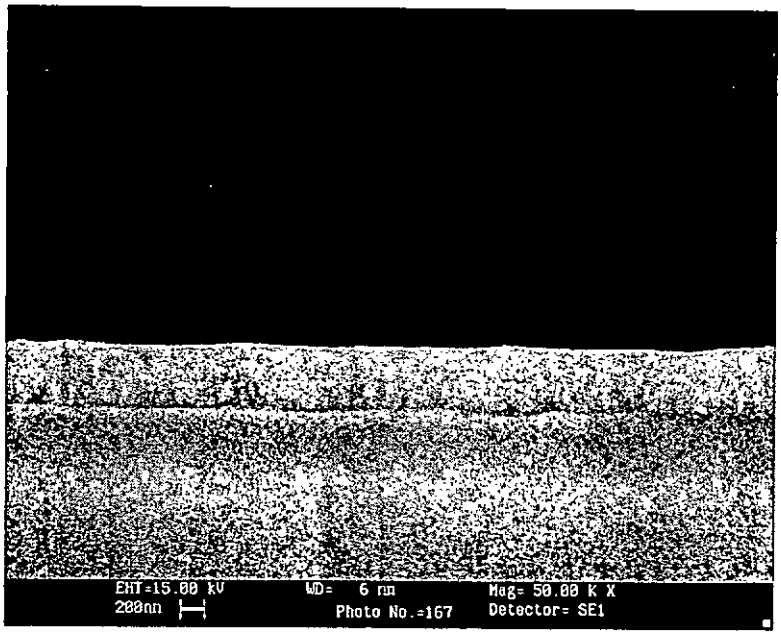

Fig. 4.6(a) SEM Micrograph of the Cross Sectional View of PZT Film on RuO_2(240nm)/SiO_2/Si Substrate

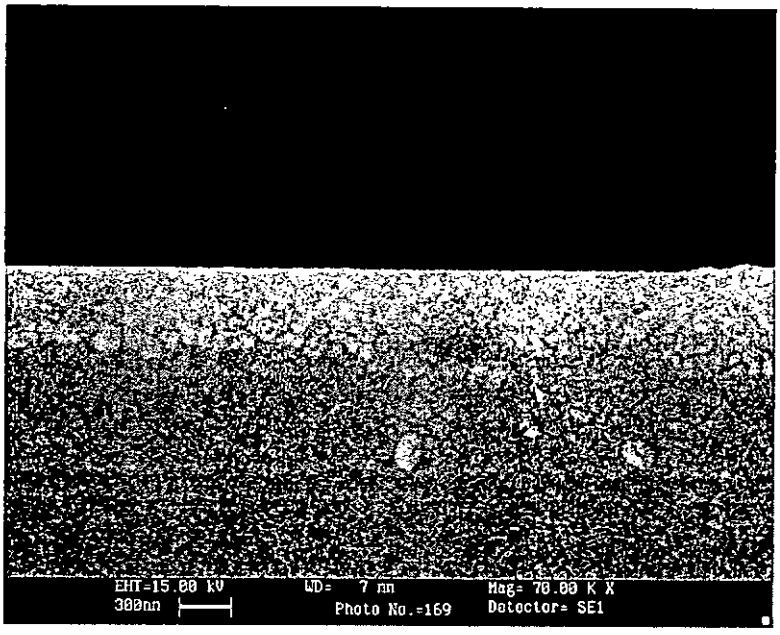

Fig. 4.6(b) SEM Micrograph of the Cross Sectional View of PZT Film on RuO_2(80nm)/SiO_2/Si Substrate

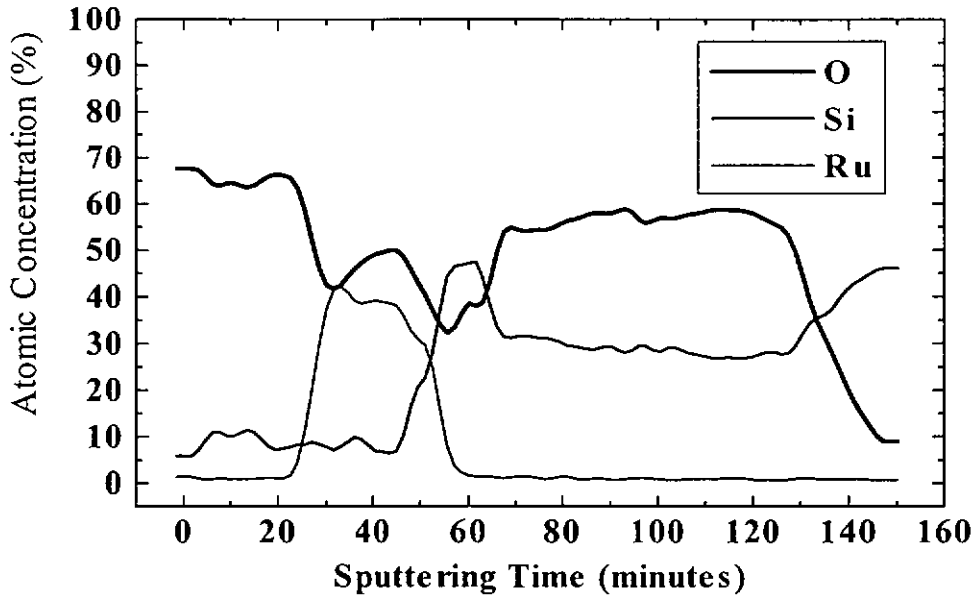

Fig. 4.7(a) AES Spectra of PZT/RuO_x(240nm)/SiO_2(600nm)/Si

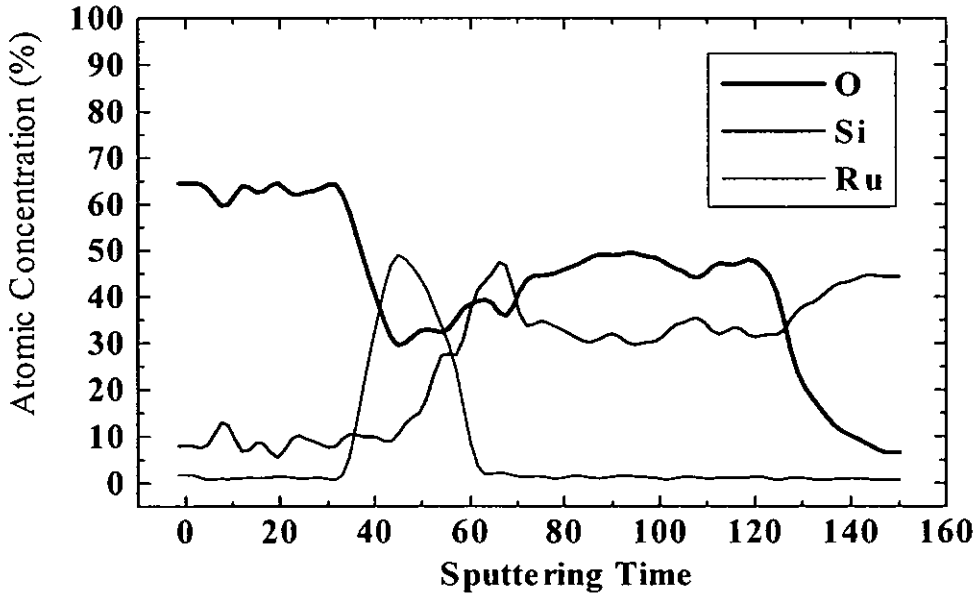

Fig. 4.7(b) AES Spectra of PZT/RuO_x(100nm)/SiO_2(560nm)/Si

4.8 Conclusions

Sol-gel PZT thin-film capacitors with reactive sputtered RuO_x electrodes were fabricated. In conclusion, we have investigated the dependence of the fatigue properties of sol-gel PZT thin films on the reactive sputtered RuO_x electrodes, including the effects of the electrode oxygen content and the thickness of the bottom electrodes.

Regarding the effect of electrode oxygen content, our results show that increase in oxygen content in the electrodes would improve the fatigue properties of the capacitors. With higher oxygen content in the electrodes, we measured better fatigue results for the capacitors. This is completely consistent with the oxygen vacancy fatigue mechanism. We believe that RuO_x electrodes with higher oxygen content provide much oxygen for filling up the trapped oxygen vacancies. We can conclude that oxygen vacancies play a key role in the fatigue of ferroelectric capacitors. It is related to the ferroelectric film-electrode interface and domain mobility. Other than using conductive oxide electrodes, we believe that the fatigue problem can be alleviated through controlling vacancy concentration and interface states. The concentration of oxygen vacancies can be controlled when adjusting dopants and heat treatment conditions. Besides, ferroelectric film-electrode interface can be controlled by using materials with crystal structures similar to that of the ferroelectric material.

Oxygen deficiency in the thin electrodes was detected through AES measurement. When the bottom electrode thickness was below 230nm, the fatigue properties were degraded because a RuO_x layer with proper stoichiometric ratio was not formed due to oxygen diffusion. We have shown that the effect of electrode thickness is attributed to the oxygen diffusion in the bottom electrode layers. The above results

provide useful information for the RuO_x sputtering process in order to optimize the fatigue properties of the PZT films.

Chapter FIVE

Current-Voltage Characteristics

5.1 Introduction

Many reports studied the electrical conduction mechanisms in ferroelectric PZT thin film capacitors. Moazzami et al. reported that the leakage current comprised of two components: ohmic at low electric field, and electric hopping current at high field, which has an activation energy of about 0.4eV [1-2]. Sudhama et al. proposed the conduction mechanism using a two-carrier-injection model in metal-semiconductor-metal incorporating blocking contacts with a barrier height of 0.6eV [3]. Scott et al. [4], Fox and Krupanidhi [5] proposed the space-charge-limited current in fatigued PZT and PLZT thin films, respectively. However, all of the models proposed to date were inadequate to explain all properties. Since the leakage current tended to change with various measurement conditions and fabrication procedures, it was very difficult to determine the conduction mechanism unless detailed experimental results were obtained. In this chapter we present the experimental results of current-voltage (I-V) characteristics on our sol-gel PZT thin film capacitors. Other than comparing the I-V characteristics of our Pt/PZT/Pt capacitors and RuO_2/PZT/RuO_2 capacitors, we shall also report the effect of electrode oxygen content on the I-V characteristics of our RuO_x/PZT/RuO_x capacitors. Our work would contribute to the understanding of electronic conduction characteristics in sol-gel PZT.

5.2 Experiment

The I-V characteristic investigation of our PZT capacitors consists of two parts. The first part compares the I-V characteristics of Pt/PZT/Pt capacitors and RuO_x/PZT/RuO_x capacitors. We employed 10% oxygen partial pressure for the RuO_x electrodes. According to our previous RBS results in chapter 4, we denoted it as RuO_2 electrodes in this chapter. The other part considers the I-V characteristics of RuO_x/PZT/RuO_x capacitors with different electrode oxygen content. Relative oxygen partial pressures of 0%, 10% and 20% were applied to fabricate the RuO_x electrodes.

The fabrication procedures and conditions of both Pt/PZT/Pt and RuO_x/PZT/RuO_x capacitors were the same as those mentioned in Chapter 3 and Chapter 4. The leakage current was measured with HP4140B pA-meter. A top electrode of the capacitor was connected to the voltage source and the bottom electrode was grounded. The polarity is positive when a positive voltage is applied to the top electrode. The data presented in this chapter were obtained in a D.C. experiment with voltage, V, held constant for 1s. Typically, 50 data points were taken from 0V to 5V.

5.3 Results and Discussions

(a) J-E Characteristics of PZT Capacitors with Pt and RuO_2 Electrodes

In this chapter, all the current-voltage (I-V) characteristics were displayed in terms of J-E (Current Density vs. Electric Field) plot. No strict correlation was found between the J-E characteristics and the pyrolysis temperature. Two typical J-E plots of Pt/PZT/Pt capacitor and RuO_2/PZT/RuO_2 capacitor were shown in Fig. 5.1.

The J-E plots of the capacitors were found asymmetric for positive and negative voltage biases. We believed it is related to their different thermal experienced electrodes. As the bottom electrodes, during capacitor fabrication, were subjected to high temperature cycles during the annealing of PZT films but the top electrodes received less heat treatment, the bottom and top interfaces of a real ferroelectric capacitor were always asymmetric. This asymmetry may form different barrier heights or contact types at bottom and top interfaces [11]. Therefore, the asymmetric leakage current levels for positive and negative voltage biases were attributed to the barrier height difference between both interfaces.

The leakage current density of Pt/PZT/Pt capacitor ($J_{Pt/PZT/Pt}$) was found to be lower than that of RuO_2/PZT/RuO_2 capacitor ($J_{RuO2/PZT/RuO2}$). Typically, $J_{Pt/PZT/Pt}$ is of the order of 10^{-7} Acm^{-2} whereas $J_{RuO2/PZT/RuO2}$ is of the order of $5x\ 10^{-5}$ Acm^{-2} when the E-field is 100 $kVcm^{-1}$. When the E-field is above 200 $kVcm^{-1}$, it was observed that both leakage current levels were very close to each other. This result has confirmed that the capacitors with RuO_2 electrodes have higher leakage current than those capacitors with Pt electrodes [6-7]. We believed that Pt/PZT/Pt capacitors have lower leakage current because of the higher work function of Pt electrodes.

J is strongly dependent on the applied E-field (E) when E is less than $50kVcm^{-1}$. J reaches a saturation current forming a kink when E > $50kVcm^{-1}$. The saturation current density is about $8x10^{-8}$ Acm^{-2} for positive bias and $3x10^{-7}$ Acm^{-2} for negative bias. The kink for negative bias is much narrower than that for positive bias. When E > 100 $kVcm^{-1}$, J increased rapidly again towards 10^{-4} Acm^{-2}.

When the J-E plot of Pt/PZT/Pt capacitors is plotted again in terms of Log(J/E) vs. $\sqrt{E}$ in Fig. 5.2, we found when E > $100kVcm^{-1}$, Log(J/E) is almost linearly

proportional to $\sqrt{E}$ with a slope of 3.5. This shows that the conduction process of the Pt/PZT/Pt capacitors may obey Frenkel-Poole Emission process at high E-field greater than 100 $kVcm^{-1}$.

Regarding the J-E plot of RuO_2/PZT/RuO_2 capacitors, the leakage current had an ohmic leakage current at relatively low electric field ranging from 0 to 10 $kVcm^{-1}$. The leakage current density increased with a decreasing slope as the E-field increased, which indicates that the current density was relative less E-field dependent at higher E-field. Both positive and negative J-E characteristics at relative low field agreed with the ohmic-current model stated in Ref. [12].

In summary, we have confirmed that the PZT capacitors with RuO_2 electrodes offer higher leakage current when comparing with the capacitors with Pt electrodes. This is consistent with the reports by Takashi et al and X. Chen et al. [8-9]. We have shown that the bottom electrodes control the leakage characteristics of PZT ferroelectric capacitors.

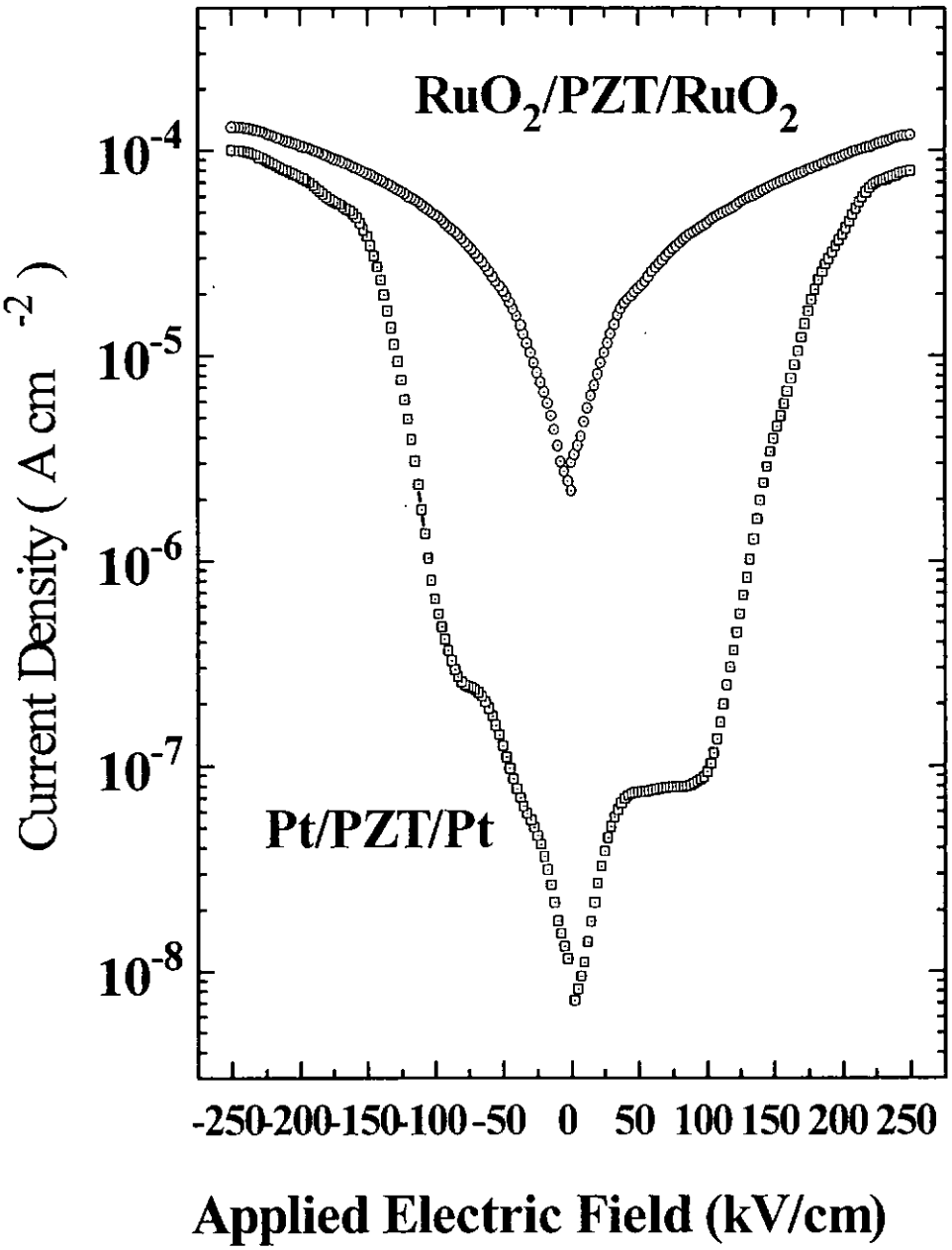

Fig. 5.1 **Current Density vs. E-Field Plots of Typical Pt/PZT/Pt and RuO_2/PZT/RuO_2 Capacitors**

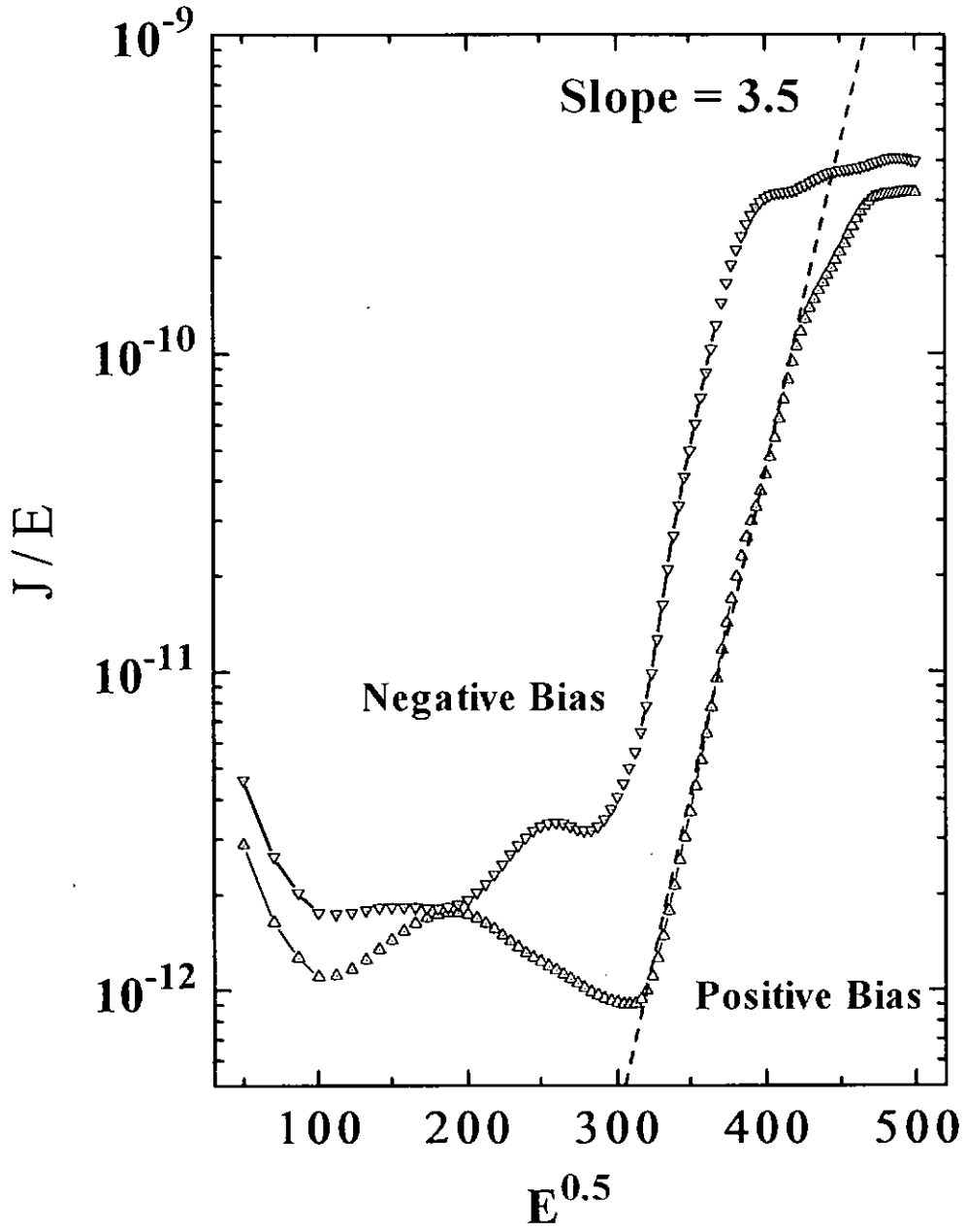

Fig. 5.2 **(J/E) vs. $E^{0.5}$ Plot of Typical Pt/PZT/Pt Capacitors**
(J - Current Density [A cm^{-2}])
(E - Electric Field [V cm^{-1}])

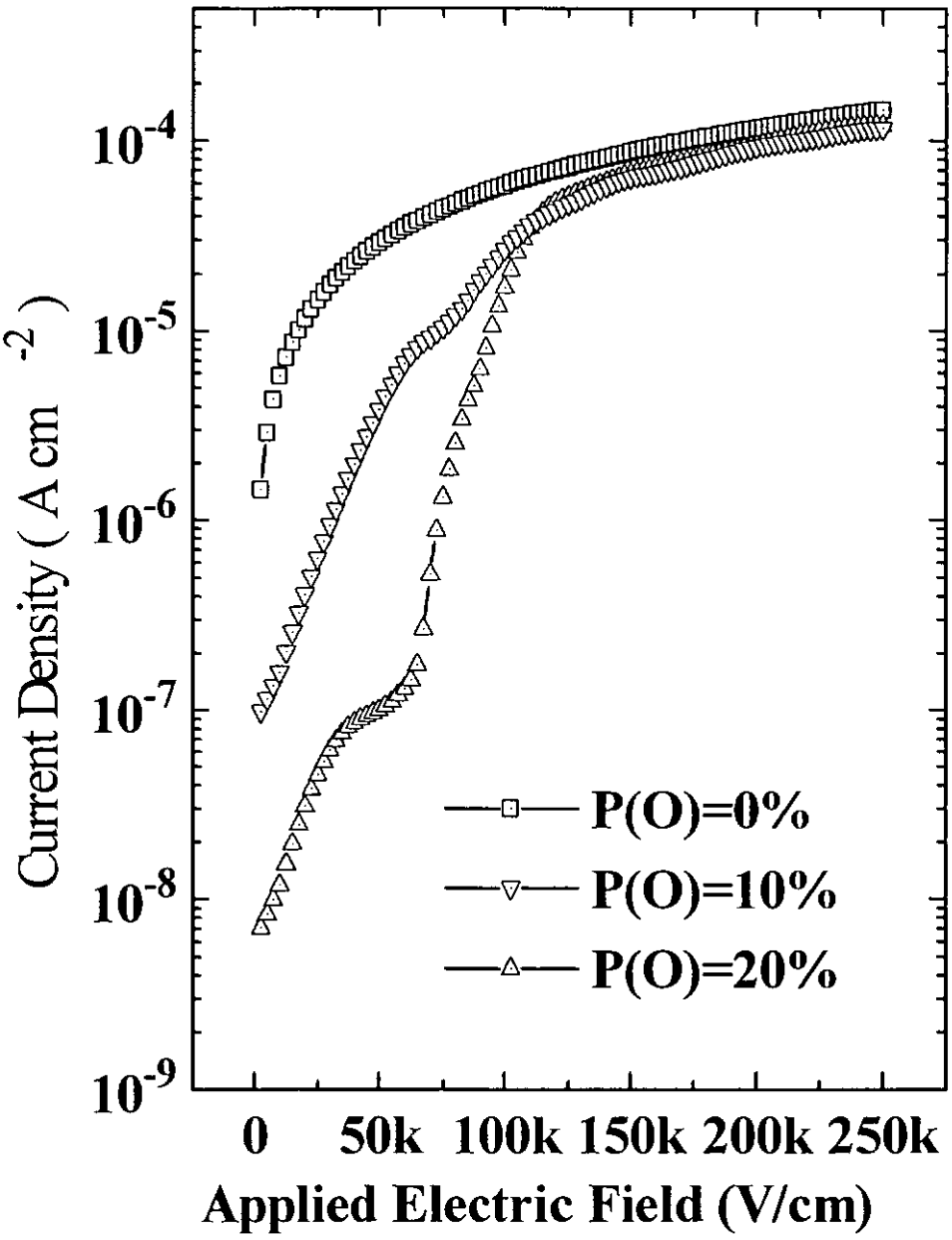

Fig. 5.3 **Current Density vs. E-Field Plot of Typical PZT Capacitors with RuO_x Electrodes of Different Relative Oxygen Partial Pressure**

(b) J-E Characteristics of RuO_x/PZT/RuO_x Capacitors with Different Oxygen Content

The current density-electric field (J-E) curves of the PZT capacitors with varying oxygen partial pressure for the RuO_x electrodes were measured and shown in Fig. 5.3. Typically, the leakage current of RuO_x/PZT/RuO_x capacitors was reported to range from 10^{-6} to 10^{-4} Acm^{-2} at bias below +5V [7, 10]. The values of leakage current obtained in our measurement completely agree with the published results.

When the E-field is below $120kVcm^{-1}$, the observed current decreased with increasing the oxygen partial pressure. This means that increasing oxygen content of the RuO_x electrodes reduces the leakage current of the capacitors. Hence the leakage current levels strongly depend on the applied E-field when $E < 120kVcm^{-1}$. Regarding the capacitors with 0% and 10%, the leakage current density increased with a decreasing slope when the E-field increased. For 20% partial pressure, we found a saturation current region again at the E-field ranging from $40kVcm^{-1}$ to $50kVcm^{-1}$. We guess the strong oxygen content dependent leakage current may be attributed to the change in the amount of oxygen vacancies at the bottom electrode interface.

According to the report in Ref. [13], oxygen vacancies can trap the charge carrier in PZT. This may affect the current due to Frenkel-Poole emission. With increasing electrode oxygen content, the amount of oxygen vacancies is reasonably decreased as mentioned in chapter 4. If we regard oxygen vacancies as charge trapping centers, this would lower the leakage current by Frenkel-Poole emission. However, further research work is still needed to confirm this point.

When the E-field is above $120kVcm^{-1}$, the leakage current was saturated at about $10^{-4}Acm^{-2}$. The leakage current level increased very gently with increasing the applied

E-field. So the current was independent of the oxygen content of electrodes with E-field above 120kVcm^{-1}.

5.4 Conclusions

In summary, the leakage current density of the PZT capacitors was observed to be independent of pyrolysis temperature. The PZT capacitors with RuO_2 electrodes possess degraded J-E characteristics, compared to those with Pt electrodes. Asymmetric current levels for positive and negative biases were measured for both types of capacitors. This asymmetric characteristic was traced back to their different thermal experienced electrodes.

The conduction process of PZT capacitors with Pt electrodes obeys the Frenkel Poole Emission model when the E-field was above 100kVcm^{-1}. In the J-E curve of the above PZT capacitors, a very narrow saturation kink region was observed. The leakage current was increased by three order of amplitude (from 10^{-7} to 10^{-4} Acm^{-2} under 100 kVcm^{-1}) when the RuO_2 electrodes were used instead of Pt electrodes. The RuO_2/PZT/RuO_2 capacitors possess ohmic-like current at very low field region below 10kVcm^{-1}.

We have investigated the J-E characteristics of the PZT capacitors with varying the oxygen content in the RuO_x electrodes. The oxygen content was controlled by the oxygen partial pressure during sputtering of the electrodes. The leakage current varied with the oxygen partial pressure during sputtering of the RuO_x electrodes when the electric field was below 120kVcm^{-1}. The current was not affected by the electrode oxygen content when the E-field is above 120kVcm^{-1}. At relative low field region, it

was observed that increasing oxygen content of the RuO_x electrodes made the capacitors to have less leakage current. We guess this is due to the decreased amount of oxygen vacancies, which is considered as charge trapping centers.

When 20% partial pressure is applied for the RuO_x electrodes, a very narrow saturation current region was observed in the corresponding J-E curve. However, the reason for the appearance of these saturation current regions in Pt/PZT/Pt capacitor J-E curve and RuO_x/PZT/RuO_x (with 20% oxygen partial pressure) capacitor J-E curve was not known. We admitted that further research work is still needed for the J-E characteristics of PZT capacitors.

Chapter SIX

Conclusions and Future Work Suggestion

6.1 Conclusions

The effect of pyrolysis temperature (300°C-600°C) on the ferroelectric properties and texture of the PZT thin films grown on Pt coated and RuO_2 coated substrate was investigated. For the Pt/PZT/Pt capacitors, the highest remanent polarization was obtained when the pyrolysis temperature of 400°C was applied. The small signal relative permittivity of the PZT thin films obtained at pyrolysis temperature at or below 400°C was higher than those obtained at pyrolysis temperature of 450°C or above. We believe that the degradation in remanent polarization of the PZT capacitors for pyrolysis temperature below 400°C is attributed to the strong (100) orientation of the PZT films. Also, the significant drop in remanent polarization and small signal relative permittivity of the capacitors for the pyrolysis temperature at or above 450°C is believed to be due to the existence of pyrochlore phase in the PZT films. We have also shown that our PZT thin films should consist of dominantly c-domains for the pyrolysis temperature at 400°C. For the RuO_2/PZT/RuO_2 capacitors, there is no considerable effect of pyrolysis temperature at or below 400°C on their ferroelectric properties. However, the pyrochlore phase was found to result in significant reduction in remanent polarization and small signal relative permittivity of the PZT capacitors for the pyrolysis temperature at or above 450°C.

The ferroelectric properties of the RuO_x/PZT/RuO_x capacitors were also investigated with different oxygen content of the RuO_x electrodes. The oxygen content was adjusted by varying the relative oxygen partial pressure during sputtering of the electrodes. The capacitors possess the highest remanent polarization when 10% partial pressure was applied whereas their small signal relative permittivity was at the highest value when applying 0% partial pressure. The highest remanent polarization of the RuO_x/PZT/RuO_x capacitors was attributed to the strongest (110) texture of the PZT thin films. We also believe that the strongest (110) texture of the RuO_x substrates yields the strongest (110) texture of the PZT thin films. For the small signal relative permittivity, we guess that its degradation is due to the presence of an interfacial layer between the PZT and the RuO_x electrode.

With varying RuO_2 bottom electrode thickness, the corresponding ferroelectric properties of the RuO_2/PZT/RuO_2 capacitors were investigated. Both the remanent polarization and small signal relative permittivity of the capacitors increased when the thickness was increased from 80nm to 230nm. When the thickness was above 230nm, both the polarization and perimittivity were found to be almost independent on the bottom electrode thickness. The poor ferroelectric properties of capacitors with thinner electrodes were attributed to their incomplete formation of perovskite phase in PZT films.

Fatigue property of the RuO_x/PZT/RuO_x capacitors was found to be dependent on the electrode oxygen content and the bottom electrode thickness. With increasing relative oxygen partial pressure, the number of fatigue free cycles increased and reduction in remanent polarization decreased. This fatigue result is consistent with the oxygen vacancy fatigue mechanism. We believe that higher oxygen content in the

electrodes provides much amount of oxygen to fill up the oxygen vacancies and hence improves the fatigue property.

When the RuO_2 bottom electrode thickness of PZT capacitors decreased from 380nm to 80nm, both the number of fatigue free cycles and remanent polarization reduction were degraded. Thinner bottom electrode was confirmed by AES spectra to provide less amount of oxygen and hence degrades both the fatigue property of the capacitors and crystallinity of the PZT thin films. Typically $RuO_{1.3}$ bottom electrode was detected with AES when the thickness is 100nm.

We have investigated the current-voltage characteristics of PZT capacitors with Pt and RuO_2 electrodes. The leakage current density of the Pt/PZT/Pt capacitors was lower than that of the RuO_2/PZT/RuO_2 capacitors. Pt/PZT/Pt capacitors were found to obey the Frenkel Poole conduction process when $E > 100kVcm^{-1}$. However, no single conduction process can be confirmed for both types of capacitors. The leakage current density decreased with increasing the relative oxygen partial pressure for the RuO_2/PZT/RuO_2 capacitors when $E < 120\ kVcm^{-1}$. When $E > 120kVcm^{-1}$, there is no considerable effect of oxygen content on the leakage current density of the RuO_x/PZT/RuO_x capacitors.

In summary, we have optimized the pyrolysis temperature in sol-gel process to obtain the most desirable ferroelectric properties for the Pt/PZT/Pt and RuO_2/PZT/RuO_2 capacitors. We have investigated the effect of RuO_x electrode thickness and oxygen content on the PZT thin film capacitors. High oxygen content in RuO_x electrode is desirable in order to improve the fatigue and leakage current characteristics.

6.2 Future Work Suggestion

Although the fatigue property of PZT capacitors was improved by using RuO_x instead of Pt electrodes, the higher leakage current level of RuO_x/PZT/RuO_x capacitors has led to another research problem. Besides, more work is still needed to understand in detail the leakage current mechanisms in PZT capacitors with different electrodes.

It was suggested to use Pt-RuO_x hybrid electrodes for the PZT capacitors in order to lower the leakage current level. However, further work is required in order to understand many capacitor properties. For example, is there any uncertain inter-diffusion behavior in the hybrid electrodes, which would degrade the capacitors? Do the hybrid structure electrodes affect the ferroelectric properties of the capacitors? Since the remanent polarization of the capacitors always depends on their bottom electrode orientation, proper control of the orientation of the hybrid electrodes is necessary. Can we properly control the orientation of the hybrid electrodes?

Regarding the leakage current characteristics of PZT capacitors, we suggest to study the temperature and time dependence of the I-V characteristics of RuO_x/PZT/RuO_x capacitors. We expected that the conduction mechanism would be further understood after studying the temperature effect on I-V characteristics and its time dependence.

REFERENCES

Chapter One

1. M. E. Lines & A. M. Glass, *"Principles and Applications of Ferroelectrics and Related Materials"*, Clarendon Press, Oxforde, 1977
2. B. Jaffe, W. R. Cooke & H. Jaffe, *"Piezoelectric Ceramics"*, Academic Press, New York, 1971
3. J. B. Goodenough & J. M. Longo, *"Landolt-Bornstein Numerical Data and Functional Relationship in Science and Technology"*, Springer-Verlag, Berlin, **12**, 126, 1978
4. J. Franco & G. Shirane, *"Ferroelectric Crystals"*, Pergemon Press, Oxford, 1962
5. J. F. Scott & C. A. Paz de Araujo, *Science*, **246**, 1400, 1989
6. G. H. Haertling, *"Electronic Ceramics: Properties, Devices and Applications"*, edited by L. M. Levinson, Marcel Dekker Inc., New York, 371, 1988
7. S. B. Krupanidhi, *"Multicomponent and Multilayered Thin Films for Advanced Microtechnologies: Techniques, Foundamentals and Devices"*, edited by O. Auciello & J. Engemann, Klumer Academics Publishers, 209, 1993
8. I. S. Zheludev, *"Crystalline Dielectrics, vol. 2, Electrical Properties"*, Plenum Press, New York, 227, 1971
9. J. Carrano, C. Sudhama, V. Chikarmane, J. Lee, A. Tasch, W. Shepherd & N. Abt, *IEEE Transactions on Ultrasonics, Ferroelectric and Frequency Control*, **38**, [6], 690, 1991
10. D. P. Vijay & S. B. Desu, *J. Electrochem. Soc.*, **140**, [9], 2640, 1993
11. B. A. Tuttle, H. N. Al-Shareef, W. L. Warren, M. V. Raymond, T. J. Headley, J. A. Voigt, J. Evans & R. Ramesh, *Microelectronic Eng.*, **29**, 223, 1995

12. C. A. Paz de Araujo, J. D. Cuchlaro, L. D. McMillan, M. C. Scott & J. F. Scott, *Nature*, **374**, 627, 1995
13. I. K. Yoo & S. B. Desu, *Mat. Sci. and Eng.*, **B13**, 319, 1992
14. W. L. Warren, D. Dimos, B. A. Tuttle & D. M. Smyth, *J. Am. Ceram. Soc.*, **77**, [10], 2753, 1994

Chapter Two

1. J. B. Goodenough & J. M. Longo, *"Landolt-Bornstein Numerical Data and Functional Relationship in Science and Technology"*, Springer-Verlag, Berlin, **12**, 126, 1978
2. G. H. Haertling & C. E. Land, *J. Am. Ceram. Soc.*, **54**, [1], 1, 1971
3. E. Sawaguchi, G. Shirane & Y. Takagi, *J. Phys. Soc. Japan*, **6**, 333, 1951
4. G. Shirane, S. Hoshino & K. Suzuki, *Phys. Rev.*, **80**, 1105, 1950
5. M. E. Lines & A. M. Glass, *"Principles and Applications of Ferroelectrics and Related Materials"*, Clarendon Press, Oxforde, 1977
6. B. Aurivillius, *Arkiv Kemi*, **1**, [54], 463, 1949
7. M. A. Subramanian, G. Aravamudan & G. V. Subbarao, *Prog. in Solid State Chem.*, **15**, 55, 1983
8. J. R. Oliver, R. R. Neurgaonkar & L. E. Cross, *J. Am. Ceram. Soc.*, **72**, [2], 202, 1989
9. Reza Moazzami, *Semiconductor Science and Technology*, **10**, 375 (1995).
10. R. A. Roy, K. F. Etzold, J. J. Cuomo & T. J. Watson, *"Ferroelectric Thin Films"*, Edited by Edward R. Myers & Angus I. Kingon, 141, 1990
11. G. Yi, Z. Wu & M. Sayer, *J. Appl. Phys.*, **64**, [5], 2717, 1988
12. S. K. Dey & R. Zuleeg, *Ferroelectrics*, **108**, 37, 1990
13. G. A. C. M. Spierings, M. J. E. Ulenaers, G. L. M. Kampschoer, H. A. M. van Hal & P. K. Larsen, *J. Appl. Phys.*, **70**, [4], 2290, 1991
14. B. Jaffe, W. R. Cook Jr. & H. Jaffe, *"Piezoelectric Ceramics"*, Academic Press London and New York, 1971
15. F. P. Gnadinger, *IEEE, VLSI and Computer Peripherals*, **1**, 20, 1989

16. S. S. Eaton, D. B. Butler, M. Parris, D. Wilson & H. McNeillie, *IEEE Solid State Circuits Conference*, **329**, 130, 1988
17. D. Bondurant & F. Gnadinger, *IEEE Spectrum*, 7, 30, 1989
18. C. Jeffrey Brinker & George W. Scherer, *Sol-Gel Science*, Academic Press.
19. R. Moazzami, C. Hu & W. H. Shepherd, *Technical Digest - International Electron Devices Meeting, IEEE Service Center*, Piscataway, New Jersey, 417, 1990
20. D. E. Fisch, N. E. Abt, F. N. Bens, W. D. Miller, T. Pramanik, W. Saiki & W. H. Shepherd, *IEEE Reliability Phys. Symp., IEEE Service Center*, Piscataway, New Jersey, 237, 1990
21. I. K. Yoo, S. B. Desu & J. Xing, *Mat. Res. Soc. Symp. Proc.*, **310**, 165, 1993
22. M. Okuda, H. Naito & T. Matsushita, *Jpn. J. Appl. Phys.*, **31**, [2B], 466, 1992
23. T. Mihara, H. Wantanable & C. A. Paz de Araujo, *Jpn. J. Appl. Phys.*, **32**, [9B], 4168, 1993
24. J. F. Scott, B. M. Melnick, L. D. Mcmillan, C. A. Paz de Araujo & M. Azuma, *Ferroelectrics*, **150**, [1-2], 209, 1993
25. Q. Zhang, W. Cao & L. E. Cross, *J. Am. Ceram. Soc.*, **77**, [1], 211, 1994
26. A. Y. Kudzin, T. U. Panchenko & S. P. Yudin, *Sov. Phys. Solid State*, **16**, [8], 1589, 1975
27. G. Rohrer, S. Narayan, L. McMillan & A. Kulkarni, *J. Vac. Sci. Tech.*, **A6**, [3], 1756, 1988
28. H. M. Guiker, P. D. Beale, J. F. Scott, C. A. Paz de Araujo, B. M. Melnick, J. D. Cuchlaro & L. D. McMillan, *J. Appl. Phys.*, **68**, [11], 5783, 1990
29. R. Waser, T. Baiatu & K. Haerdtl, *J. Am. Ceram. Soc.*, **73**, [6], 1645, 1990
30. M. V. Raymond & D. M. Smyth, *Integrated Ferroelectrics*, **4**, [2], 145, 1994
31. A. V. Dixit, N. R. Rajopadhye & S. V. Bhoraskar, *J. Mat. Sci.*, 21, 2798, 1996
32. J. Robertson, W. L. Warren & B. A. Tuttle, *J. Appl. Phys.*, **77**, [8], 3975, 1995
33. H. M. Duiker, P. D. Beale, J. F. Scott, C. A. Paz de Araujo, B. M. Melnick, J. D. Cuchlaro & L. D. McMillan, *J. Appl. Phys.*, **68**, [11], 5783, 1990
34. T. Mihara, H. Watanabe, C. A. Paz de Araujo, *Jpn. J. Appl. Phys.*, **33**, [9B], 5281, 1994
35. J. F. Chang & S. B. Desu, *J. Mat. Res.*, **9**, [4], 955, 1994

36. C. H. Seager, W. L. Warren, B. A. Tuttle, R. D. Nasby & D. Dimos, *Mat. Res. Soc. Symp. Proc.*, **284**, 493, 1993
37. W. L. Warren, D. Dimos, B. A. Tuttle, D. Nasby & D. M. Smyth, *J. Am. Ceram. Soc.*, **77**, [10], 2753, 1994
38. W. L. Warren, D. Dimos, B. A. Tuttle, R. D. Nasby & G. E. Pike, *Appl. Phys. Lett.*, **65**, [8], 1018, 1994
39. B. Jiang, J. Kim, R. Khamankar, I. Lee & J. C. Lee, *Mat. Res. Soc. Symp. Proc.*, **361**, 85, 1995
40. S. D. Bernstein, T. Y. Wong, Y. Kisler & R. W. Tustison, *J. Mat. Res.*, **8**, [1], 12, 1993
41. T. Nakmura, Y. Nako, Q. Kamisawa & H. Takasu, *Jpn. J. Appl. Phys.*, **33**, [9B], 5207, 1994
42. B. a. Tuttle, H. N. Al-Shareef, W. L. Warren, M. V. Raymond, T. J. Headley, J. A. Voigt, J. Evans & R. Ramesh, *Microelectronic Eng.*, **29**, [1-4], 223, 1995
43. C. Bjormander, A. M. Grishin, B. M. Moon, J. Lee & K. V. Rao, *Appl. Phys. Lett.*, **64**, [26], 3646, 1994
44. R. Ramesh, T. Sands, V. G. Keramidas & D. K. Fork, *Mat. Sci. Eng.*, **B22**, 283, 1994
45. K. D. Budd, S. K. Dey & D. A. Payne, *Br. Ceram. Proc.*, **36**, 107, 1985
46. S. Y. Chen, X. Du, I. Wei & Chen, *Mat. Res. Soc. Symp. Proc.*, **361**, 15, 1995
47. H. N. Al-Shareef, K. R. Bellur, O. Auciello & A. I. Kingon, *Thin Solid Films*, **256**, [1], 73, 1995
48. C. Hsueh & M. L. Mecartney, *J. Mat. Res.*, **7**, [9], 2521, 1992
49. B. A. Tuttle, T. J. Headley, B. C. Bunker, R. W. Schwartz, T. J. Zender, C. L. Hernandez, D. C. Goodnow, R. J. Tissot, J. Michael & A. H. Carim, *J. Mat. Res.*, **7**, [7], 1876, 1992
50. M. J. Lefevre, D. B. Dimos & J. S. Speck, *Proceedings - Annual Meeting, Microscopy Soc. of America*, 582, 1994
51. T. Tani, Z. Xu, Zhengkui & D. A. Payne, *Mat. Res. Soc. Symp. Proc.*, **310**, 269, 1993
52. K. Fujimoto, S. Yoshimura & K. Kubota, *Thin Solid Films*, **173**, [2], L139, 1989

53. L. A. Wills, W. A. Feil, B. W. Wessels, L. M. Tonge & T. J. Marks, *J. Crystal Growth*, **107**, [1-4], 712, 1991
54. S. D. Ghonge, E. Goo, R. Ramesh, R. Haakenaasen & D. K. Fork, *"Ferroic Materials: Design, Preparation and Characteristics"*, edited by A. S. Bhalla, K. M. Nair, I. K. Lloyd, H. Yanagida & D. A. Payne, Am. Ceramic Soc., 165, 1994
55. S. Y. Chen & I. W. Chen, *J. Am. Ceram. Soc.*, 77, [9], 2332, 1994
56. S. Y. Chen & I. W. Chen, *J. Am. Ceram. Soc.*, 77, [9], 2337, 1994
57. K. Arita, E. Fujii, Y. Shimada, Y. Uemoto, M. Azuma, S. Hayashi, T. Nasu, A. Matsuda, Y. Nagano, S. Katsu, T. Otsuki, G. Kano, L. D. Mcmillan & C. A. Paz de Araujo, *IEEE Transactions on Electronics*, **E77-C**, [3], 392, 1994
58. W. A. Gideman, S. Y. Wu, L. E. Sanchez, B. P. Maderic, W. M. Liu, I. K. Naik & S. H. Wayanable, *IEEE 7 Int. Symp. Appl. Ferroelectr.*, 258, 1992
59. C. M. Foster, R. Csencsits, P. M. Baldo, G. R. Bai, Z. Li, L. E. Rehn, L. A. Wils, R. R. Hiskes, *Proceedings of SPIE*, **2441**, 279, 1995
60. G. R. Fox, S. Trolier-McKinstry, S. B. Krupanidhi & L. M. Casas, *J. Mat. Res.*, **10**, [6], 1508, 1995
61. H. N. Al-Shareef, K. D. Gifford, S. H. Rou, P. D. Hren, O. Auciello, A. I. Kingon, *Integrated Ferroelectrics*, **3**, [4], 321, 1993
62. R. E. Jones, Jr., P. D. Maniar, R. Moazzami, P. Zurcher, J. Z. Witowski, Y. T. Lii, P. Chu & S. J. Gillespie, *Thin Solid Films*, **270**, 584, 1995

Chapter Three

1. C. Chen & D. F. Ryder, *J. Am. Ceram. Soc.*, **72**, 1495, 1989
2. S. K. Dey & R. Zuleeg, *Ferroelectrics*, **112**, 309, 1990
3. L. N. Chapin & S. A. Myers, *Mater. Res. Soc. Symp. Proc.*, **200**, 153, 1990
4. Y. Huang, I. M. Reaney & A. J. Bell, *Ferroelectrics*, **134**, 285, 1992
5. Katsuhiro Aoki, Yukio Fukuda, Ken Numata & Akitoshi Nishimura, *Jpn. J. Appl. Phys.*, **34-I**, 746, 1995
6. Y. L. Tu & S. J. Milne, *J. Materials Science*, **30**, 2507, 1995
7. H. Hu, C. J. Peng & S. B. Krupanidhi, *Thin Solid Films*, **223**, 327, 1993

8. M. Klee, A. de Veirman, D. J. Taylor & P. K. Larsen, *Integrated Ferroelectrics*, **4**, 197, 1994
9. Keith G. Brooks, Ian M. Reancy, Radosveta Klissurska, Y. Huang, L. Bursill & N. Setter, *J. Mater. Res.*, **9**, 2540, 1994
10. C. A. Paz de Araujo, J. D. Cuchiaro, L. D. McMillan, M. C. Scott & J. F. Scott, *Nature*, **374**, 627, 1995
11. Keiko Kushida-Abdelghafar, Hiroshi Miki, Kazuyoshi Torii & Yoshihisa Fujisaki, *Appl. Phys. Lett.*, **69**, 3188, 1996
12. H. N. Al-Shareef, K. R. Bellur, O. Auciello & A. I. Kingon, *Integrated Ferroelectrics*, **2**, 185, 1994
13. D. P. Vijay & S. B. Desu, *J. Electrochem. Soc.*, **140**, 2640, 1993
14. H. N. Al-Shareef, A. I. Kingon, X. Chen & K. R. Bellur, *J. Mater. Res.*, **9**, 2968, 1994
15. H. N. Al-Shareef, O. Auciello & A. I. Kingon, *J. Appl. Phys.*, **77**, 2146, 1995
16. A. Gril, D. Beach, C. Smart & W. Kane, *"Ferroelectric Thin Films III, Mater. Res. Soc. Poc."*, edited by E. R. Myers, B. A. Tuttle, S. B. Besu & P. K. Larsen, **310**, 189, 1993
17. R. Ramesh, A. Inam, W. K. Chau, F. Tillerot, B. Wilkens, C. C. Chang, T. Sands, J. M. Tarascon & V. G. Keramidas, *Appl. Phys. Lett.*, **59**, 3542, 1991
18. D. P. Vijay, S. B. Desu & W. Pan, *"Ferroelectric Thin Films III, Mater. Res. Soc. Poc."*, edited by E. R. Myers, B. A. Tuttle, S. B. Besu & P. K. Larsen, **310**, 133, 1993
19. T. Horikawa, N. Mikami, T. Makita, J. Tanimura, M. Kataoka, K. Sato & M. Nunoshita, Jpn. J. Appl. Phys., 32, 4126, 1993
20. S. D. Bernstein, T. Y. Wong, Yanina Kisler & R. W. Tustison, *J. Mater. Res.*, **8**, 12, 1993
21. Jeong-gun Lee, Suk-ki Min & Sung Ho Choh, *Jpn. J. Appl. Phys.*, **33**, 7080, 1994
22. Q. Wang, Wayne L. Gladfelter, D. Fennell Evans, Yue Fan & Alfonso Franciosi, *J. Vac. Sci. Technol. A.*, **14**, 747
23. M. Klee, R. Eusemann, R. Waser, W. Brand & H. Van Hal, *J. Appl. Phys.*, **72**, 1566, 1992

24. Katsuhiro Aoki, Yukio Fukuda, Ken Numata & Akitoshi Nishmura, *Jpn. J. Appl. Phys.*, **34**, 746, 1995
25. Y. Huang, I. M. Reaney & A. J. Bell, *Ferroelectrics*, **134**, 285, 1992
26. L. L. Hench, J. K. West, *"Principles of Electronic Ceramics"*, Wiley, 1990
27. K. No, C. J. Kim, D. S. Yoon, J. S. Lee, C. G. Choi, W. J. Lee & B. S. Bae, *Integrated Ferroelectrics*, **9**, [1-3], 159, 1995
28. N. J. Wu, A. Ignatiev, A. Mesarwi, H. Lin, K. Xie, H. Shih, *Jpn. J. Appl. Phys.*, **32**, [11A], 5019, 1993
29. G. A. C. M. Spierings, G. J. M. Dormans, W. G. J. Moors, M. J. E. Ulenaers & P. K. Larsen, *J. Appl. Phys.*, **78** ,1926, 1995

Chapter Four

1. C. A. Paz de Araujo, J. D. Cuchiaro, L. D. McMillan, M. C. Scott & J. F. Scott, *Nature*, **374**, 627, 1995
2. Keiko Kushida-Abdelghafar, Hiroshi Miki, Kazuyoshi Torii & Yoshihisa Fujisaki, *Appl. Phys. Lett.*, **69**, 3188, 1996
3. H. N. Al-Shareef, K. R. Bellur, O. Auciello & A. I. Kingon, *Integrated Ferroelectrics*, **2**, 185, 1994
4. D. P. Vijay & S. B. Desu, *J. Electrochem. Soc.*, **140**, 2640, 1993
5. H. N. Al-Shareef, A. I. Kingon, X. Chen & K. R. Bellur, *J. Mater. Res.*, **9**, 2968, 1994
6. H. N. Al-Shareef, O. Auciello & A. I. Kingon, *J. Appl. Phys.*, 77, 2146, 1995
7. A. Gril, D. Beach, C. Smart & W. Kane, *"Ferroelectric Thin Films III, Mater. Res. Soc. Poc."*, edited by E. R. Myers, B. A. Tuttle, S. B. Besu & P. K. Larsen, **310**, 189, 1993
8. R. Ramesh, A. Inam, W. K. Chau, F. Tillerot, B. Wilkens, C. C. Chang, T. Sands, J. M. Tarascon & V. G. Keramidas, *Appl. Phys. Lett.*, **59**, 3542, 1991
9. D. P. Vijay, S. B. Desu & W. Pan, *"Ferroelectric Thin Films III, Mater. Res. Soc. Poc."*, edited by E. R. Myers, B. A. Tuttle, S. B. Besu & P. K. Larsen, **310**, 133, 1993

10. T. Horikawa, N. Mikami, T. Makita, J. Tanimura, M. Kataoka, K. Sato & M. Nunoshita, Jpn. J. Appl. Phys., 32, 4126, 1993
11. S. D. Bernstein, T. Y. Wong, Yanina Kisler & R. W. Tustison, *J. Mater. Res.*, **8**, 12, 1993
12. Jeong-gun Lee, Suk-ki Min & Sung Ho Choh, *Jpn. J. Appl. Phys.*, **33**, 7080, 1994
13. Q. Wang, Wayne L. Gladfelter, D. Fennell Evans, Yue Fan & Alfonso Franciosi, *J. Vac. Sci. Technol. A.*, **14**, 747
14. I. K. Yoo & S. B. Desu, *Phys. Stat. Sol. (a)*, **133**, 565, 1992
15. S. B. Majumder, Y. N. Mohapatra & D. C. Agrawal, *Appl. Phys. Lett.*, **70**, 138, 1997
16. H. N. Al-Shareef, K. R. Bellur, O. Auciello, A. I. Kingo, *Thin Solid Films*, **256**, 73, 1995
17. Kohta Yoshikawa, Takafumi Kimura, Hideyuki Noshiro, Seigen Otani, Masao Yamada & Yuji Furumura, *Jpn. J. Appl. Phys.*, **33**, L867, 1994
18. Byung Gyu Chae, Su Jae Lee, Yong Suk Yang, Seong Hyun Kim & Min Su Jang, *J. Korean Physical Society*, **31**, [6], 874, 1997
19. Xingjiao Li, Jianshe Liu, Dexin Lu, Jianhong Zhao, Longbo Huang & Jiangde Xuan, *Jpn. J. Appl. Phys.*, **34**, L51, 1995
20. B. Guttler, U. Bismayer, P. Groves & E. Salje, *Semicond. Sci. Technol.*, **10**, 245, 1995
21. W. L. Warren, D. Dimos, B. A. Tuttle, R. D. Nasby & G. E. Pike, *Appl. Phys. Lett.*, **65**, [8], 1018, 1994
22. W. L. Warren, G. E. Pike, B. A. Tuttle & D. Dimos, *Appl. Phys. Lett.*, **70**, [15], 2010, 1997
23. Takashi Mihara, Hitoshi Watanabe & Carlos A. Paz de Araujo, *Jpn. J. Appl. Phys.*, **33**, [I-7A], 3996, 1994

Chapter Five

1. R. Moazzami, C. Hu & W. H. Shepherd, *IEEE Trans. Electron Devices*, **11**, 454, 1990
2. R. Moazzami, C. Hu & W. H. Shepherd, *IEEE Trans. Electron Devices*, **39**, 2044, 1992

3. C. Sudhama, A. C. Campbell, P. D. Maniar, R. E. Jone, R. Moazzami, C. J. Mogab & J. C. Lee, *J. Appl. Phys.*, **75**, 1014, 1994
4. J. F. Scott, C. A. Araujo, B. M. Melnick, L. D. McMillan & R. Zuleeg, *J. Appl. Phys.*, **75**, 1014, 1994
5. G. R. Fox & S. B. Krupanidhi, *J. Appl. Phys.*, **74**, 1949, 1993
6. S. D. Bernstein, T. Y. Wong, Yanina Kisler & R. W. Tustison, *J. Mater. Res.*, **8**, [1], 12, 1993
7. H. N. Al-Shareef, A. I. Kingon, X. Chen & K. R. Bellur, *J. Mater. Res.*, **9**, [11], 2968, 1994
8. Takashi Mihara & Hitoshi Watanabe, *Jpn. J. Appl. Phys.*, **34**, 5674, 1995
9. X. Chen, A. I. Kingon, H. Al-Shreef & K. R. Bellur, *Ferroelectrics*, **151**, 133, 1994
10. H. N. Al-Shareef, O. Auciello & A. I. Kingon, *J. Appl. Phys.*, **77**, [5], 2146, 1995
11. Lirong Zheng, Chenglu Lin & Tso-ping Ma, *J. Phys. D: Appl. Phys.*, **29**, 457, 1996
12. Takashi Mihara & Hitoshi Watanabe, *Jpn. J. Appl. Phys.*, **34**, 5664, 1995
13. M. V. Raymond & D. M. Smyth, *J. Phys. Chem. Solids.*, **57**, [10], 1507, 1996